DANIEL EBKE

COBALT-BASED HEUSLER COMPOUNDS IN MAGNETIC TUNNEL JUNCTIONS

BIELEFELD UNIVERSITY

This work was done by myself. Text and figures were partly taken from corresponding publications originate directly from this work.

(Daniel Ebke)

Reviewers:

Prof. Dr. Andreas Hütten
Prof. Dr. Walter Pfeiffer

Copyright © 2010 Daniel Ebke

BIELEFELD UNIVERSITY, DEPARTMENT OF PHYSICS

THIN FILMS & PHYSICS OF NANOSTRUCTURES

Ph.D. thesis

First printing, July 2010

Contents

Publications and Conferences 9

The optimal seed layer system 13

Optimization of the Heusler layer 21

Various Co-based Heusler compounds 29

Transport properties 55

Industrial applicability 79

Conclusions 87

Appendix 91

Schaffe, schaffe Heusler baue!

Introduction

Spintronic devices have attracted a lot of attention in recent years due to possible new applications, e.g., a magnetic random access memory (MRAM), logic and sensors.[1] The spin of the electrons is used as an additional degree of freedom in contrast to common electronic devices. The main constituent of many spintronic devices is the magnetic tunnel junction (MTJ) where two ferromagnets are separated by a thin insulating tunnel barrier.[2] The resistance of such a device depends on the magnetic orientation of the ferromagnets. Usually, R_{AP} (antiparallel) is higher than R_P (parallel) and a tunnel magnetoresistance (TMR) can be defined as $TMR = \frac{R_{AP}-R_P}{R_P}$. For small voltages the resistance is connected to the spin dependent density of states (DOS) at the Fermi level of the ferromagnets. Hence, the TMR value is also given by $TMR = \frac{2P_1P_2}{1-P_1P_2}$[3] with the spin polarization $P_{1,2}$.

Therefore, materials with a high spin polarization are eligible for applications. A half metallic behavior, i.e., they are 100% spin polarized at the Fermi level E_F which has been theoretically predicted for some oxide compounds such as Fe_3O_4 and CrO_2[4], perovskites (e.g. $LaSrMnO_3$[5]), zinc-blende-type CrAs[6] and Heusler compounds[7]. In particular, Co-based Heusler compounds are promising materials for spintronic applications due to the required high Curie temperatures T_C.[8] Here a Heusler compound is given by the composition X_2YZ and a crystallographic $L2_1$ structure exists. X and Y are transition metal elements and Z is a group III, IV or V element.

In 2004, room temperature TMR ratios of more than 100% were reported for MgO-based MTJs.[9] Recently Ikeda presented TMR ratios of over 600% at room temperature and over 1100% at low temperatures[10] for a single MgO tunnel barrier. With the concept of a double barrier system these values can be increased and TMR ratios of more than 1000% at room temperature have been reported.[11]

[1] S. A. Wolf, Science **294**, 1488 (2001); and G. A. Prinz, Science **282**, 1660 (1998)

[2] J. S. Moodera et al., Phys. Rev. Lett. **74**, 3273 (1995); and M. Julliere, Phys. Lett. A **54**, 225 (1975)

[3] M. Julliere, Phys. Lett. A **54**, 225 (1975)

[4] J. Coey et al., J. Appl. Phys. **91**, 8345 (2002)

[5] W. Pickett et al., J Magn Magn Mater **172**, 237 (1997)

[6] H. Akinaga et al., Jpn J Appl Phys 2 **39**, L1118 (2000)

[7] R. D. Groot et al., Phys. Rev. Lett. **50**, 2024 (1983)

[8] P. Webster, J Phys Chem Solids **32**, 1221 (1971)

[9] S. Yuasa et al., Nat Mater **3**, 868 (2004); and S. S. P. Parkin et al., Nat Mater **3**, 862 (2004)

[10] S. Ikeda et al., Appl Phys Lett **93**, 082508 (2008)

[11] L. Jiang et al., Applied Physics Express (2009)

High room temperature TMR ratios have also been reported for MTJs containing Heusler compounds as electrodes: 217% for Co_2MnSi[12] and very recently 386% for $Co_2Fe_{0.5}Al_{0.5}Si$[13]. The latter was grown by using molecular beam epitaxy in place of sputtering deposition. However, sputtering is the preferred and established method for industrial applications. From a technological point of view, the aim is also to achieve high TMR ratios by sputtering. The actuality of this topic can by recognized by recent press releases. For example, Toshiba announced the development of a spin transport electronics based metal oxide semiconductor field-effect transistor (MOSFET)[14] cell with a full Heusler compound.[15] However, the predicted half-metallicity for Heusler compounds should lead to much higher TMR ratios.

[12] S. Tsunegi et al., Appl Phys Lett **93**, 112506 (2008)

[13] N. Tezuka et al., Appl Phys Lett **94**, 162504 (2009)

[14] Most common device for switching and amplifying electronic signals.

[15] http://www.physorg.com/news179572434.html

Nevertheless, one has to meet two challenges to achieve half metallicity:

- crystallization of the Heusler electrode(s) in $L2_1$ structure
- coherent interfaces of the Heusler compound and the MgO tunnel barrier

In this work we have investigated different Co-based Heusler compounds. We have integrated them into so called half junctions to investigate the crystal growth and magnetic properties of the Heusler electrode and into full MTJs for the transport properties.

We describe the optimization of a required seed layer system to induce the preferred (001) texture of the Heusler thin films. Furthermore, we have optimized the Heusler layer in an attempt to achieve a high atomic ordering, represented by a high magnetic moment and a maximum (001) texture. We investigated the transport properties of the full junctions at room temperature and low temperature (13K) respectively, and discuss them in terms of annealing temperature, bias voltage and temperature dependence.

Finally, the industrial applicability and integration of Heusler compound electrodes into conventional GMR/TMR systems will be verified. Consequently, Heusler junctions prepared by Singulus NDT GmbH will be compared to our samples. In particular, the growth properties of the Heusler layer will be addressed to determine differences within the sputtering process of the Heusler thin films.

Publications and conferences

Publications

2006

1. A. Hütten, J. Schmalhorst, A. Thomas, S. Kämmerer, M. Sacher, **D. Ebke**, N.-N. Liu, X. Kou and G. Reiss: *Spin-electronic devices with half-metallic Heusler alloys*, Journal of Alloys and Compounds, **423**, 148 (2006)

2. **D. Ebke**, J. Schmalhorst, N.-N. Liu, A. Thomas, G. Reiss and A. Hütten: *Large tunnel magnetoresistance in tunnel junctions with Co_2MnSi /Co_2FeSi multilayer electrode*, Appl. Phys. Lett., **89**, 162506 (2006)

3. A. Thomas, D. Meyners, **D. Ebke**, N.-N. Liu, M.D. Sacher, J. Schmalhorst, G. Reiss, H. Ebert and A. Hütten: *Inverted spin polarization of Heusler alloys for spintronic devices*, Appl. Phys. Lett., **89**, 012502 (2006)

2007

4. J. Schmalhorst, A. Thomas, S. Kämmerer, O. Schebaum, **D. Ebke**, M.D. Sacher, G. Reiss, A. Hütten, A. Turchanin, A. Gölzhäuser and E. Arenholz: *Transport properties of magnetic tunnel junctions with Co_2MnSi electrodes: The influence of temperature-dependent interface magnetization and electronic band structure*, Physical Review B (Condensed Matter and Materials Physics), **75**, 014403 (2007)

5. J. Schmalhorst, **D. Ebke**, M.D. Sacher, N.-N. Liu, A. Thomas, G. Reiss, A. Hütten, and E. Arenholz, *Chemical and interface properties of tunnel junctions with Co_2MnSi / Co_2FeSi multilayer electrode showing large tunnel magnetoresistance*, IEEE Trans. Magn., **43**, 2806 (2007)

6. A. Castrup, S. Dasgupta, T. Scherer, H. Rösner, J. Ellrich, R. Kruk, M. Ghafari, H. Hahn, A. Hütten, **D. Ebke**, N.-N. Liu, I. Ennen, A. Thomas, J. Schmalhorst and G. Reiss: *Half-metallic Co_2MnSi/Co_2FeSi multilayered Heusler electrodes in magnetic tunnel junctions*, J. Magn. Magn. Mater. **310**, 2009 (2007)

2008

7. A. Thomas, A. Weddemann, **D. Ebke**, N.-N. Liu, A. Hütten, J. Schmalhorst and G. Reiss: *Evidence for band structure effects in the magnetoresistance of Co-based Heusler compounds*, J. Appl. Phys., **103**, 023903 (2008)

8. **D. Ebke**, A. Thomas, A. Hütten, B. Balke, C. Felser, J. Schmalhorst and G. Reiss: *Preparation of Heusler thin films: The quaternary alloy $Co_2Mn_{0.5}Fe_{0.5}Si$*, Physica Status Solidi (a), **205**, 2298 (2008)

9. J. Schmalhorst, **D. Ebke**, A. Weddemann, A. Hütten, A. Thomas, G. Reiss, A. Turchanin, A. Gölzhäuser, B. Balke and C. Felser, *On the influence of bandstructure on transport properties of magnetic tunnel junctions with $Co_2Mn_{1-x}Fe_xSi$ single and multilayer electrode*, J. Appl. Phys, **104**, 043918 (2008)

10. S. Dasgupta, R. Kruk, **D. Ebke**, A. Hütten, C. Bansal and H. Hahn: *Electric field induced reversible tuning of resistance of thin gold films*, J. Appl. Phys., **104**, 103707 (2008)

2009

11. J. Schmalhorst, **D. Ebke**, M. Meinert, A. Thomas, G. Reiss and E. Arenholz: *Element-specific study of the temperature dependent magnetization of Co-Mn-Sb thin films*, J. Appl. Phys, **105**, 053906 (2009)

12. S. Wurmehl, J. T. Kohlhepp, H. J. M. Swagten, B. Koopmans, C. G. F. Blum, V. Ksenofontov, H. Schneider, G. Jakob, **D. Ebke** and G. Reiss: *Off-stoichiometry in Co_2FeSi thin films sputtered from stoichiometric targets revealed by nuclear magnetic resonance*, Journal of Physics D: Applied Physics, **42**, 084017 (2009)

13. **D. Ebke**, V. Drewello, M. Schäfers, G. Reiss and A. Thomas: *Tunneling spectroscopy of MgO based magnetic tunnel junctions with Co_2FeAl electrode*, Appl. Phys. Lett., **95**, 232510 (2009)

14. **D. Ebke**, P. Thomas, O. Schebaum, M. Schäfers, D. Nissen, V. Drewello, A. Hütten and A. Thomas, *Low B2 crystallization temperature and high tunnel magnetoresistance in Co_2FeAl / MgO / Co-Fe magnetic tunnel junctions*, J. Magn. Magn. Mat., **322**, 996-998 (2010)

15. M. Meinert, J. Schmalhorst, **D. Ebke**, N.-N. Liu, A. Thomas, G. Reiss, J. Kanak, T. Stobiecki and E. Arenholz: *Structural and magnetic properties of Co-Mn-Sb thin films*, J. Appl. Phys., **107**, 063901 (2010)

16. **D. Ebke**, Z. Kugler, P. Thomas, O. Schebaum, M. Schäfers, D. Nissen, J. Schmalhorst, A. Hütten, E. Arenholz and A. Thomas, *X-ray absorption and magnetic circular dichroism studies of Co_2FeAl in magnetic tunnel junctions*, IEEE Trans. Magn., **46**, 1925-1928 (2010)

17. O. Schebaum, **D. Ebke**, A. Niemeyer, G. Reiss and A. Thomas, *Direct measurement of the spin polarization of Co_2FeAl in combination with MgO tunnel barriers*, J. Appl. Phys., **107**, 09C717 (2010)

Conferences

1. D. Ebke, N.-N. Liu, M. Sacher, J. Schmalhorst, G. Reiss and A. Hütten, *Co_2FeSi - an alternative for the Co_2MnSi Heusler electrode integrated in magnetic tunnel junctions*, DPG spring meeting, Dresden (2006), MA 3.5

2. D. Ebke, J. Schmalhorst, A. Thomas, S. Kämmerer, O. Schebaum, M. Sacher, A. Hütten and G. Reiss, *Transport properties of magnetic tunnel junctions with Co_2MnSi electrode: influence of temperature-dependent interface magnetization and electronic band structure*, SNI-meeting, Hamburg (2006), D-P255

3. D. Ebke, J. Schmalhorst, A. Hütten, G. Reiss, B. Balke and C. Felser, *Transport properties of magnetic tunnel junctions with the quaternary Heusler alloy $Co_2Mn_{0.5}Fe_{0.5}Si$* ,DPG spring meeting, Regensburg (2007), MA 12.2

4. D. Ebke, J. Schmalhorst, M. Sacher, N.-N. Liu, A. Thomas, A. Hütten, E. Arenholz and G. Reiss, *Chemical and magnetic interface properties of tunnel junctions with Co_2MnSi/Co_2FeSi multilayer electrode*, DPG spring meeting, Regensburg (2007), MA 15.98

5. D. Ebke, J. Schmalhorst, A. Thomas, A. Hütten and G. Reiss, *Magnetic properties of Co_2FeSi thin films deposited by magnetron sputtering using different target compositions*, 424. WE-Heraeus-Semiar, Magnetism meets Semiconductor, Bad Honnef (2009)

6. D. Ebke, J. Schmalhorst, A. Thomas, A. Hütten and G. Reiss, *Magnetic properties of Co_2FeSi thin films deposited by magnetron sputtering using different target compositions*,DPG spring meeting, Dresden (2009), MA 40.108

7. D. Ebke, P. Thomas, O. Schebaum, M. Schäfers, D. Nissen, A. Hütten and A. Thomas, *Low ordering temperature and high tunnel magnetoresistance in Co_2FeAl / MgO / Co-Fe magnetic tunnel junctions*, 11th Joint MMM-Intermag Conference, Washington, DC (2010), BA12

8. D. Ebke, Z. Kugler, P. Thomas, O. Schebaum, M. Schäfers, D. Nissen, J. Schmalhorst, A. Hütten and A. Thomas, *Magnetic properties and high room temperature TMR ratios of Co_2FeAl in magnetic tunnel junctions*, DPG spring meeting, Dresden (2010), MA 28.1

The optimal seed layer system

To realize a high spin polarized full Heusler compound (X_2YZ) thin film, it is necessary to enforce the crystallization in a $L2_1$ type structure. As illustrated in Figure 1, this is given by four interpenetrating fcc lattices that are shifted by $1/4$ lattice constant a. Each sub-lattice contains one kind of atom. An atomic disorder of the Y and Z components is defined as $B2$ structure, a disorder of the X and Y components $D0_3$, respectively. The A2 type structure has no ordered sub-lattices, i.e. it is a simple bcc lattice.

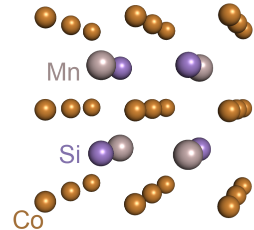

Figure 1: Crystallographic $L2_1$ type structure of a Co_2MnSi Heusler compound.

It is reported by Picozzi that some type of disorder might lead to additional states at the Fermi level E_F and the spin polarization is reduced.[16]

In addition to the atomic order the crystallographic orientation of the Heusler thin film is also important. It is reported by Oogane[17] that a (001) texture of a Co-based Heusler compound is essential because Co atoms at the interface may break the half metallicity in (011) textured Heusler layers.

In general one has to consider the base for the Heusler layer in order to induce the crystal growth and the preferred orientation. The previous works of our lab were founded on a (011) textured Heusler film.[18] Here, the layers were deposited on V buffered thermally oxidized Si wafer to induce a maximum texture. Later, we realized first experiments of a (001) textured Heusler compound, which are described in the Master's thesis of Keseberg.[19] The V buffer was replaced by a MgO/Cr buffer to achieve a more (001) oriented growth. Probably due to the Si substrate, (011) textured parts of the Heusler layer were still present.

In this work we will create a more effective layer stacking. The thin films will be optimized layer by layer. Therefore the first step is to find a new and simple seed layer system to get a highly (001) oriented Heusler compound. For different reasons[20] it is most suitable to pass on a metallic seed layer, such as Cr which is often used on insulating MgO as an additional seed layer.[21]

[16] S. Picozzi et al., Phys. Rev. B **69**, 1 (2004)

[17] M. Oogane et al., ATI and IFCAM International Workshop on Spin-Currents, Tohoku University (2007)

[18] S. Kämmerer, PhD thesis, Bielefeld University (2004); J. Schmalhorst et al., Phys. Rev. B **75**, 1 (2007); and D. Ebke et al., Appl Phys Lett **89**, 162506 (2006)

[19] F. Keseberg, Master's thesis, Bielefeld University (2007)

[20] excluding additional sources of diffusion; required for the layer stacking to realize spin polarized tunneling into superconductor experiments

[21] Y. Sakuraba et al., Appl Phys Lett **88**, 192508 (2006); S. Tsunegi et al., Appl Phys Lett **93**, 112506 (2008); and K. Inomata et al., Sci. Technol. Adv. Mater. **9**, 014101 (2008)

The most promising reported methods to form a highly (001) textured thin film are the following:

MgO substrates: (001) MgO substrates are used. [22] The expected lattice mismatch of about 5% to the 45 degrees rotated MgO ($a_{MgO} = 4.21\,\text{Å} \times \sqrt{2} = 5.95\,\text{Å}$) allows a epitaxial growth of the Heusler compound ($a_{Heusler} \approx 5.70\,\text{Å}$). The disadvantage of MgO substrates are their high costs when compared to the established SiO_2 wafer. This is caused by the small standard substrate sizes and therefore a direct industrial application is challenging. Furthermore, MgO substrates are very sensitive to moisture and require special storage.

[22] S. Tsunegi et al., Appl Phys Lett **93**, 112506 (2008)

Si substrates: The Si lattice constant of $a_{Si} = 5.43\,\text{Å}$ is also in good agreement with the treated Heusler compounds of this work ($a_{Heusler} = 5.65\,\text{Å}$- $5.70\,\text{Å}$). The disadvantage of Si is the elaborate cleaning process of the surface. It is reported, that this can be done subsequently by isopropyl, diluted H_2SO_4 and HF.[23]

[23] G. X. Miao et al., Appl Phys Lett **93**, 142511 (2008)

The latter method was used for Fe thin films instead of Heusler compounds. Nevertheless it is comparative because the lattice constant of Fe ($a_{Fe} = 2.866\,\text{Å}$)[24] is almost half of the lattice constant of the investigated Heusler compounds ($a_{Heusler} \approx 5.70\,\text{Å}$). Additionally, Fe growths in (011) texture on standard thermally oxidized SiO_2 wafer, too.

[24] Reference Database, International Centre for Diffraction Data (1999)

Therefore, we used Fe in the first step, instead of a Heusler compound, in order to find an optimum seed layer system with regard to the required (001) texture. Its advantage is that an annealing process is not essential for atomic ordering, as it is in the case of Heusler thin films. Furthermore, a confusion of texture and order related diffraction peaks can be avoided in X-ray diffraction (XRD) measurements. To prevent surface contaminations, all substrates were covered by various thicknesses of a MgO buffer layer.

Therefore, we prepared the following two systems on different substrates and performed XRD measurements to estimate the growth properties:

1. MgO substrate / MgO (x nm) / Fe (20 nm)
2. Si substrate / MgO (x nm) / Fe (20 nm)

Here, x is a varying MgO buffer thickness of $1, 2, 5, 10, 15$, or $20\,\text{nm}$. One and two nm were only investigated for the MgO substrates. All prepared samples were measured in the as prepared

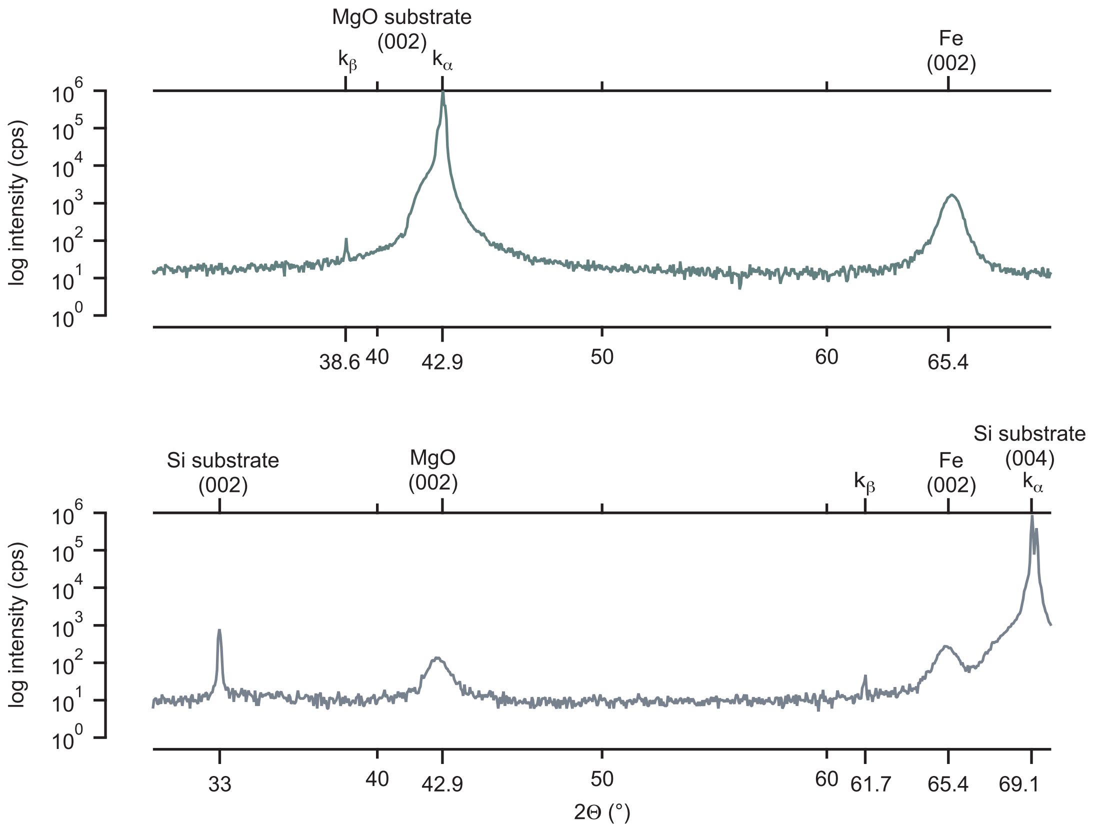

Figure 2: Overview of XRD pattern for 20 nm Fe on MgO (top) and Si (bottom) substrate. The samples were annealed for 1h at 400°C.

state and after subsequent annealing for 1h in steps of 200°C, 300°C, 400°C and 500°C.

We use DC/RF sputtering for the preparation of the thin films. This is the established method for industrial applications. All films were deposited at room temperature. A base pressure of 1.0×10^{-7}mbar of the sputtering system was used; the Argon process pressure was between 1.5×10^{-2}mbar and 1.5×10^{-3}mbar.

XRD is a standard method for the characterization of the crystal growth properties of thin films. It is possible to determine the layer thickness and to conclude orientation and texture of the sputtered films. The constructive interference of radiation in a lattice can be described by Bragg's law:[25]

$$n\lambda = 2d_{hkl} \sin\theta \quad (1)$$

where n is an integer, λ is the wavelength of the incident beam and d_{hkl} the lattice plane distance in (hkl) direction. The XRD measurements were performed by an X'pert PRO MPD diffrac-

[25] Einführung in die Festkörperphysik, C. Kittel, R. Oldenbourg Verlag München Wien (2006)

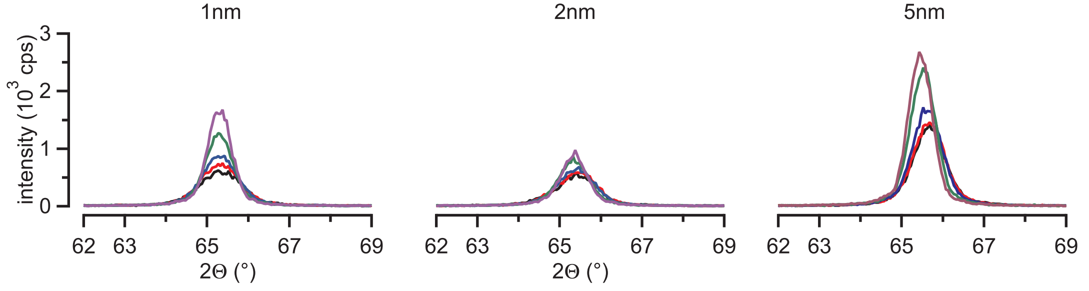

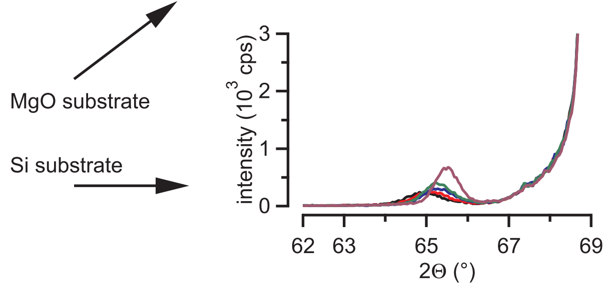

Figure 3: XRD pattern of the Fe (002) peak for 1 nm, 2 nm and 5 nm (left) and 10 nm, 15 nm and 20 nm (right) MgO buffer thickness on MgO (top) and Si substrates (bottom).

tometer by Philips. The copper anode emits a wavelength of $\lambda = 1.54056$ Å for Cu K_{α_1} and the average of K_{α_1} and K_{α_2} is determined to $\lambda = 1.54184$ Å. With the angle of constructive interference θ the plane distance is given by

$$d_{hkl} = \frac{n\lambda}{2\sin\theta}. \tag{2}$$

Hence, the lattice constant of the investigated material can be calculated by:

$$a = \sqrt{h^2 + k^2 + l^2} \cdot d_{hkl}. \tag{3}$$

The obtained peak intensities, or rather the peak net areas, represent, in a first approximation, the degree of texture of the sputtered film and are used to estimate the optimum seed layer.[26]

[26] The observed intensity is a superposition of different effects and is influenced by disorder effects, too. For the investigated Fe this is neglected.

Figure 2 depicts an overview of the obtained XRD pattern for a 20 nm thick Fe film, deposited on a MgO substrate (top) and Si substrate (bottom), respectively. The MgO buffer layer thickness is 5 nm. Both samples were ex-situ vacuum annealed for 1h at 400°C. The MgO substrate peak at 42.9 degrees on the top of Figure 2 and the Si substrate peak at 33 and 69.1 degrees on the bottom are clearly visible. The corresponding smaller k_β substrate peaks are also labeled. The Fe (002) peak can be identified at 65.4 degrees

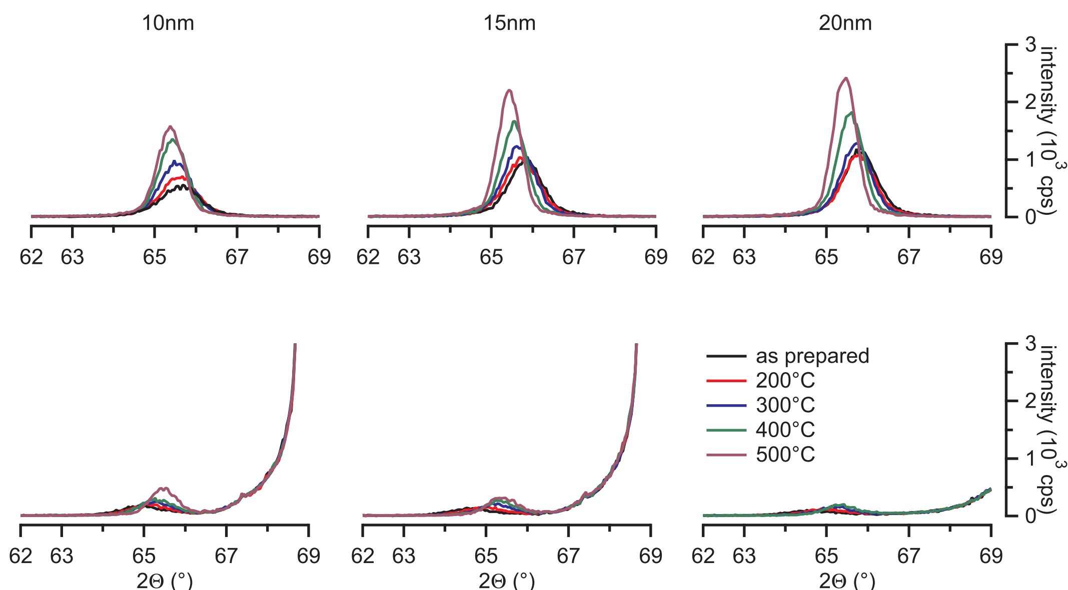

for both types of substrate. The peak of the sputtered MgO layer is overlaid by the MgO substrate peak but can be found in case of the Si substrate at 42.5 degrees.

For further characterization of the crystal growth properties of the Fe layer, the analysis is focused on the Fe (002) peak. This is shown for different MgO buffer thicknesses and for varying annealing temperatures in Figure 3. The Fe (002) peak intensities are lowered for all MgO buffer layer thicknesses in case of the Si substrate compared to the MgO substrate. The highest intensities can be found for 5 nm and 20 nm MgO buffered Fe on MgO substrate. For the Si substrate, the highest peak can be found for 5 nm MgO, as well. But the height is only a fourth of the highest corresponding height on the MgO substrate. Due to the strongly degraded growth of the Fe layer on Si wafers, MgO substrates were used in the following work.

To determine the optimum MgO buffer layer thickness, the net area of the Fe (002), as a function of annealing temperature, is shown in Figure 4. An increasing net area for increasing annealing temperatures can be found for all MgO thicknesses which indicate an improvement of (001) texture. Only the net area of the 2 nm MgO buffered Fe is nearly on a constant level. The 5 nm buffered Fe clearly results in the largest peak net area for all annealing

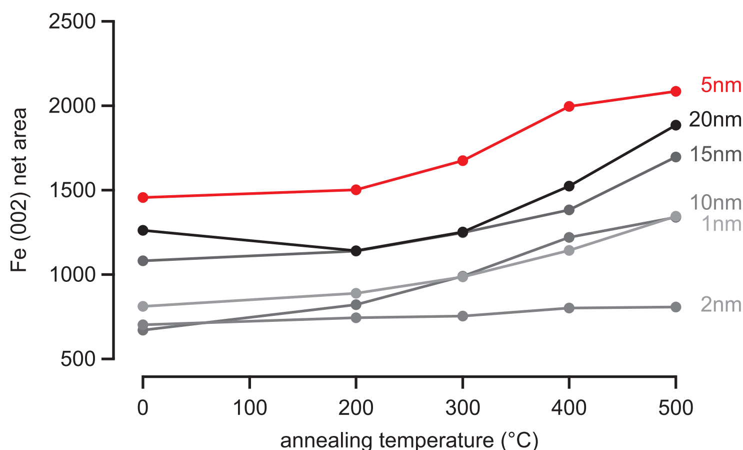

Figure 4: net area of Fe (002) peak as a function of annealing temperature for different MgO buffer thicknesses. All samples were deposited on (001) MgO substrates and subsequently ex situ vacuum annealed.

temperatures. Hence, this thickness is assumed to be the best seed layer and it will be used for all Heusler compounds that were investigated in this work.

The obtained shift in the maximum peak intensities, in Figure 3, can be attributed to a change of the Fe lattice constant. This is shown for varying annealing temperatures in Figure 6. All achieved values are close to the Fe bulk value, represented by the dashed line. The deviation is larger for thicker MgO layers in the as prepared state. With increasing annealing temperatures all lattice constants approach the bulk value. This might indicate a slightly degraded crystal growth of the thicker MgO layers which can be compensated by moderate annealing. Remarkably, all changes are only in the order of $1/100$ Å.

Furthermore, it is reported that film deposition on heated MgO substrates can improve the crystal growth properties.[27] Therefore, the optimized layer system was deposited on an in situ annealed MgO substrate. A maximum temperature of about 400°C could be achieved in the current sputtering system. For a similar treatment, the deposited layers were also subsequently ex-situ annealed at varying temperatures. The corresponding XRD pattern of the Fe (002) peak is shown in Figure 5. Compared to the same layer stacking shown in Figure 3, no improvement of the Fe films can be achieved for any annealing temperature. The maximum peak intensity is only about a third of the highest intensity for the similar non pre-annealed MgO substrate. Furthermore, nearly no difference in peak intensity can be found with increasing annealing temperature, as might be expected by the 400°C in situ annealing temperature.

[27] K. Inomata et al., J. Phys. D: Appl. Phys. **39**, 816 (2006)

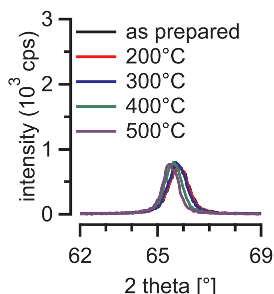

Figure 5: Fe (002) peak intensities for 5 nm thick MgO buffer deposited on a heated MgO substrate.

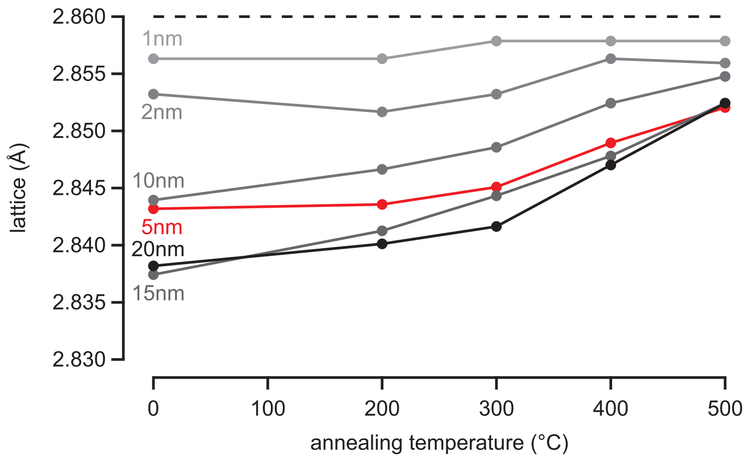

Figure 6: Lattice constants for different MgO buffered Fe layers as a function of annealing temperature. The dashed line represents the bulk value.

In summary, the required seed layer for Heusler compounds was optimized. Because of similar growth properties[28] to a Heusler compound, Fe was used to estimate the optimum seed layer. The different seed layers were investigated by XRD with in an attempt to achieve a maximum (002) Fe peak height and net area, respectively. According to the obtained results, a 5 nm MgO buffer is the preferred seed layer on (001) MgO substrate in order to obtain a (001) textured Heusler thin film.

[28] cubic lattice, Fe lattice is half of the Heusler lattice, (011) oriented growth on standard SiO_2 wafer

Optimization of the Heusler layer

This chapter deals with the optimization of the Heusler layer with regard to getting a high magnetic moment and a good (001) textured growth. The influence of layer thickness, as well as ex situ annealing temperature, will be investigated. Here, the well known compound Co_2MnSi is used as a representative for all Heusler compounds that will be investigated in this work. From earlier works, it is known that Co_2MnSi is amorphous in the as prepared state. Therefore, an annealing process is required to initiate the crystallization and to induce the atomic ordering. Founded on previous results, an initial annealing temperature of $400°C$ was chosen.[29]

[29] S. Kämmerer, PhD thesis, Bielefeld University (2004); and A. Hütten et al., Journal of Alloys and Compounds **423**, 148 (2006)

thickness dependence

Co_2MnSi thin films with a varying layer thickness were deposited on the optimized seed layer system MgO(001)/MgO(5 nm) to investigate thickness dependent crystalline growth and the magnetic properties of the Heusler compound. The samples were prepared under the same conditions as described previously for the Fe thin films.

Figure 7 shows the obtained XRD pattern of 10 nm, 20 nm, 50 nm and 100 nm thick Co_2MnSi layers. All layers were ex situ vacuum annealed for 1h at 450°C, for crystallization and atomic ordering of the Heusler compound. The baselines of the achieved patterns were shifted with regard to the Heusler thickness. As previously described, the MgO substrate peak can be found at 42.9 degrees (k_α) and 38.6 degrees (k_β). The Co_2MnSi (004) peaks at 66.3 degrees and the (002) peaks at 31.8 degrees are visible in all cases. As expected, the obtained peak intensities are increased by increasing Co_2MnSi thickness. For the 50 nm and 100 nm thick layers, a slight (022) peak at 24.4 degrees can be imagined. The induced (001) growth direction by the MgO seed probably vanishes

Figure 7: Co_2MnSi XRD pattern for different Co_2MnSi thickness at an annealing temperature of 450°C. The baselines are shifted with regard to the annealing temperature.

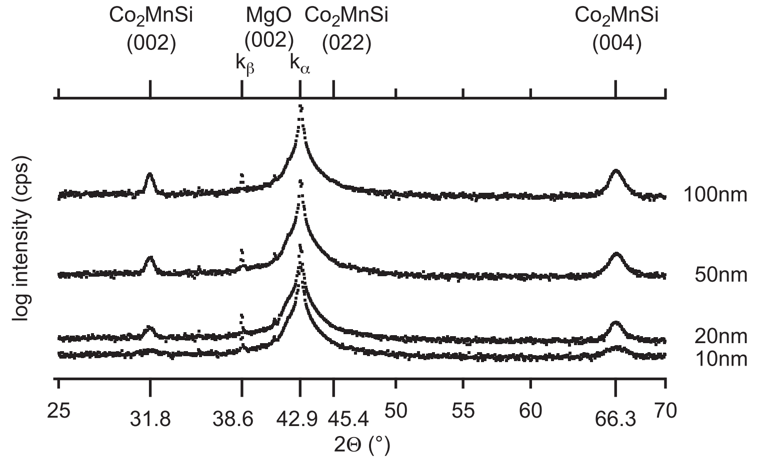

for thick layers and the Heusler film forms partial (011) crystals.

The peak intensities are proportional to the layer thickness. Due to the different deposited thicknesses of Co_2MnSi, an extended peak analysis is required to distinguish the optimum Heusler thickness. Therefore, the net area of the Heusler (004) peak is divided by the corresponding layer thickness and defined as the textured fraction:

$$textured\ fraction = \frac{peak\ net\ area}{layer\ thickness} \tag{4}$$

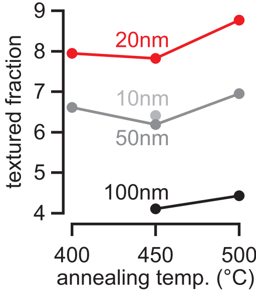

Figure 8: Textured fraction of different Heusler thicknesses and varying annealing temperatures.

The results are shown in Figure 8 as a function of annealing temperature. The highest textured fraction can be found for the 20 nm thick Co_2MnSi and all investigated annealing temperatures of 400°C, 450°C and 500°C. The values of the 50 nm thick layer were slightly reduced. For the 400°C and 500°C annealed 10 nm Co_2MnSi films, no clear (004) peak was detectable and the net area could not even be estimated. The same behavior was a also found for the 400°C annealed 100 nm thick Heusler sample. Here, higher annealing temperatures were required for crystallization. The epitaxial growth of the Co_2MnSi onto the buffered (001) MgO substrate can be proven by an XRD pole figure scan, which was taken by an Euler cradle. Here, the sample can additionally be rotated on a tilting stage. The diffraction angle of θ is set to a fixed value. For every angle ψ (0 to 90 degrees) of the tilted stage a diffraction pattern is taken with a varying angle ϕ (0 to 360 degrees) of the rotating sample. Figure 9 depicts the results of the obtained pole figure scans of the MgO substrate[30] (left) and 20 nm thick Co_2MnSi layer (right) for a 500°C subsequently annealed sample. The fixed angle was set to the MgO (022) peak position of $2\theta = 62.3$ degrees and to the Co_2MnSi (022) peak posi-

[30] The intensity of the 5 nm thick MgO buffer can be neglected.

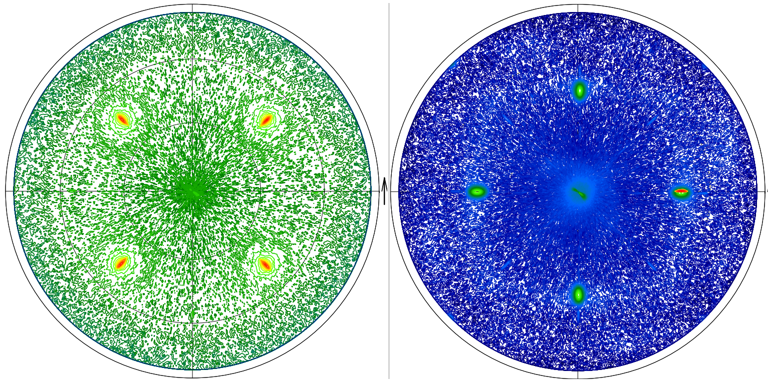

Figure 9: Left: pole figure of the MgO substrate. The fixed angle is set to the MgO (022) peak position at $2\theta = 62.3$ degrees. Right: corresponding pole figure of the 20 nm thick Co_2MnSi layer. The angle is set to the (022) peak position at 45.5 degrees. The sample was subsequently annealed to a maximum temperature of 500°C.

tion of 45.5 degrees. The four visible areas with higher intensities show the (022) peak of the MgO substrate and represent the cubic crystal structure. Consequently, the corresponding (022) peak of the Co_2MnSi film is rotated by $\phi = 45$ degrees, i.e., the intended epitaxial growth of the Heusler compound in (001) direction was present. As expected, the lattice was rotated by 45 degrees to the MgO substrate and the buffer did not alter the intended growth, due to the low lattice mismatch.

In addition to a good (001) texture, a high magnetic moment of the Heusler thin films should be achieved. A lowered moment could be attributed to a certain atomic disorder.

Room temperature alternating gradient magnetometer (AGM) measurements were performed to investigate the magnetic moment of the Co_2MnSi thin films. Here, samples of about 3 mm x 3 mm were placed onto a sample holder that was connected to a piezo crystal. In a magnetic field of a pair of coils, the sample behaves like a dipole. An additional oscillating magnetic gradient field leads to a vibration of the sample. The generated voltage of the piezo crystal can be monitored with a lock-in amplifier. The magnetic state of the sample will be changed by the variation of the homogeneous field, which leads to a different signal at the lock-in amplifier. Calibrated with a known magnetic moment, the moment of the investigated sample can be determined. The magnetization M can be calculated from the relation $M = m/V$, where m is the measured magnetic moment and V the magnetic volume of the investigated magnetic material. The volume can be calculated from the known thickness of the sputtered films and the sample area. The latter can be estimated via the substrate density and the weight of the treated sample.

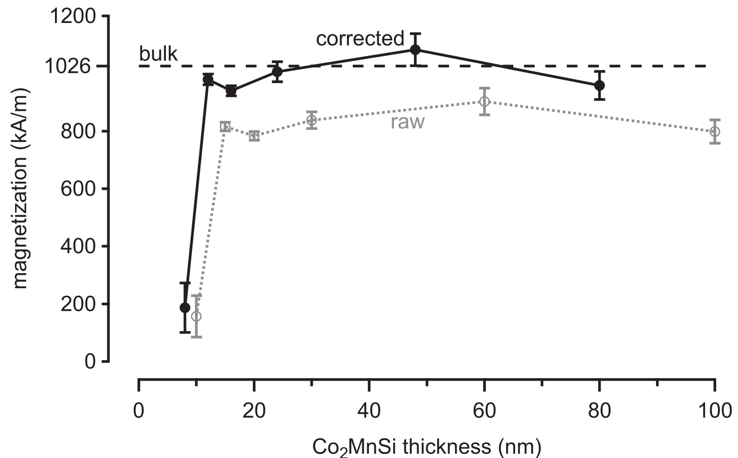

Figure 10: Room temperature magnetization of Co_2MnSi measured by AGM as a function of supposed (grey) and correct(black) Heusler thickness. The layers were annealed for 1h at 400°C.

In Figure 10 the results of the performed AGM measurements are shown for different Co_2MnSi films which were deposited on the optimized seed layer. The obtained magnetization of the Co_2MnSi layer is given as a function of thickness (grey dots). All samples were ex situ annealed for 1h at $400°C$. The plotted values are the average values of three similar samples. The error bars are estimated from the corresponding standard deviation of the three measurements. The dashed line represents the predicted full bulk magnetic moment of 1026 kA/m ($5.008\mu_B$[31] and assuming the experimental lattice constant of 5.64 Å). For a Co_2MnSi layer thicker than 15 nm, a magnetization of abut 900 kA/m can be reached which corresponds to about 88% of the predicted bulk value. The magnetization is almost constant, within the range of 15 nm to 100 nm Heusler thickness. Thinner layers show a strongly reduced magnetization which indicates an atomic disorder or absence of the crystal structure. The present lowered experimental magnetization of Co_2MnSi, compared to the predicted bulk magnetization, can be explained by an overestimated thickness of the Heusler layer. The thickness of the sputtered films are given by a certain deposition time that is determined from a calibration sample. Here, a thick layer is deposited for an exact time ($\sim$ 100 s). Afterwards the thickness is determined by X-ray reflection (XRR) or atomic force microscopy (AFM) on the non-annealed sample. Because of the amorphous growing of Co_2MnSi, a difference of about 20 % in layer thickness can be found for the non-annealed and annealed sample, respectively. This results in a 20 % lower calculated magnetic moment.

[31] I. Galanakis, Phys. Rev. B **71**, 1 (2005)

The corrected values, represented by the black dots in Fig-

ure 10, measure up to the predicted full bulk magnetization of 1026 kA/m (corresponding to about $5\mu_B$) for a corrected film thickness of 12 nm and above.

In addition to the magnetization, the coercive field H_C, of the estimated soft magnetic Co_2MnSi layers, can be determined from AGM measurements, as well. In Figure 11 the coercive field is depicted as a function of Co_2MnSi thickness. A minimum H_C of 3 Oe can be found for the 15 nm thick Co_2MnSi layers. With increasing layer thickness, the coercive field increases, as well. With regard to the XRD results, the change of coercive field might be attributed to the crystal quality of the Heusler compound. The lowest values of H_C are found for the highest textured fraction of Co_2MnSi. Therefore, the progression of coercive field can be used as a first approximation to estimate the Heusler quality.

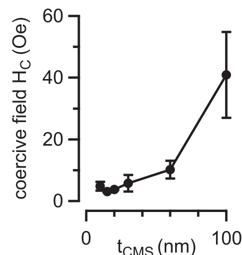

Figure 11: Coercive field of Co_2MnSi annealed for 1h at 400°C as a function of Heusler thickness.

In summary, the performed XRD and AGM measurements of the Co_2MnSi layers, deposited on the optimized seed layer system MgO(001)/MgO(5 nm), show an optimal Heusler thickness of about 20 nm, with regard to the atomic ordering and crystal growth in (001) direction. Below 15 nm, a strongly degraded magnetic moment is found, as well as an increased coercive field. The crystalline growth of a 10 nm Co_2MnSi layer is lower when compared to 20 nm. Thicker Heusler layers show an increased coercive field and a degraded crystalline growth, as well. Therefore, we assumed a Heusler thickness of 20 nm as the optimal layer thickness for the following experiments and all other compounds that we will investigate in this work.

annealing temperature dependence

The annealing temperature of the Heusler layer is important for atomic ordering and crystallization. Analogous to the above discussed influence of Heusler layer thickness, structural and magnetic measurements were performed to verify the optimal annealing temperature. Figure 12 depicts the XRD pattern of a 20 nm thick Co_2MnSi layer, that was deposited on the optimized seed layer system for different annealing temperatures. The baselines of the patterns were shifted with regard to this temperature. Prior to annealing at $350°C$, no (002) and (004) Heusler peaks at 31.8 degrees and 66.3 degrees can be found. For higher temperatures, both peaks are visible. The (002) k_α and k_β peak of the MgO sub-

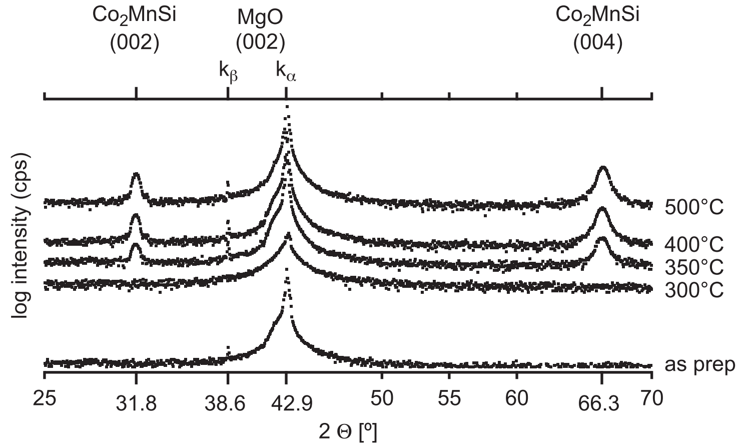

Figure 12: XRD pattern of 20 nm thick Co2MnSi layers annealed at varying temperatures. The crystallization process starts at about 350°C.

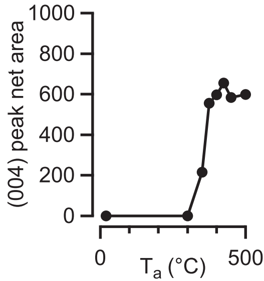

Figure 13: (004) peak net area of 20 nm thick Co_2MnSi as a function of annealing temperature. The crystallization process starts at about 350°C.

strate are located at 42.9 and 38.6 degrees, respectively. The required annealing temperature to initiate the crystal growth of the Heusler compound Co_2MnSi in (001) direction can be estimated from the (004) peak net area. The achieved patterns are shown in Figure 13 as a function of annealing temperature. Below $300°C$ the Co_2MnSi layer is amorphous and, therefore, no peak is present. In the range of $300°C$ to $375°C$ the crystallization process takes place and the (004) peak net area increases with increasing temperature. Higher annealing results in a fairly constant net area. The maximum value can be found for the $425°C$ annealed sample.

A similar step like behavior is present in the obtained magnetization of the Heusler thin films. The results of the room temperature

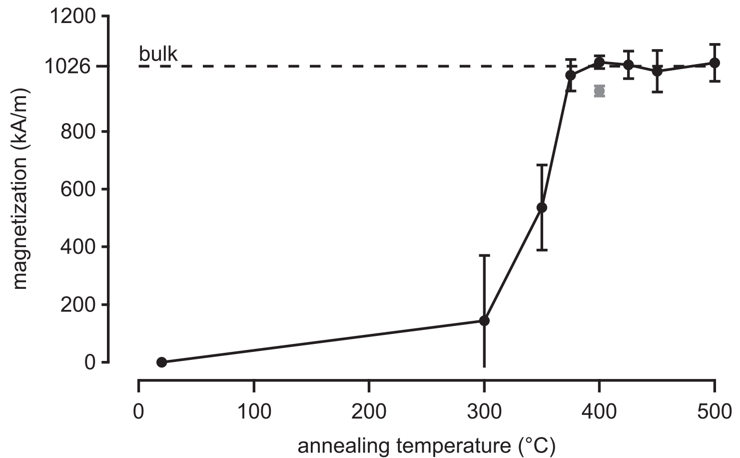

Figure 14: Room temperature magnetization of Co_2MnSi, measured by AGM, as a function of annealing temperature for 20 nm thick Heusler layer. The grey marker refers to the corresponding measurements of Co_2MnSi thickness dependence.

AGM measurements are illustrated in Figure 14. The dashed line represents the predicted bulk magnetization of 1026 kA/m (corresponding to 5.008μ_B[32]). Within the temperature range of 375°C to 500°C, the magnetization is almost constant and a maximum of 1039 kA/m can be achieved for the 400°C annealed sample.

[32] I. Galanakis, Phys. Rev. B **71**, 1 (2005)

The overestimated thickness of the Co_2MnSi layers was already taken into account. The grey marker refers to the corresponding measurements of Co_2MnSi thickness dependence. It is slightly lowered but within experimental accuracy.

The coercive fields of the Heusler compound were investigated by AGM, as well. The obtained results are depicted in Figure 15 as a function of annealing temperature. A very high H_C is present for the 350°C annealed sample. In addition to the previously discussed XRD measurements, it indicates the structural change at this temperature. For temperatures above 375°C a low coercive field can be achieved for the crystalized and atomically ordered Co_2MnSi layers.

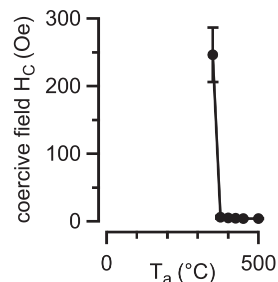

Figure 15: Coercive field of 20 nm thick Co_2MnSi layers annealed at varying temperatures.

In summary, the growth direction of the Co_2MnSi layer was successfully changed from (011) to (001) orientation with the new seed layer system, which was previously introduced and investigated for Fe. The full predicted bulk magnetization and thus the magnetic moment of the Heusler compound was reached. The best results, with regard to the induced atomic ordering and an optimal (001) textured growth, were achieved for 20 nm thick Co_2MnSi layer deposited on 5 nm MgO buffered (001) MgO substrates, which were annealed for 1h at 400°C.

Various Co-based Heusler compounds

The half-metalic behavior has been theoretically predicted for different Heusler compounds[33], but the resulting giant TMR ratios could not be observed. The reasons for this can be manifold and some are listed in the below:

[33] R. D. Groot et al., Phys. Rev. Lett. **50**, 2024 (1983); and I. Galanakis et al., Phys. Rev. B **66**, 1 (2002)

- Fabrication of the required $L2_1$ structure: Often the half-metallicity is predicted only for $L2_1$ type structure. The density of states (DOS) can be sensitive to the crystal structure and so a disordered compound ($B2$-, $A2$-type structure) may have a reduced spin polarization[34]
- Correct film composition: The calculated DOS of compounds with a deviation from the X_2YZ composition shows, for some materials, additional states close to the Fermi level. This may lead to a reduced spin polarization, as well.
- Mn oxide problem: Heusler compounds that contain Mn often show a decreased magnetic moment. In particular, the barrier interface moment might be lowered due to the formation of MnO, which might also reduce the spin polarization.[35]
- Coherent growth: Coherent growth of the barrier is preferred to get coherent tunneling. Therefore, materials with a low lattice mismatch are most promising.
- Layer roughness: A rough surface of the sputtered Heusler bottom electrode can reduce the quality of the tunnel barrier and would lead to a reduced TMR ratio.

[34] S. Picozzi et al., Phys. Rev. B **69**, 1 (2004)

[35] A. Hütten et al., Journal of Alloys and Compounds **423**, 148 (2006)

The challenge is to find a Heusler compound with the best properties regarding the above mentioned difficulties. In particular, the following compounds are very promising. The pros and cons will be pointed out in detail.

Co_2MnSi (CMS) is the Heusler compound with the highest reported TMR values at low temperatures.[36] Several experimental and theoretical publications can be found and it is very well

[36] S. Tsunegi et al., J. Phys. D: Appl. Phys. (2009)

understood. It is predicted to be a half metal but the position of the Fermi level is reported to be close to the edge of the valence band. This might reduce the room temperature TMR because of thermal smearing.[37] Some years of experience in preparing Co_2MnSi thin films are present in Bielefeld. Unfortunately, the containing Mn is supposed to reduce the spin polarization due to the formation of MnO at the barrier interface.[38]

[37] B. Balke et al., J Magn Magn Mater **310**, 1823 (2007)

[38] A. Hütten et al., Journal of Alloys and Compounds **423**, 148 (2006)

Co_2FeAl (CFA) contains the same number of electrons (29) as Co_2MnSi, and regarding the Slater-Pauling behavior[39], the same magnetic moment is expected. Half metallicity is predicted for band structure calculations using the SPR-KKR program package of H. Ebert[40]. The spin polarization is lowered for the approach of Akai, used by Miura.[41] The FPLO method leads also to a reduced spin polarization.[42] In contrast to other compounds, the high spin polarization is almost conserved, even for $B2$ type structured Co_2FeAl.

[39] I. Galanakis et al., Phys. Rev. B **66**, 1 (2002)

[40] http://olymp.cup.uni-muenchen.de/ak/ebert/SPRKKR/

[41] Y. Miura et al., Phys. Rev. B **69**, 144413 (2004)

[42] S. Wurmehl et al., J. Phys. D: Appl. Phys. **41**, 115007 (2008)

Co_2FeSi (CFS) has the highest reported Curie temperature T_C and bulk magnetic moment of $6\mu_B$.[43] Furthermore, it is reported to be easily fabricated in the required $L2_1$ structure.[44] With regard to the latter two compounds, the position of the Fermi level is shifted to higher energies. For some DOS calculations, it ends up in the conductance minority band and the predicted half metallicity can not be conserved. But the exact position of E_F is disputed.[45]

[43] S. Wurmehl et al., Phys. Rev. B **72**, 1 (2005)

[44] N. Tezuka et al., Appl Phys Lett **89**, 112514 (2006)

[45] A. Thomas et al., J. Appl. Phys. **103**, 023903 (2008); and B. Balke et al., Phys. Rev. B **74**, 1 (2006)

Co_2MnAl (CMA) contains 28 valence electrons. According to the Slater-Pauling behavior, it has the lowest magnetic moment within this list, which is interesting for current induced switching. The position of E_F is shifted to lower energies, with regard to the above listed compounds. Very few publications can be found about this compound. The included Mn might oxidize, as reported for Co_2MnSi, but the role of Al or Si, respectively, with regard to prevention of oxidation is unclear.

$Co_2Mn_{0.5}Fe_{0.5}Si$ (CMFS) is predicted to have E_F located in the middle of the band gap.[46] Therefore, high TMR ratios at low temperature are also expected to be conserved at room temperature.

[46] B. Balke et al., J Magn Magn Mater **310**, 1823 (2007)

In summary, Heusler compounds with 28 (Co_2MnAl) to 30 (Co_2FeSi) valence electrons will be investigated. The corresponding predicted bulk magnetic moment is in a range of $4\mu_B$ to $6\mu_B$. A half metallic behavior can be predicted for all compounds and the dif-

ferent number of valence electrons lead to different positions of the Fermi level, with regard to the band gap.[47] Within this list of Heusler compounds, the role of the different elements can probably be verified, as well as the connection to Fermi level, bias voltage and temperature dependence. A similar lattice constant is expected for all compounds and the for Co_2MnSi optimized seed layer will be used, as well. First, half junctions (see Figure 16) of all compounds were prepared to investigate the crystal growth and magnetic properties of the Heusler thin film. This was necessary for evaluation and in order to understand the results of corresponding full junctions, which will be discussed later in this work.

[47] The position of the Fermi level E_F can be assumed roughly by the number of electrons.

Figure 16: Layer stacking of a half magnetic tunnel junctions with a bottom Heusler electrode.

film stoichiometry

Due to different sticking coefficients the film composition might be different to the target composition. However, the correct film composition is essential for the atomic ordering and a high spin polarization. Therefore, sputtered layers of all Heusler compounds were analyzed by inductively coupled plasma optical emission spectrometry (ICP-OES) to verify the exact film composition. Here, the sputtered films of about 600 nm were deposited on GaAs wafers for Heusler compounds containing Si and on SiO_2 wafer for compounds without Si. A substrate size of about 30 mm x 30 mm was used to provide enough material to verify the film stoichiometry. The ICP analysis was realized by Currenta GmbH & Co. OHG. The obtained stoichiometries for different Heusler compounds are given in Table 1 as well as the corresponding target composition.

compound	target composition (at%)	film composition (at%)
Co_2MnAl	Co 2 Mn 1 Al 1	Co 2 Mn 0.957 Al 0.8
Co_2MnSi	Co 2 Mn 1.28 Si 1.29	Co 2 Mn 0.985 Si 0.968
Co_2FeAl	Co 2 Fe 1 Al 1	Co 2 Fe 0.98 Al 0.985
Co_2FeSi	Co 2 Fe 1 Si 1	Co 2 Fe 0.953 Si 0.925
$Co_2Mn_{0.5}Fe_{0.5}Si$	Co 2 Mn 0.5 Fe 0.5 Si 1	Co 2 Fe 0.473 Mn 0.383 Si 0.912

Table 1: comparison of used target compositions and the resulting film compositions

The best agreement of film stoichiometry and intended Heusler composition (X_2YZ) was found for Co_2FeAl and Co_2MnSi. The latter composition was investigated in earlier experiments, which allowed an adjustment of the target composition, with regard to an optimized film composition. These two compounds are the most promising. The required $L2_1$ structure might be formed. A high magnetic moment and high TMR ratios are expected, be-

cause off-stoichiometrical Heusler films might show a reduced moment and spin polarization.

crystalline growth

The crystalline growth properties of the different Heusler compounds were investigated by XRD, as previously discussed for Co_2MnSi. The optimized layer stack of a 5 nm MgO buffered 20 nm thick Heusler compound was deposited under the same conditions, as mentioned before on single crystalline MgO (001) substrates. The layers were covered with an additional MgO layer of 1.8 nm to prevent surface contaminations. All layers were ex-situ vacuum annealed for 1h at different temperatures.

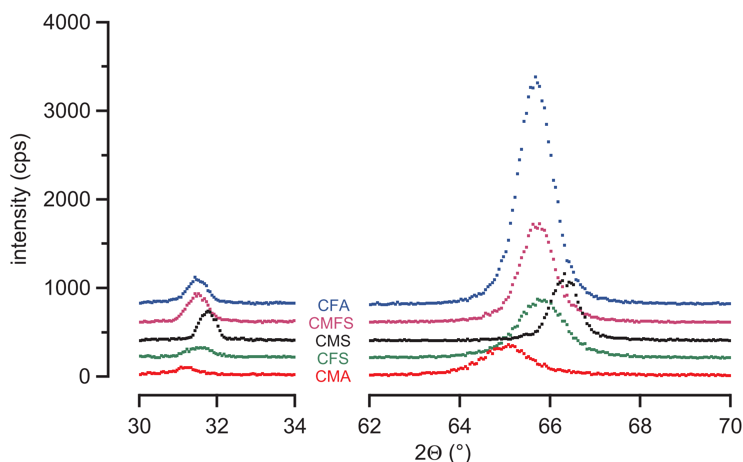

Figure 17: XRD pattern of the (002) and (004) peak of different Heusler compounds at 400°C annealing temperature. The layer stacking is: MgO(001) / MgO (5 nm) / Heusler (20 nm) / MgO (1.8 nm).

Figure 17 depicts the obtained Heusler (004) and (002) peaks for the 400°C samples, including the previously discussed Co_2MnSi. A shift in the maximum peak intensities for different compositions, which is attributed to a slightly different lattice constant, is clearly visible. The intensity of the peaks is correlated with layer thickness, on the one hand, and on the other hand with the amount of crystallinity. Here, the highest (004) peak can be found for Co_2FeAl and the highest (002) peak for Co_2MnSi respectively. But the indented (001) orientation is present for all investigated compounds.

Furthermore, Figure 18 shows the (004) peak net area as a function of annealing temperature. Except for Co_2MnSi, all compounds are crystalline prior annealing. For Co_2MnAl, the net area is nearly unaffected by annealing temperature within the investi-

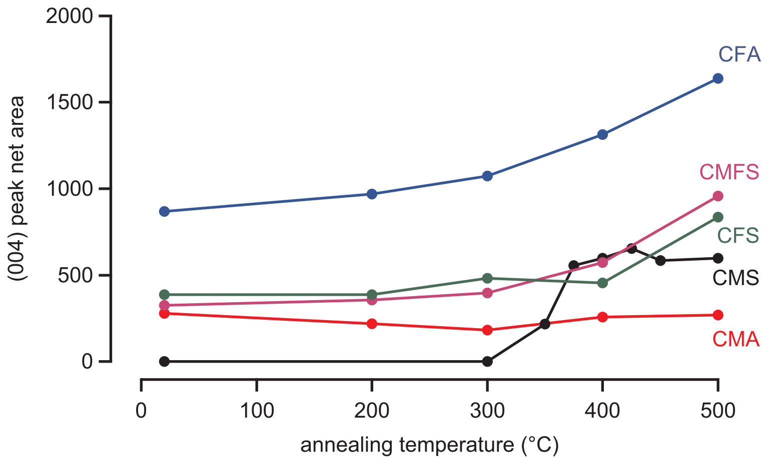

Figure 18: (004) peak net area of the different Heusler compounds for varying annealing temperatures.

gated range. For all other compounds, an increase of the Heusler (004) peak net area can be found for increasing annealing temperatures. This increase indicates a improved crystal growth. In contrast to the step like behavior of Co_2MnSi, the compounds Co_2FeAl and $Co_2Mn_{0.5}Fe_{0.5}Si$ show a continuos increase with annealing temperature. For Co_2FeSi, only high annealing at 500°C creates a crystallographic improvement.

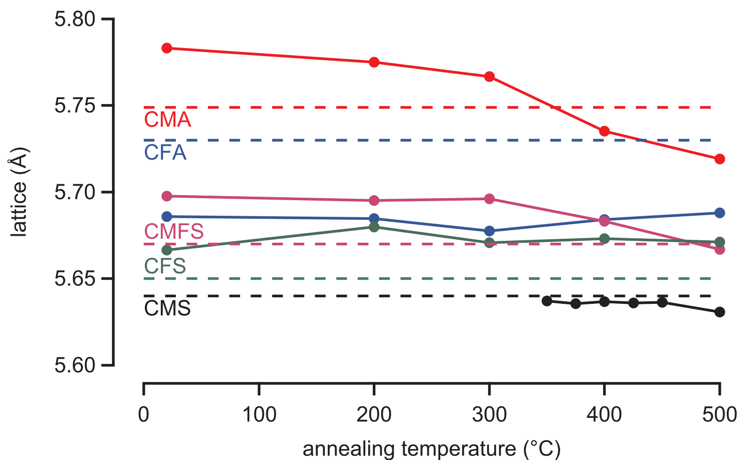

Figure 19: Lattice constant for all investigated Heusler compounds at different annealing temperatures. The dashed lines represent the reported bulk values.

Figure 19 represents the progression of the lattice constant for increasing annealing temperatures and different Heusler compounds. The dashed lines represent the particular predicted values found in literature (Co_2MnSi[48], Co_2MnAl and Co_2FeAl[49], Co_2FeSi[50], $Co_2Mn_{0.5}Fe_{0.5}Si$[51]). The lattice constant was obtained by applying the Bragg equation to the corresponding (002) and (004) peaks and averaging them. Therefore, the lattice constant re-

[48] U. Geiersbach et al., J Magn Magn Mater **240**, 546 (2002)

[49] K. Buschow et al., J Magn Magn Mater **38**, 1 (1983)

[50] S. Wurmehl et al., Phys. Rev. B **72**, 1 (2005)

[51] M. Kallmayer et al., J. Phys. D: Appl. Phys. **39**, 786 (2006)

flects only the out of plane component of the lattice. If not marked otherwise, a cubic lattice is assumed.

As shown in Figure 19 the lattice constants of the compounds Co_2MnSi, Co_2FeSi and Co_2FeAl are almost independent of annealing temperature. The lattice constant of Co_2MnSi measures up to the predicted value of 5.64 Å. For Co_2FeSi the values are slightly raised, when compared to the reference, probably due to the stoichiometrical disagreement. By contrast, the lattice of Co_2FeAl is clearly reduced. This might be due to a deformation of the lattice. The lattice of the neighboring top and bottom MgO growths 45 degrees rotated to the Heusler lattice. This results in a MgO buffer lattice size of $\sqrt{2}$ x $a_{MgO} = 5.95$ Å that might spread out the in plane lattice of the Heusler ($a_{Heusler} \approx 5.70$ Å) to get coherent interfaces. Assuming a constant volume of the Heusler cell this would reduce the measured out of plane lattice constant.

The strongest change in lattice constant can be detected for Co_2MnAl. Here, the lattice is larger than the reference value in the as prepared state and decreases with increasing annealing temperatures. For annealing temperatures of 400°C and above, the lattice constant drops clearly below the literature value. In the case of the quaternary compound $Co_2Mn_{0.5}Fe_{0.5}Si$, the experimental lattice is slightly higher than the reported reference for annealing temperatures to 300°C. For higher temperatures the lattice decreases and measures up to the reference for the 500°C annealed sample.

To determine the crystallographic Heusler structure, pole figure scans have to be performed, as discussed previously. But another approach would be to use the obtained diffraction peaks. In the case of e.g., an fcc cell, the centered atoms cause an additional reflection plane at the half distance. This can make some peaks vanish by destructive interference. To estimate the allowed peaks of an XRD pattern one has to consider the internal structure of the unit cell. The total intensity I_{hkl} that is registered by the detector is directly proportional to the squares of the crystallographic structure factor F_{hkl}.[52]

[52] Powder Diffraction: The Rietveld Method and the Two-Stage Method, G. Will, Springer Verlag (2006)

$$I_{hkl} \propto |F_{hkl}|^2 \tag{5}$$

The structure factor F_{hkl} is a complex quantity which is given by:

$$F_{hkl} = \sum_{k=1}^{N} f_k \exp(2\pi i(hu_k + kv_k + lw_k)) \tag{6}$$

with f_k, the atomic scattering factor of the different atoms k, (hkl) the Miller indices and u_k, v_k and w_k, the relativ positions of the atoms in the unit cell. N is the corresponding number of atoms within in the unit cell.

In the case of a full[53] Heusler compound, three different types of reflection can be identified from the four interpenetrating fcc lattices. Planes (hkl) with all even Miller indices or all odd indices lead to a non-vanishing reflected intensity. The even indices can further be distinguished into even and odd ratios of $(hkl)/2$. Therefore, the following peaks can be connected to the corresponding structure factors, which represent the crystallographic type of structure.[54]

[53] A half or a full Heusler compound are given by a XYZ or a X_2YZ composition, respectively.

[54] S. Kämmerer, PhD thesis, Bielefeld University (2004)

all odd (hkl) peaks represent the presence of a $L2_1$ structure (e.g. (111), (113), (133), (333), ...) and the structure factor is given by: $|F_{hkl}|^2 = 16\left[(f_A - f_C)^2 + (f_B - f_D)^2\right]$ with $h + k + l = (2n + 1)$

all odd (hkl)/2 peaks represent the presence of a $B2$ structure (e.g. (002), (222), (024), (006), ...) and the structure factor is given by: $|F_{hkl}|^2 = 16\left[(f_A + f_C) - (f_B + f_D)\right]^2$ with $h + k + l = 2(2n - 1)$

all even (hkl)/2 peaks represent the presence of a $A2$ structure (e.g. (022), (004), (224), (044), ...) and the structure factor is given by: $|F_{hkl}|^2 = 16\left[(f_A + f_B + f_C + f_D)\right]^2$ with $h + k + l = 4n$

However, the (004) peak is fundamental for the $A2$ type structure. Here, the Heusler atoms are randomly distributed in a bcc lattice. The existence of an additional (002) peak indicates a $B2$ type structure. Here, only the sub-lattices Y and Z of the compound X_2YZ are disordered. The proof of a $L2_1$ structure can be

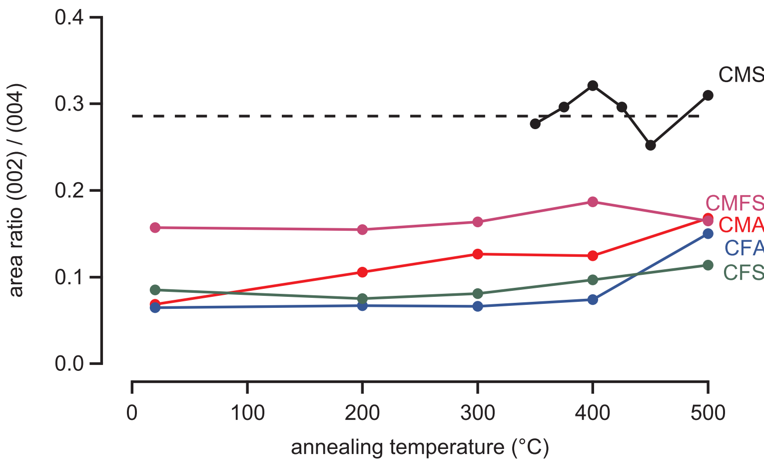

Figure 20: Calculated area ratio of the (002) to (004) peaks for the investigated Heusler compounds at different annealing temperatures.

given by detection of the (111) peak. An Euler cradle is required to realize these measurements. Alternatively, a comparison of the (002)/(004) peak ratio to powder diffraction data is often used as an indicator for the $L2_1$ structure.

The corresponding ratio for all investigated Heusler compounds as a function of annealing temperature is given in Figure 20. The dashed lines represent the predicted ratio, which hints to a $L2_1$ structure.[55] The best agreement can be found for Co_2MnSi. The required (111) peak to prove the $L2_1$ type structure could not be observed from the pole figure scans. But it was found in more detailed scans with higher resolution on similar samples that were annealed for 1h at 400°C.[56] For all other compounds, the ratio is clearly lowered and an absent $L2_1$ type structure can be assumed. In particular, no (111) peaks were found for the Co_2FeAl half junctions. However, the obtained (002) peaks for the different compounds indicate at least a $B2$ type structure.

[55] Reference Database, International Centre for Diffraction Data (1999)

[56] H. Wulfmeier, Diploma thesis, Bielefeld University (2010)

magnetic properties

In this section, the magnetic properties of the Heusler half junctions will be discussed in detail. The coercive field H_C as well as the bulk magnetization were determined by room temperature AGM measurements.

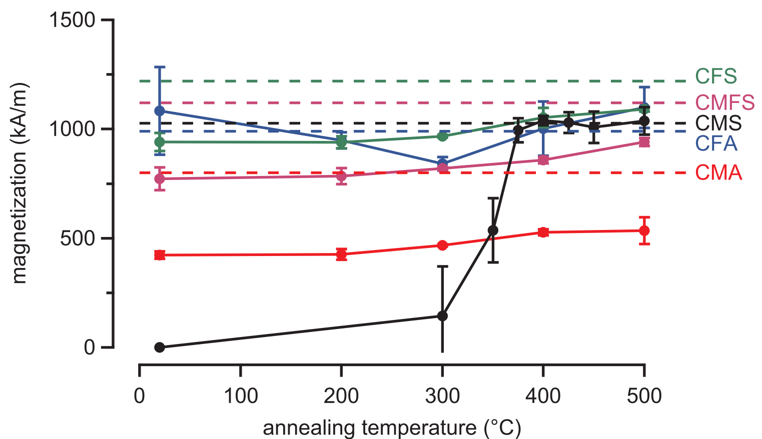

Figure 21: Magnetization of the Heusler compounds for different annealing temperatures. The dashed lines represent the values found in literature.

Figure 21 depicts the magnetization of the 20 nm thick Heusler layers for different annealing temperatures. The given values were obtained from averaging three measurements of similar half junctions. The error bars are given by the standard deviation. The theoretically predicted values of the magnetization, represented by

the dashed lines, were given by Galanakis for Co_2MnAl (800 kA/m), Co_2MnSi (1026 kA/m) and Co_2FeAl (1007 kA/m).[57] The corresponding values for Co_2FeSi (1219 kA/m) and $Co_2Mn_{0.5}Fe_{0.5}Si$ (1120 kA/m) were reported by Wurmehl[58] and Balke[59] respectively. To calculate the magnetic moment in μ_B or the magnetization in kA/m, the experimental values of the lattice parameter were used. An ideal $L2_1$ type structure was assumed in all cases. The step like progression of the Co_2MnSi magnetization has already been discussed privously. By contrast, all other investigated compounds show a magnetic behavior, even for the non annealed sample, which can be attributed to the crystal structure in the as prepared state.

[57] I. Galanakis, Phys. Rev. B **71**, 1 (2005)

[58] S. Wurmehl et al., Phys. Rev. B **72**, 1 (2005)

[59] B. Balke et al., Phys. Rev. B **74**, 1 (2006)

For Co_2FeAl the reported bulk value of 4.99 μ_B is reached almost independently of annealing temperature.

The magnetization of Co_2FeSi increases slightly with increasing annealing temperature, which indicates an improved atomic ordering. A maximum value of 1090 kA/m can be achieved for 500°C. This value is higher, when compared to similar (011) textured Co_2FeSi films.[60] Here, we reached a maximum of 901 kA/m at 400°C. Further annealing decreased the magnetization, probably due to diffusion of the V seed layer.

[60] D. Ebke et al., Appl Phys Lett **89**, 162506 (2006)

A similar behavior is present for the quaternary compound $Co_2Mn_{0.5}Fe_{0.5}Si$. Here, a maximum magnetization of 941 kA/m can also be reached for 500°C. This value is almost identical to the previously reported, for (011) textured $Co_2Mn_{0.5}Fe_{0.5}Si$ half junctions[61], but the value is only about 84% of the reported bulk value. This result is probably related to the strong deviation in the film stoichiometrie.

[61] D. Ebke et al., phys. stat. sol. (a) **205**, 2298 (2008)

The lowest magnetization of all investigated compounds is present for Co_2MnAl. As previously found in the XRD measurements, the values are nearly independent of annealing temperature and a maximum of 535 kA/m can be reached at 500°C. This is less than 70% of the corresponding predicted bulk value and can probably be attributed to the disagreement of the film stoi-

compound	maximum magnetization (kA/m)	maximum magnetic moment (μ_B)	ratio of predicted value
Co_2MnAl	535	2.70	0.68
Co_2MnSi	1039	5.02	1.00
Co_2FeAl	1099	5.45	1.09
Co_2FeSi	1090	5.36	0.89
$Co_2Mn_{0.5}Fe_{0.5}Si$	941	4.62	0.84

Table 2: Achieved maximum magnetization and corresponding magnetic moment in μ_B in comparison with the reported bulk values for all investigated Heusler compounds.

chiometrie, which might lead to a disordered Heusler layer.

The effect of the overestimated thickness in case of the Co_2MnSi layer has not been taken into account for the other investigated Heusler compounds. These compounds are already crystalline in the as prepared state and the assumed deposition rates yield the intended layer thickness.

The achieved maximum values of magnetization for the different Heusler compounds are summarized in Table 2 as well as the corresponding magnetic moments in μ_B. As mentioned above, the experimental lattice constants and a $L2_1$ structure were assumed for the calculation.

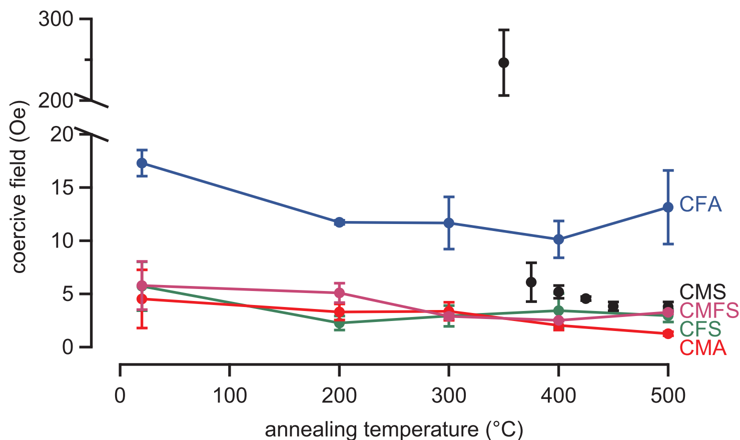

Figure 22: Coercive field H_C of the investigated Heusler compounds for varying annealing temperatures.

In Figure 22, the coercive field is given as a function of annealing temperature. With the exception of Co_2MnSi, the soft magnetic character of the Heusler compounds with the coercive fields below 20 Oe can be found in all cases. As previously described, a high H_C can be detected for Co_2MnSi in the annealing temperature range of the crystallization process. For annealing temperatures higher than 375°C, it drops clearly below 10 Oe. Apart from this drop, the H_C of Co_2FeSi, Co_2MnAl and $Co_2Mn_{0.5}Fe_{0.5}Si$ is about 5 Oe for all annealing temperatures. The coercive field of Co_2FeAl is about two times.

Beside the discussed bulk magnetic moment, the properties at the barrier interface are very important. These interfacial atoms determine the tunneling current. Therefore, the element specific magnetic moment of the Heusler layers, at the barrier interface, were examined as a function of annealing temperature by X-ray absorption spectroscopy (XAS) and X-ray magnetic circular dichroism (XMCD) respectively. The measurements were

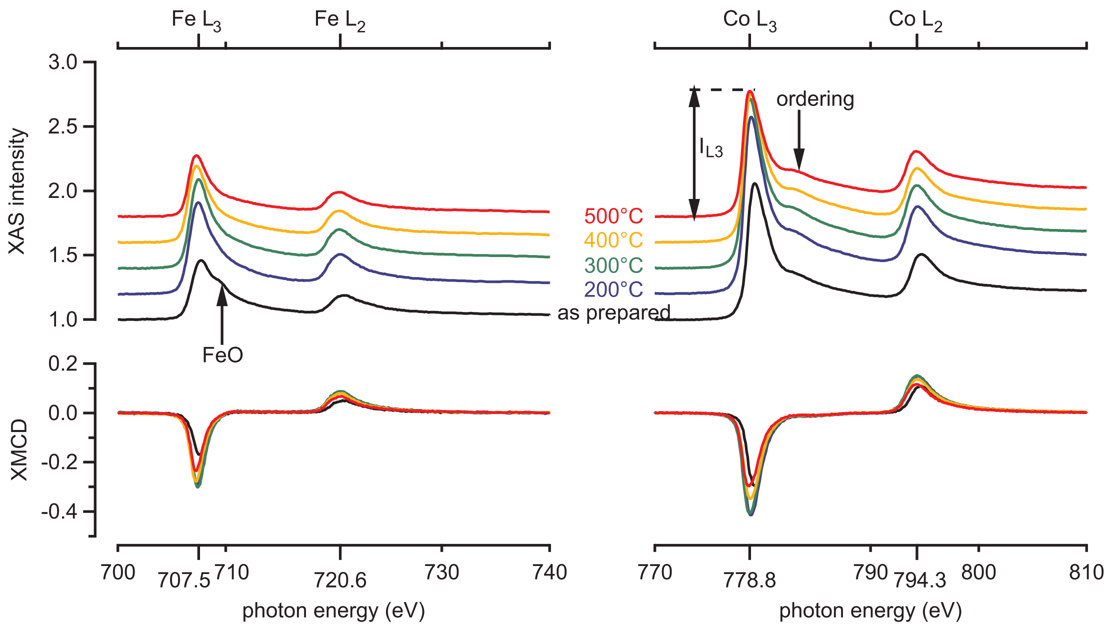

Figure 23: Room temperature XAS (top) and XMCD (bottom) spectra at the $Fe - L_{3,2}$ and $Co - L_{3,2}$ edge, respectively for different annealing temperatures of the Heusler compound Co_2FeAl. The XAS intensities were normalized to the values prior to the L3 edge. For comparison, the baseline of the measurement is shifted in regard to the annealing temperature. The arrows mark prominent XAS features.

performed at beamline 6.3.1 of the Advanced Light Source of the Lawrence Berkeley Laboratory at Berkeley, California, USA. The Co-, Mn- and Fe-$L_{3,2}$ edges were investigated. Surface sensitive total electron yield (TEY) was recorded with a grazing angle of incidence φ of 30 degrees to the sample surface. The XMCD spectra were obtained by applying a magnetic field of up to $\pm 2\,\mathrm{T}$ along the x-ray beam direction, using elliptically polarized radiation with a polarization P of 60%. The XAS intensity and the XMCD effect are defined as $(I_+ + I_-)/2$ and $I_+ - I_-$, respectively. Here, I_+ and I_- name the intensity, measured with parallel/antiparallel orientation of the photon spin to the magnetic field. The measurements were achieved at room temperature with a sampling depth of about 2 nm.[62]

[62] R. Nakajima et al., Phys. Rev. B **59**, 6421 (1999); and Y. Idzerda et al., Nuclear Instruments and Methods in Physics Research-Section A Only **347**, 134 (1994)

The obtained spectra of the investigated Heusler compound Co_2FeAl will be discussed in detail, followed by a discussion of the results for Co_2FeSi, Co_2MnSi and $Co_2Mn_{0.5}Fe_{0.5}Si$. The corresponding spectra of these compounds can be found in the appendix. For Co_2MnAl, no XAS data are available at the present time.

Figure 23 shows the Fe- and Co-XAS (top) and XMCD (bottom) spectra for the as prepared and annealed Co_2FeAl half junctions.

The measured XAS intensity was normalized to the intensity prior to the Fe-L_3 and Co-L_3 edge, respectively. The arrows indicate prominent features in the XAS. In the case of Co, the shoulder at about 4 eV above the L_3 edge, can be attributed to a certain atomic and magnetic order of the Co_2FeAl compound at the barrier interface, as previously reported for Co_2MnSi.[63] This feature is already present for the non-annealed sample and becomes pronounced with increasing annealing temperatures. The corresponding Co spectra of Co_2FeSi, Co_2MnSi and $Co_2Mn_{0.5}Fe_{0.5}Si$ (see appendix) also show a typical metallic behavior for all annealing temperatures. We found a certain atomic ordering, represented by the shoulder at about 780 eV, for $Co_2Mn_{0.5}Fe_{0.5}Si$ already in the as prepared state. This shoulder becomes pronounced with increasing annealing temperatures. For Co_2FeSi, the shoulder is only present for the 500°C sample. In case of Co_2MnSi it is present for 375°C and becomes pronounced with increasing annealing temperatures. This is in good agreement with the obtained results from XRD investigations. For the 500°C sample, this feature disappears again, probably due to oxidation.

[63] J. Schmalhorst et al., Phys. Rev. B **70**, 1 (2004)

The shoulder at about 2 eV above the L_3 edge of the Fe-XAS (Figure 23) and the non-annealed Co_2FeAl layer is attributed to FeO.[64] The Fe might be oxidized during the sputtering of the MgO barrier. For annealing temperatures higher than 200°C, no FeO can be found. The absence might be explained by the crystallization process of the barrier and the binding of O. The Fe spectra, of the 200°C and 300°C Co_2FeSi samples, also show the fingerprint of oxidized Fe. For the as prepared and higher annealed layers, a metallic Fe spectra is present. This also obtains for the Fe atoms at the barrier interface of the $Co_2Mn_{0.5}Fe_{0.5}Si$ layers. Here, we found a metallic behavior for all annealing temperatures. By contrast, the associated Mn spectra show the typical multiplet structure of MnO for the whole investigated range of annealing temperatures.[65] Most likely, the Mn prevents the oxidation of Fe because of a higher oxygen affinity. We had previously found a similar behavior for (011) textured $Co_2Mn_{0.5}Fe_{0.5}Si$ half junctions.[66] The same multiplet structure is also present in the Mn-XAS of Co_2MnSi which indicates an oxidation of the Mn atoms[67] for all temperatures, except the range of 375°C to 425°C. Here, the Mn spectra show metallic behavior.

[64] T. J. Regan et al., Phys. Rev. B **64**, 1 (2001)

[65] B. Thole et al., Phys. Rev. B **31**, 6856 (1985)

[66] D. Ebke, Diploma thesis, Bielefeld University (2007)

[67] B. Thole et al., Phys. Rev. B **31**, 6856 (1985); and J. Schmalhorst et al., Phys. Rev. B **70**, 1 (2004)

The Fe- and Co-XMCD of Co_2FeAl in Figure 23 (bottom) show an asymmetry for all annealing temperatures, i.e., a magnetic interface moment can be achieved even for the non-annealed Heusler

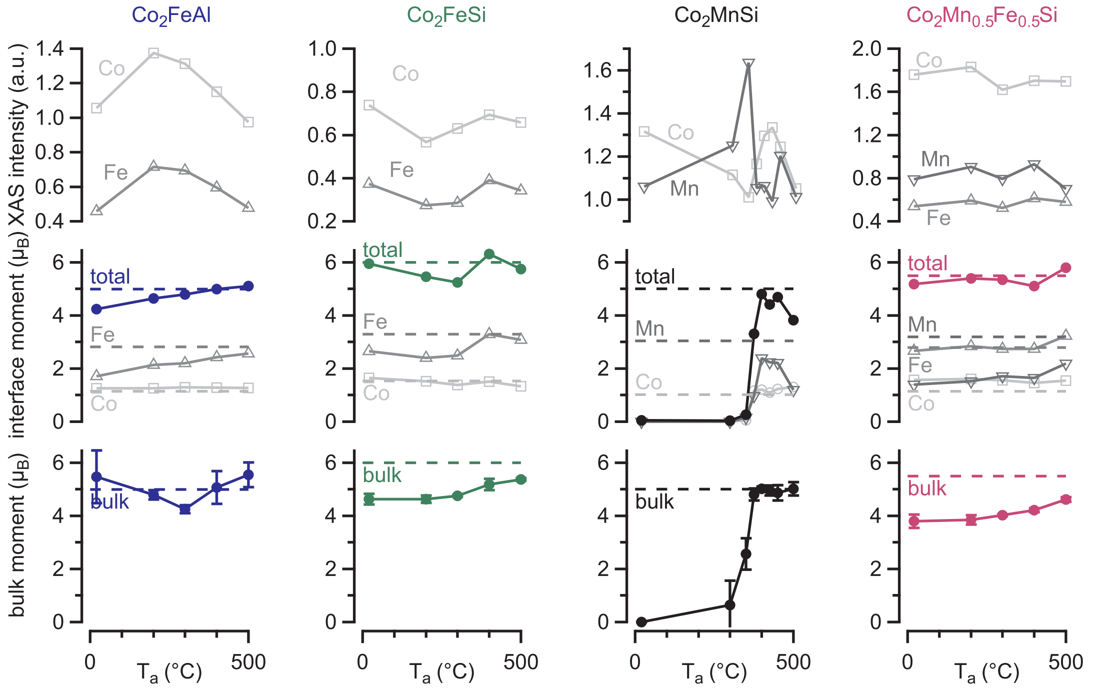

Figure 24: Top: room temperature XAS intensity at the L3 edge of Co, Fe and Mn of MgO/Heusler/MgO layers as a function of annealing temperature. Middle: element specific moment (orbital + spin) of the barrier interface and the corresponding total moment ($2 \times m_{Co} + m_X, X = Fe, Mn$). Bottom: bulk moment of the Heusler layer.

layer. As expected from the AGM investigations, an asymmetry is also present in the Co_2FeSi and $Co_2Mn_{0.5}Fe_{0.5}Si$ spectra (see appendix) for all annealing temperatures. By contrast, an XMCD effect for the Co_2MnSi layers can only be observed for temperatures higher than 350°C. In the case of Mn the effect is again reduced for the 500°C sample. This might be attributed to the formation of Mn_xSi_yO.[68]

[68] A. Hütten et al., Journal of Alloys and Compounds **423**, 148 (2006)

Figure 24 (top) shows the Fe- and Co-XAS intensity at the L3 edge (IL3, as defined in Figure 23) as a function of annealing temperature. At annealing temperatures higher than 200°C, the XAS intensity decreases for Co and Fe respectively. This might be due to an Al segregation toward the barrier interface, to improve the Heusler structure. In contrast to the progression found for Co_2FeAl, a roughly constant level can be found for the Co and Fe intensities of Co_2FeSi, and the Co, Mn and Fe intensities of $Co_2Mn_{0.5}Fe_{0.5}Si$. This indicates that a strong change in the atomic structure is not present in the investigated range of annealing temperatures. This observation is in contrast to our previously investigated V buffered (011) textured $Co_2Mn_{0.5}Fe_{0.5}Si$ half junctions. Here, we found a strong Mn diffusion toward the barrier interface for annealing temperatures higher than 400°C.[69]

[69] D. Ebke et al., phys. stat. sol. (a) **205**, 2298 (2008)

In the case of Co_2MnSi, an opposite behavior of the Co I_{L_3} curve and the Mn I_{L_3} curve was present. This behavior indicates a strong structural change at the barrier interface with varying annealing temperatures. For annealing temperatures of 375°C to 425°C, we found a maximum of Co- and a minimum of Mn-intensity. For these temperatures we found a fingerprint of metallic Mn. Most likely the Co atoms at the interface prevent the Mn atoms from oxidation. For the 500°C sample the Co- as well as the Mn-intensity at the L_3 edge drops, probably due to Si diffusion toward the barrier interface and the formation of Mn_xSi_y-oxides, as reported for similar junctions.[70]

[70] A. Hütten et al., Journal of Alloys and Compounds **423**, 148 (2006)

The element specific magnetic moment can be calculated from the XAS and XMCD by applying the sum rules.[71] The integrals r, p and q of the spectra are defined as:

[71] C. Chen et al., Phys. Rev. Lett. **75**, 152 (1995)

$$p = \int_{L_3} (I^+ - I^-) dE \quad (7)$$

$$q = \int_{L_3+L_2} (I^+ - I^-) dE \quad (8)$$

$$r = \int_{L_3+L_2} \left(\frac{I^+ + I^-}{2} - f \right) dE \quad (9)$$

The function f is a two-step function. The threshold is set to the peak positions of the L_3 and L_2 absorption edges and the relative step height is set to $2/3$ and $1/3$ respectively, of the average intensity above the L_2 edge.

The corresponding orbital and spin magnetic moment can be determined by:

$$m_{orb} = -\frac{1}{P\cos\varphi} \frac{4q}{6r} n_d \quad (10)$$

$$m_{spin} = -\frac{1}{P\cos\varphi} \frac{(6p - 4q)}{2r} n_d \quad (11)$$

The polarization P and the angle of incidence φ are set as listed above. The number of 3d holes are given in Table 3. These were carried out from SPR-KKR band structure calculations.[72]

[72] http://olymp.cup.uni-muenchen.de/ak/ebert/SPRKKR/

The resulting element specific magnetic moments (orbital + spin) are depicted in Figure 24 (middle). The total moment was determined by $2 \times m_{Co} + m_X, (X = Fe, Mn)$.

compound	$n_d(Co)$	$n_d(Fe)$	$n_d(Mn)$
Co_2FeAl	1.93	3.29	-
Co_2FeSi	2.28	3.48	-
Co_2MnSi	2.24	-	4.52
$Co_2Mn_{0.5}Fe_{0.5}Si$	2.33	3.39	4.44

Table 3: Assumed number of 3d holes for the investigated Heusler compounds. The values were determined by SPR-KKR band structure calculations.

For Co_2FeAl and Co_2FeSi, the magnetic moment of the Co atoms measure up to the predicted value of $1.14\mu_B$ and $1.54\mu_B$[73], respectively, for the full range of annealing temperature. The reference values are represented by the dashed lines. For Co_2MnSi, a Co interface moment is present for annealing temperatures of 375°C and above. The values measure up to the predicted value found in literature, as well.[74] By contrast, the Co interface moment of $Co_2Mn_{0.5}Fe_{0.5}Si$ is higher than the predicted value of $1.15\mu_B$.[75] The interface moment stays almost constant for all annealing temperatures. The Co moment fits very well with the theoretical values of the above discussed compositions. Therefore, an overestimated number of 3d holes, because of a deviating composition, can be assumed for $Co_2Mn_{0.5}Fe_{0.5}Si$.

[73] I. Galanakis, Phys. Rev. B **71**, 1 (2005); and S. Wurmehl et al., Phys. Rev. B **72**, 1 (2005)

[74] I. Galanakis, Phys. Rev. B **71**, 1 (2005)

[75] B. Balke et al., Phys. Rev. B **74**, 1 (2006)

The Fe magnetic moment in Co_2FeAl increases with increasing annealing temperatures and is close to the predicted value of $2.81\mu_B$ for the 500°C annealed sample.[76] This is most likely due to the reduction of FeO. A similar behavior was found for the total moment resulting from 2 x $m_{Co} + m_{Fe}$. The predicted bulk value of $4.99\mu_B$ can be reached for annealing temperatures higher than 400°C. In Co_2FeSi, the Fe moment is reduced for annealing temperatures below 300°C and fits with the predicted value of $3.3\mu_B$ for 400°C and above.[77] This can be explained by the previously discussed presence of FeO for these temperatures. A similar behavior can be found for the total interface moment $(2 \times m_{Co} + m_{Fe})$, which measures up to the predicted value of $6\mu_B$.[78]

[76] I. Galanakis, Phys. Rev. B **71**, 1 (2005)

[77] S. Wurmehl et al., Phys. Rev. B **72**, 1 (2005)

[78] S. Wurmehl et al., Phys. Rev. B **72**, 1 (2005)

A reduced interface moment, because of oxidation, can also be found for the Mn containing compounds. We found an optimal temperature for Co_2MnSi, with respect to a high Mn interface moment, to be in the range of 400°C to 450°C. Here, we found a metallic fingerprint in the XAS of Mn. The total interface moment given by $2 \times m_{Co} + m_{Mn}$ is in its maximum and reaches the predicted value of about $5\mu_B$.[79] The reduced Mn- and total interface moments below this temperature, and for the 500°C sample, are attributed to the oxidation of Mn atoms. As expected from previously discussed AGM investigations, we found no interface

[79] I. Galanakis, Phys. Rev. B **71**, 1 (2005)

moment for the amorphous Co_2MnSi layer below 350°C.

The Mn moment at the $Co_2Mn_{0.5}Fe_{0.5}Si$ interface is strongly reduced, when compared to the reported value of $3.19\mu_B$. Most likely this is because of the strong presence of MnO for all annealing temperatures, which we can conclude from the XAS. A slight increase of the interface moment is present only for the 500°C sample. By contrast, the achieved Fe moment measures up to the predicted value of $2.79\mu_B$. Here, we found a metallic fingerprint in the Fe-XAS for all temperatures.

Due to the roughly constant level of the Co moments of the various Heusler layers, the total interface moments are mostly determined by the Fe or/and Mn moments. For Co_2FeAl and Co_2FeSi, the predicted values can be reached for annealing temperatures higher 400°C.

However, the resulting total moment given by $2m_{Co}+ ½m_{Mn}+ ½m_{Fe}$ fits with the predicted value of $5.5\mu_B$. Here, the strongly reduced Mn moment was compensated by the probably overestimated Co moment. The overestimation might issue from a deviation in the atomic concentration of the films.

For a better comparison, the previously discussed bulk moments of the Heusler half junctions are also shown in Figure 24 (bottom). We found an almost identical progression of bulk and total interface moment for Co_2FeSi, Co_2MnSi and $Co_2Mn_{0.5}Fe_{0.5}Si$. The predicted interface moments were reached but the bulk moment of Co_2FeSi and $Co_2Mn_{0.5}Fe_{0.5}Si$ were lowered. The deviation can be explained by the assumed number of $3d$-holes, which might be different for the found film stoichiometries. Therefore, an overestimated interface moment can be assumed for the latter two compounds. For Co_2MnSi we observed nearly the same values of interface and bulk moment. The lowered interface moment of the 500°C Co_2MnSi sample, in comparison to the bulk moment, confirms the presence of MnO at the barrier interface. The roughly constant bulk moments of the Co_2FeAl layers, are in contrast with the total interface moment, which increases with increasing temperatures. This can be explained by the detected oxidized Fe at the barrier interface, which was formed during the deposition of MgO.

In summary, we have investigated the interfacial magnetic moments of the compounds Co_2FeAl, Co_2FeSi, Co_2MnSi and $Co_2Mn_{0.5}Fe_{0.5}Si$ for different annealing temperatures. We found

an oxidation of Mn atoms for all Mn containing compounds, which led to a reduced interface magnetic moment. We found, for only a small annealing temperature range of (400°C - 450°C), a fingerprint of metallic Mn in the XAS of Co_2MnSi. This might indicate an atomically ordered Heusler for these temperatures.

By contrast, the obtained Fe-XAS spectra mostly show a fingerprint of metallic Fe. Remarkably we found no oxidized Fe in the higher annealed Fe containing Heusler compounds. The predicted interfacial Fe moment was reached. A direct comparison of the Fe- and Mn-XAS, in the case of the quaternary compound $Co_2Mn_{0.5}Fe_{0.5}Si$ leads to the assumption that the Mn atoms oxidize more easily and can hinder the Fe from oxidation.

The investigated Co-XAS spectra are very similar for all compounds. A shoulder, located at about 4 eV above the Co L_3 edge, can be found for all samples. It is faintly present, even for the non-annealed samples (Co_2FeAl and $Co_2Mn_{0.5}Fe_{0.5}Si$), and becomes pronounced with increasing annealing temperatures. This feature indicates a certain atomic ordering. It is reported by Tsunegi[80] that this feature is correlated to the $L2_1$ structure of the Heusler compound. But we observed a $L2_1$ structure only in Co_2MnSi half junctions.

[80] S. Tsunegi et al., J. Phys. D: Appl. Phys. (2009)

We found that neither Si nor Al prevents Fe from oxidation at low annealing temperatures. The XAS of Co_2FeSi and Co_2FeAl are very similar. But we deduce a connection of the found FeO and the atomic ordering, represented by the magnetic moment and the shoulder in the Co-XAS. A direct comparison of the results for Co_2FeAl and Co_2FeSi shows that oxidized Fe disappears at lower annealing temperatures (for Co_2FeAl). Correspondingly, the (004) peak net area increases (see XRD), the magnetic moment increases (see AGM) and the shoulder in the Co-XAS appears.

different compositions of Co-Fe-Si

One of the most promising Heusler compounds for spintronic applications is Co_2FeSi. In the class of Co-based Heusler compounds, it has the highest predicted magnetic moment of $6\,\mu_B$ and the highest Curie temperature of about $1100\,K$.[81] Furthermore, it is reported to be easily fabricated in $L2_1$ structure[82]. We can conclude from the XAS and XMCD measurements, that a Fe containing composition is preferred to Mn, due to the reduced formation of oxides at the interface which might reduce the spin polarization.

[81] S. Wurmehl et al., Phys. Rev. B **72**, 1 (2005)

[82] N. Tezuka et al., J. Appl. Phys. (2006)

DOS calculations of Heusler compounds (in particular Co_2MnSi) have shown that antisite defects might destroy the half metallicity due to additional states at the Fermi level.[83] Consequently, the composition of the Heusler is very important. The investigation of off-stoichiometrical films might help to reveal magnetic and crystallographic properties. Therefore, the influence of Heusler film composition was investigated. We used two additional Co-Fe-Si targets that resulted in a

[83] S. Picozzi et al., Phys. Rev. B **69**, 1 (2004)

- strongly Fe enriched film composition and a
- strongly Si enriched film composition.

The specific film compositions were determined by ICP-OES[84] and are given in Table 4.

[84] The measurements were performed by Currenta GmbH & Co. OHG

Table 4: Film compositions of the three different Co-Fe-Si targets verified by ICP analysis.

	target composition (at%)	film composition (at%)
balanced	Co 2 Fe 1 Si 1	Co 2 Fe 0.953 Si 0.925
Fe enriched	Co 2 Fe 1.43 Si 1.22	Co 2 Fe 1.313 Si 0.894
Si enriched	Co 2 Fe 1.09 Si 1.37	Co 2 Fe 1.019 Si 1.205

The off-stoichiometrically Heusler layers were investigated with regard to the crystal growth and magnetic properties. Half junctions, consisting of 20 nm of Co-Fe-Si and 1.8 nm of MgO, were deposited on 5 nm MgO buffered (001) MgO substrates.

Figure 25 depicts the obtained (002) and (004) XRD peaks at about 32 and 66 degrees, respectively, for the three different Co-Fe-Si compositions. The samples were annealed for 1h at 400°C. For the Si enriched film composition, both peaks nearly vanished. The crystallization was strongly reduced when compared to the

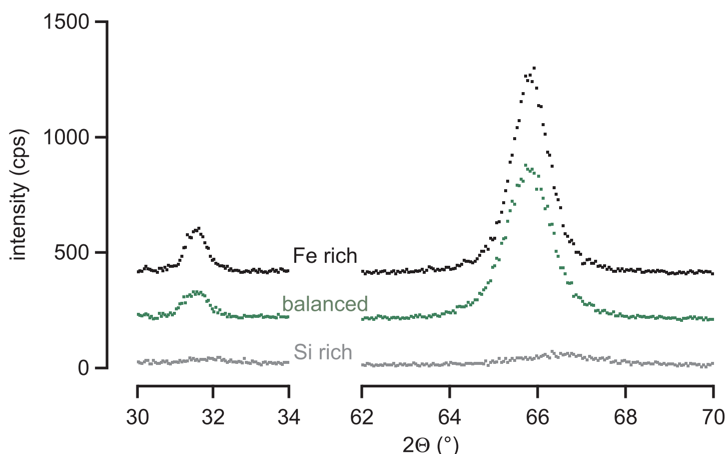

Figure 25: XRD pattern overview for three different Co_2FeSi compositions annealed at 400°C. The layer stacking is: MgO(001) / MgO (5nm) / Co_2FeSi (20nm) / MgO (1.8nm).

balanced and Fe enriched film composition. Nearly the same intensities with a similar peak shape were present for the latter two compositions. The (022) Heusler peak at about 45 degrees, could not be found in any case.

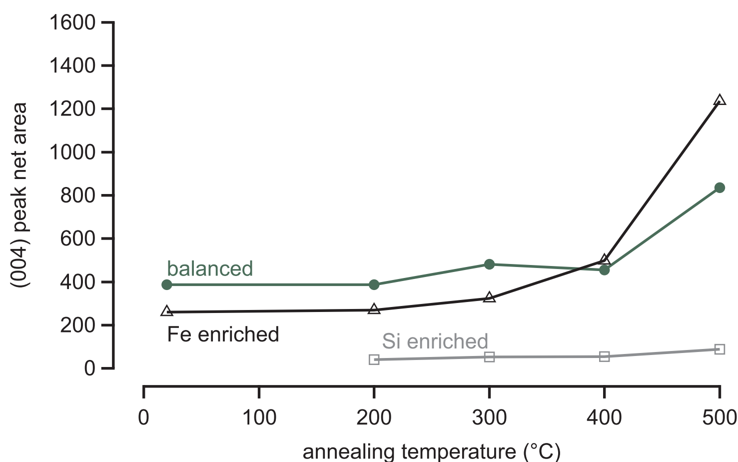

Figure 26: (004) peak net area for the different Co_2FeSi Heusler compounds at varying annealing temperatures.

In Figure 26 the particular (004) peak net area is shown as a function of annealing temperature. The Si enriched layer is amorphous in the as prepared state. With an increasing annealing temperature a slight increase of net area can be estimated but the achieved intensities are considerably lower when compared to all other investigated Heusler compounds. By contrast, the balanced and Fe enriched layers were already crystalline prior annealing. We detected an increasing net area with increasing annealing temperatures. The slope of the Fe enriched (004) peak net area was slightly

stronger when compared to the balanced film, which indicates an improved crystal growth without taking into account the present type of structure.

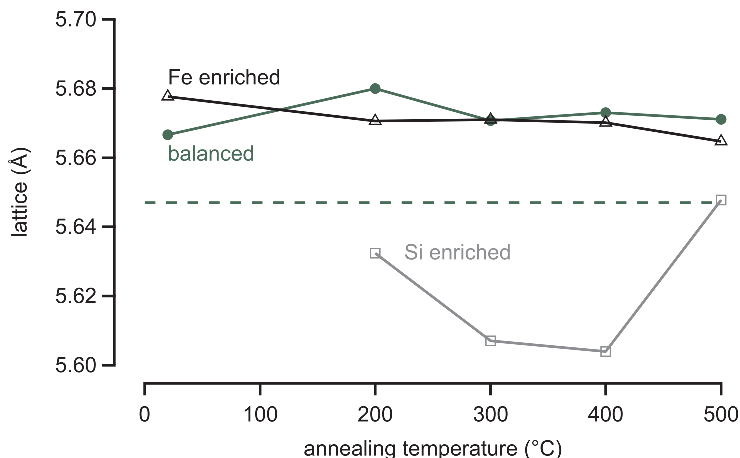

Figure 27: Lattice constant for the different Co_2FeSi Heusler compounds at varying annealing temperatures. The dashed line represents the reported bulk value.

The annealing temperature dependence of the out of plane lattice constant is illustrated in Figure 27. The balanced and Fe enriched layers show similar behavior. Both lattices are slightly higher than the reported bulk value[85] and keep almost constant for the whole range of annealing temperatures. The Fe enriched lattice faintly approaches the bulk value with increasing annealing temperatures. This is in contrast to the behavior of the Si enriched lattice constant. For annealing temperatures of 200°C and 500°C, the lattice constant is close to the bulk value. Apart from this, it is strongly reduced for the 300°C and 400°C annealed samples. This effect can be explained by a strong crystallographic change or distorted unit cell.

[85] S. Wurmehl et al., Phys. Rev. B **72**, 1 (2005)

To estimate the present type of crystal structure for the different compounds, the (002) and (004) peak ratios were calculated and are depicted in Figure 28 for different annealing temperatures. The dashed line represents the expected value for a $L2_1$ structure. The peak ratios of the balanced and Fe enriched Heusler layers are considerably lower and a $B2$ type structure can be assumed for these compounds. By contrast, the ratio of the Si enriched layer increases with increasing annealing temperature and measures up to the expected value for a $L2_1$ structure. As reported by Tezuka[86], it seems that Si can somehow provide the preferred $L2_1$ structure. But the found peak intensities leads to the assumption that a mostly amorphous film is present in the case of the Si enriched half junctions.

[86] N. Tezuka et al., J. Appl. Phys. **99**, 08T314 (2006)

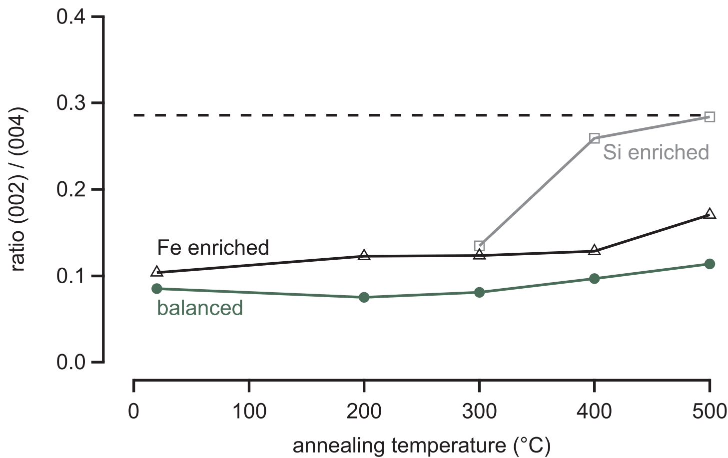

Figure 28: Ratio of (002)/(004) peak area for the different Co_2FeSi Heusler compounds at varying annealing temperatures. The dashed line represents predicted value of $L2_1$ structure?

However, the proof can only be determined by pole figure scans and the detection of the (111) Heusler peak. Due to the low peak intensities, the scans were skipped at this point but planed for higher annealed samples. Higher temperatures might lead to higher intensities and an improved crystal Heusler layer.

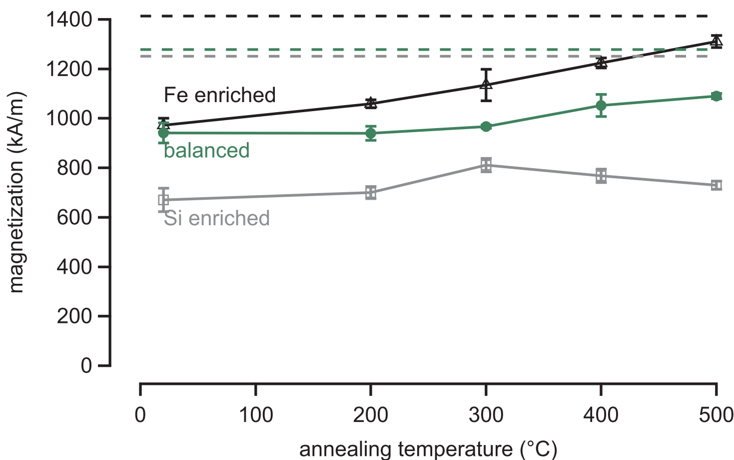

Figure 29: Magnetization of the different Co-Fe-Si compounds as a function of annealing temperature. The dashed lines represent the values found in literature.

We have performed room temperature AGM measurements to investigate the bulk magnetization and coercive field of the Co-Fe-Si compounds. The obtained results are given in Figure 29 for different annealing temperatures. The dashed lines represent the predicted bulk values, assuming $L2_1$ structure and the experimentally determined lattice constant. The predicted off-soichiometrically values were roughly estimated by taking the particular element specific moment of Co_2FeSi [87] and the obtained film stoichiometry.

[87] S. Wurmehl et al., Phys. Rev. B **72**, 1 (2005)

The achieved magnetization of the Fe enriched layers is similar to the balanced layer for the as prepared state. With increasing annealing temperatures a continuous slope is present and a maximum magnetization of 1310 kA/m can be reached for the 500°C annealed sample. Therefore, a higher magnetization when compared to the balanced Heusler layer is present, which might be attributed to the higher amount of Fe.

In contrast, we found a roughly constant magnetization of the Si enriched layers. A maximum magnetization of 811 kA/m is present for the 300°C annealed layers. This value is only about 60% of the estimated magnetization. Higher annealing resulted in a decrease of magnetization. In combination with the obtained XRD results this hints at a certain atomic disorder. A magnetic moment is already present in the as prepared state although the Si enriched Heusler layers were amorphous. This in contrast to the results we found for the Co_2MnSi half junctions.

Table 5: Magnetic moments for different Co-Fe-Si film stoichiometries. The experimental values of the lattice parameter were used to calculate the magnetic moment in μ_B.

compound	maximum magnetization (kA/m)	maximum magnetic moment (μ_B)	ratio of predicted value
balanced	1090	5.36	0.89
Fe enriched	1310	6.42	0.92
Si enriched	811	3.47	0.58

The achieved highest values are summarized in Table 5. The ideal $L2_1$ type structure and the experimental lattice constant were assumed to determine the corresponding magnetic moment in μ_B/f.u.

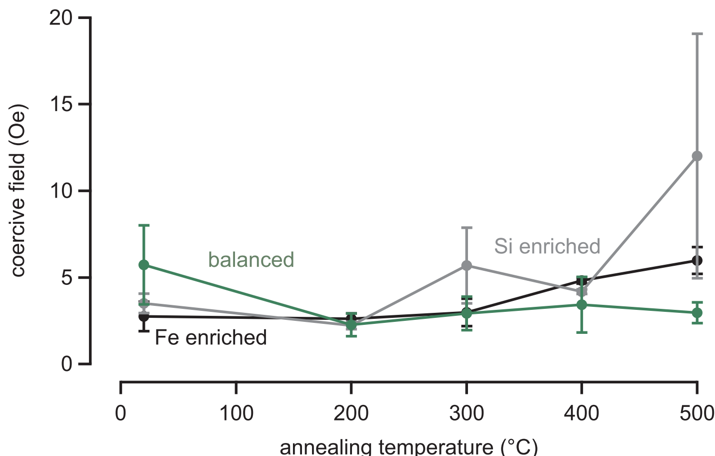

Figure 30: Coercive field of the different Co-Fe-Si compounds as a function of annealing temperature.

The corresponding coercive fields of the off-stoichiometrically Co-Fe-Si layers are depicted in Figure 30 as a function of annealing temperature and are compared to the achieved values of the balanced Co_2FeSi layers. A similar low H_C can be found for all annealing temperatures. In particular, the coercive field of the amorphous grown Si enriched layers is below 5 Oe, which contrasts with the achieved high H_C of the crystalizing Co_2MnSi. Only a slight increase is present for the 500°C annealed sample.

The element specific properties at the barrier interface were investigated by XAS and XMCD. The obtained spectra of the Fe- and Si-enriched Co-Fe-Si films can be found in the appendix. We found a fingerprint of metallic Fe in the XAS for both off stoichiometric compounds and all investigated annealing temperatures. This in contrast to the results we found previously for the balanced Co_2FeSi layers. The Co-XAS also show a metallic behavior for all annealing temperatures. We found a shoulder at about 4 eV above the L_3 edge for the 500°C samples, which can be attributed to a certain atomic and magnetic order.[88] For lower temperatures the shoulder is clearly weakened. As expected from the AGM measurements, a Fe- and Co-XMCD effect was achieved for all annealing temperatures.

[88] J. Schmalhorst et al., Phys. Rev. B **70**, 1 (2004)

The corresponding progression of the calculated interface moments, as well as the XAS intensities, are illustrated in Figure 31 (middle) and (top), respectively. For better comparison, the results of the previously discussed balanced Co_2FeSi are also given.

The Co-XAS intensities are almost constant for all annealing temperatures, except a dip at 300°C for the Si enriched sample. We also found a similar dip in the corresponding Fe-XAS, which might indicate a higher amount of Si at the barrier interface. However, we also observe a structural change from the XRD investigations at this temperature.

An increasing Fe-XAS intensity in connection with increasing temperatures can be assumed for the Fe enriched Heusler half junctions. Most likely, the containing smaller amount of Si forms the Heusler structure inside the layer and excessive Fe segregates at the barrier interface or rather the Si segregates into the layer. But compared to the priviously discussed XAS of the other compounds, especially to Co_2FeAl and Co_2MnSi, the changes were only in a small range.

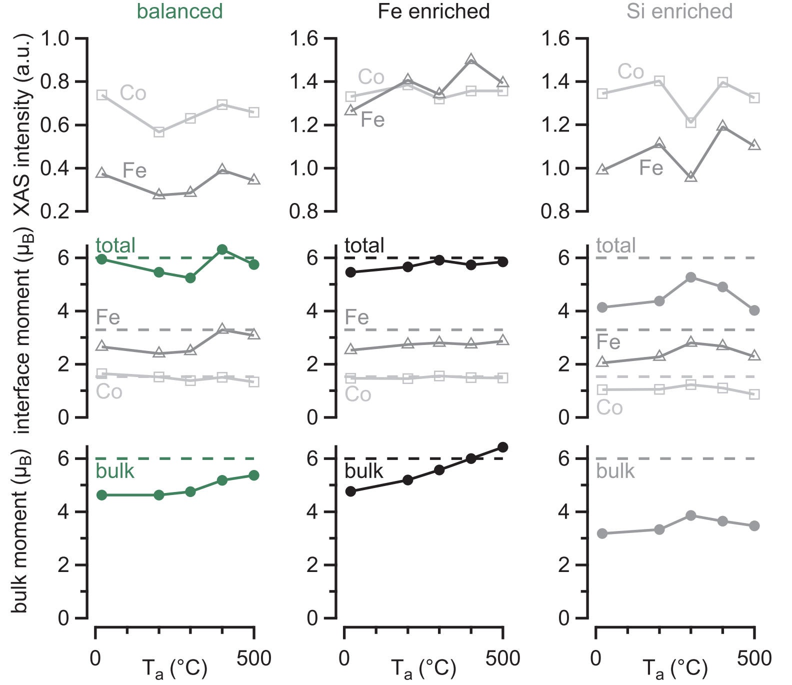

Figure 31: Top: room temperature XAS intensity at the L3 edge of Co and Fe of MgO/Co-Fe-Si/MgO layers as a function of annealing temperature. Middle: element specific moment (orbital + spin) of the barrier interface and the corresponding total moment ($2 \times m_{Co} + m_{Fe}$). Bottom: bulk moment of the Co-Fe-Si layer.

We have estimated the interface moments (Figure 31 (middle)) by applying the sum rules.[89] We have assumed the same number of 3d holes as previously for the balanced Co_2FeSi, that is to say, $n_d = 2.28$ for Co and $n_d = 3.48$ for Fe.

[89] C. Chen et al., Phys. Rev. Lett. **75**, 152 (1995)

For the Fe enriched layers, we found, that the magnetic interface moment of Co measured up to the predicted value of $1.54\mu_B$ for Co_2FeSi.[90] By contrast, the interface moment of Fe was lower than the predicted moment. A slight increase with increasing annealing temperature can be estimated. The total interface moment ($2 \times m_{Co} + m_{Fe}$) behaved similarly. The predicted value of Co_2FeSi was reached for temperatures higher 300°C. This is in contrast to the continuous increase of the bulk moment with increasing annealing temperatures, which we found previously in the AGM measurements.

[90] S. Wurmehl et al., Phys. Rev. B **72**, 1 (2005)

For the Si enriched layers, we found a maximum of about $5.2\mu_B$ for the total interface moment ($2 \times m_{Co} + m_{Fe}$) after annealing at 300°C. The Co, as well as the Fe interface moments are in their maximum. With regard to the obtained XAS, the highest moment can be found for the lowest Co and Fe absorption intensities. A higher amount of Si at the interface can be concluded.

We found the same behavior for the investigated bulk moment, as depicted in the bottom of Figure 31. The achieved lower values lead to the assumption that the estimated number of 3d holes

results in an overestimated interface moment. Nevertheless, the trend of the element specific moments are in good agreement with the obtained bulk values.

IN SUMMARY we have investigated two off-stoichiometrical Co-Fe-Si half junctions. With regard to crystal growth, the Fe enriched layers show comparable behavior, as previously found for the balanced Co_2FeSi films. By contrast, the Si enriched Co-Fe-Si layers are amorphous in the as prepared state and only a weak crystal structure can be obtained after annealing.

We found a similar behavior for the magnetization and (interface) magnetic moments. We observe increasing moments by increasing annealing temperatures for the Fe enriched layers. By contrast, the magnetization and interface moment of the Si enriched layers were reduced. We found both maxima for the 300°C annealed sample. No FeO was found in the XAS of the Fe enriched layers nor in the Si enriched layers which is in contrast to the balanced film.

We can conclude that the Heusler Co_2FeSi is considerably influenced by additional Si atoms, whereas added Fe led to an almost identical behavior when compared to the balanced compound.

Our results contrast with similar MgO/Cr buffered Co-Fe-Si half junctions that we deposited from identical targets. Apart from the Co-Fe-Si (004) and (002) peaks, we also detect a (022) peak in the XRD pattern. This leads to the assumption that a lower degree of (001) texture was present due to the buffer layer we used. Furthermore, a bulk magnetization of about only 800 kA/m could be achieved by AGM measurements, independent of target and annealing temperature. The observed corresponding high coercive fields of about $100 Oe$ leads us to expect a less ordered Heusler film.

Transport properties

The transport properties of full magnetic tunnel junctions with different Heusler compound electrodes were investigated and the results are discussed in this chapter. As shown in Figure 32, the full tunnel junctions contain the optimized lower 20 nm thick Heusler electrode on a 5 nm MgO buffered (001) MgO substrate. An MgO barrier thickness of 1.8 nm or 2.1 nm was used. The counter electrode was formed by a 5 nm Co-Fe layer that was pinned to a 10 nm antiferromagnetic Mn-Ir layer. For good conductance these layers were covered with a 40 nm Ru and 20 nm Au capping layer. The final junctions were subsequently ex-situ vacuum annealed for 1h to induce crystallization and ordering of the lower layer stack up to the Co-Fe electrode. The samples were cooled in a magnetic field of 0.65 T in order to set the exchange bias of the pinned electrode and were patterned, by optical lithography and ion beam etching, to junctions with a size of $7.5\,\mu m \times 7.5\,\mu m$, $12.5\,\mu m \times 12.5\,\mu m$ and $22.5\,\mu m \times 22.5\,\mu m$. The transport properties of the magnetic tunnel junctions were measured as a function of the magnetic field. All transport characterizations were carried out by conventional 2-terminal measurements. Except as noted otherwise, all measurements were done at room temperature. The applied bias voltage was 10 mV and the annealing time was 1 h.

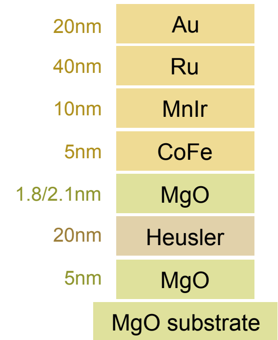

Figure 32: Layer stacking of the full tunnel junctions for all investigated different Heusler compounds.

annealing temperature stability

The resulting room temperature TMR ratios for the subsequently annealed full Heusler junctions are shown in Figure 33. An increasing TMR ratio with increasing annealing temperature, most likely due to an improvement of the crystallinity of the Heusler / tunnel barrier interface, was found in all cases. This is commonly found in conventional Co-Fe-B/MgO/Co-Fe-B MTJs, too.[91] The highest ratios of about 150% were achieved for Co_2FeAl junctions

[91] S. Ikeda et al., Appl Phys Lett **93**, 082508 (2008)

Figure 33: Achieved room temperature TMR ratios of full MTJs containing Co_2MnSi, Co_2FeSi, Co_2FeAl, Co_2MnAl and $Co_2Mn_{0.5}Fe_{0.5}Si$ at varying ex-situ annealing temperatures. The dashed lines represent a 1.8 nm thick MgO barrier, the solid 2.1 nm MgO, respectively. The squares and triangles indicate the two different subsequently annealed Co_2FeAl samples for the 1.8 nm thick MgO barrier.

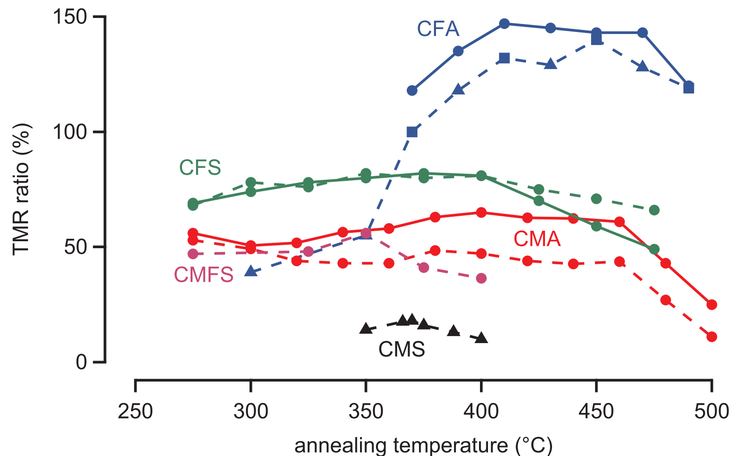

with a 2.1 nm MgO barrier that were annealed at 450°C. The junctions show good annealing temperature stability. The TMR ratio stays roughly constant for temperatures between 410°C and 470°C. This is in contrast to other studies where the Mn diffusion of the Mn-Ir, toward the upper barrier interface, was thought to be responsible for the decrease of the TMR ratio beyond 400°C.[92] On the other hand, similar behavior was reported by Kant and Palusker[93]

[92] J. Hayakawa et al., Appl Phys Lett **89**, 232510 (2006)

[93] P. V. Paluskar et al., J. Appl. Phys. **97**, 10C925 (2005); C. H. Kant et al., Appl Phys Lett **84**, 1141 (2004); and C. H. Kant et al., J Magn Magn Mater **286**, 154 (2005)

For the Co_2FeSi junctions, a maximum TMR ratio of about 80% can be found for annealing temperatures in the range of 350°C to 400°C. The differences between the 1.8 nm and 2.1 nm thick MgO barriers were small. Higher temperatures led to a decrease of the TMR. This decrease might be attributed to Mn diffusion towards the upper barrier interface. The decay is stronger for the thicker barrier.

The Co_2MnAl junctions show a nearly constant TMR ratio, on a low level of about 60%, with varying annealing temperatures. The ratios of the 2.1 nm thick barrier are higher than for the 1.8 nm thick MgO. A strong decay occured for temperatures higher than 460°C, and likewise for Co_2FeAl. The achieved TMR ratios are similar to the reported values of Oogane at el. for AlO_X based *B*2 ordered (001) Co_2MnAl junctions, but the annealing temperature stability is much better.[94]

[94] M. Oogane et al., J. Phys. D: Appl. Phys. **39**, 834 (2006)

The expected high TMR values of the quaternary compound $Co_2Mn_{0.5}Fe_{0.5}Si$, due to a shift of the Fermi level into the band gap, could not be found. Ratios of about 50% were achieved for the 350°C annealed junctions.

The lowest TMR ratios were achieved for Co_2MnSi although

it is a composition with reported high room temperature TMR values[95]. Here, the TMR ratios remain below 20%, whereas high magnetic bulk and interface moments were present. A slight maximum was found for an annealing temperature of 366°C. A phase change is present for this temperature region as we observed in the XRD pattern. Furthermore, the XAS showed a presence of oxidized Mn at the barrier interface. Higher annealing temperatures would improve the crystal structure. But higher temperatures also led to Mn diffusion toward the barrier interface which lowered the TMR ratios.

[95] S. Tsunegi et al., J. Phys. D: Appl. Phys. (2009)

In conclusion, compounds containing Fe lead to higher ratios than similar compounds containing Mn. Heuslers containing Al lead to higher TMR than Si. The TMR ratios of Si containing compounds are less stable against annealing than similar compounds containing Al. Here, a decay of the TMR is present for annealing temperatures above 470°C. Most likely, the Al containing compounds form larger grains at lower annealing temperatures in comparison with the Si containing compounds. Because grain boundary diffusion occurs much faster than bulk diffusion this seems to lead to more temperature stable TMR ratios.

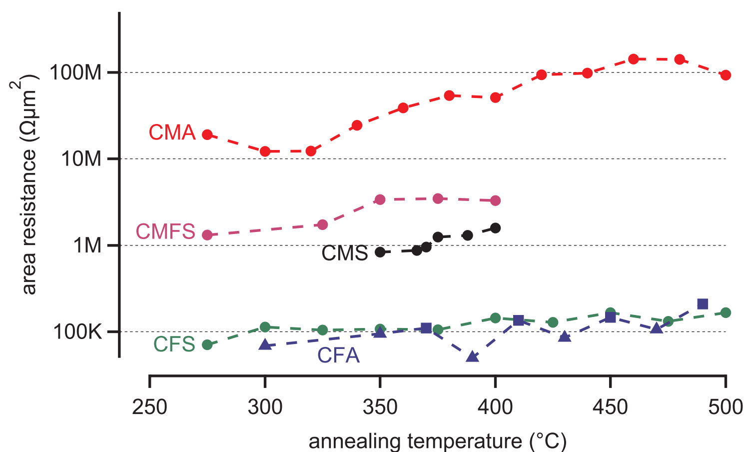

Figure 34: Area resistance (AR) of the Heusler full MTJs as a function of annealing temperature for a 1.8nm thick MgO barrier. The squares and triangles indicate the two different subsequently annealed Co_2FeAl samples.

The corresponding products of area resistance are given in Figure 34 for different Heusler electrodes and annealing temperatures. The MgO barrier thickness is 1.8 nm. The values are approximately 100 K$\Omega\mu$m^2 for Co_2FeSi and Co_2FeAl, and more than 100 M$\Omega\mu$m^2 for Co_2MnAl. An increase of resistance can be found for all compounds. This increase indicates an improvement of the barrier quality. In particular, no strong decay can be found which would indicate a break within the barrier or short cuts. The ob-

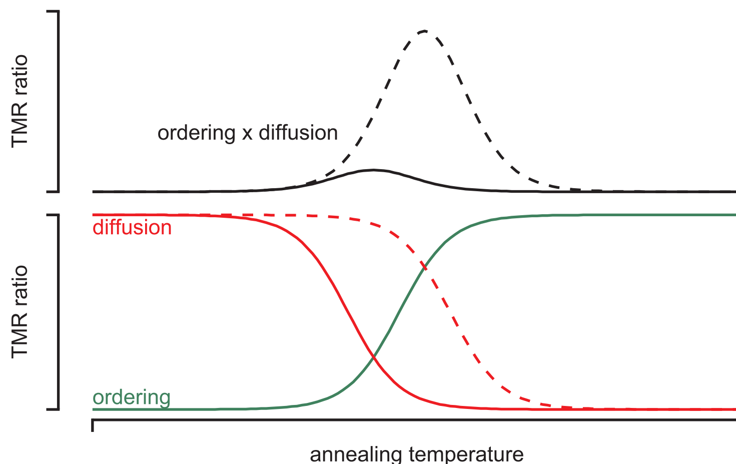

Figure 35: Bottom: model for influence of atomic ordering and diffusion to the obtained low TMR value in the case of Co_2MnSi. A shift (dashed line) of the diffusion process to higher annealing temperatures would increase the TMR, which can be estimated by the product (top) of ordering and diffusion.

tained higher resistant for Mn containing compounds can be explained by an additional thin insulating MnO layer, at the lower barrier interface.

The low TMR ratio of Co_2MnSi can be explained by the following model: The crystallization process of Co_2MnSi is in the annealing temperature range of 350°C to 400°C. The low TMR ratios may be attributable to diffusion taking place before the crystallization is completed. Figure 35 illustrates the impact of atomic ordering (green line) and diffusion (red line) on the TMR ratios. The TMR ratio can be estimated by the product (black) of both lines. As shown by the dashed lines, a relative shift of one effect would lead to higher TMR values. Therefore, the following procedures to improve the TMR ratios are imaginable:

Temperature stable counter electrode: Higher ex-situ annealing temperatures are necessary to induce the required atomic ordering and crystallization of the Heusler compound Co_2MnSi. To generate a more stable layer stacking and to suppress possible Mn diffusion, the antiferromagnetic Mn-Ir could be omitted. The free Co-Fe counter electrode is supposed to show a different magnetic switching behavior, which is in fact required to achieve an antiparallel state of the electrodes and to obtain a TMR ratio.

In-situ annealing: The integration of an in-situ annealing step for the crystallization of the Co_2MnSi electrode, prior to the deposition of Mn-Ir, might reduce Mn diffusion toward the upper barrier interface, which is supposed to limit the TMR.

Lowering the crystallization temperature: A reduction of the Co_2MnSi crystallization and ordering temperature might lead to higher TMR ratios.

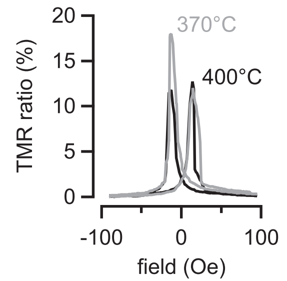

Figure 36: Co_2MnSi junction with unpinned Co-Fe counter electrode to realize hard/soft switching.

temperature stable counter electrode

A second MgO layer of 1 nm is deposited on top of the upper electrode to eliminate potential diffusion of the final Ru conductance layer. Due to the different coercive fields of Co-Fe and Co_2MnSi, an antiparallel state of the electrodes can be achieved. A major loop of a 370°C and 400°C annealed sample is given in Figure 36. The loops are very spiky and a clear antiparallel state could not be achieved. Compared to the Co_2MnSi junctions above, no higher TMR ratios could be found and a decay of the TMR ratio was also present with increasing annealing temperature.

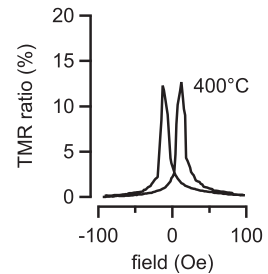

Figure 37: Co_2MnSi junction with artificially pinned Co-Fe counter electrode.

To create an antiparalell state of the two electrodes, the Co-Fe counter electrode was pinned to a second 6 nm thick Co-Fe layer. These were separated by a 0.92 nm Ru spacer layer which resulted in a antiferromagnetic coupling between the two Co-Fe layers. The major loop of a 400°C annealed sample is depicted in Figure 37. As was the case for the above investigated samples, no clear antiparallel state of the electrodes was present and a low TMR ratio of about 12% could be reached. The supposed diffusion of Mn as source for a lowered TMR can not be concluded from this experiment.

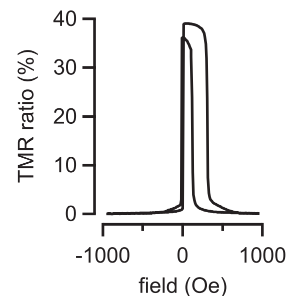

Figure 38: Major loop of an in-situ annealed Co_2MnSi junction.

in-situ annealing

The utilized Leybold sputtering system also provides an in situ heating system. Here, a heating wire is mounted in a second process chamber (oxidation chamber). Annealing temperatures of about 350°C to 400°C can be reached which are sufficient for the crystallization and ordering of Co_2MnSi. To keep the barrier interface clean the annealing step was added after depositing the Co-Fe counter (sample A) and within half of the Co-Fe electrode (sample B). Hereafter, Mn-Ir and Ru were deposited for pinning and conductance. The full junctions were ex situ annealed for 10 minutes at 275°C and cooled in a magnetic field to activate the exchange bias. The samples were subsequently annealed at different temperatures for an identical sample treatment.

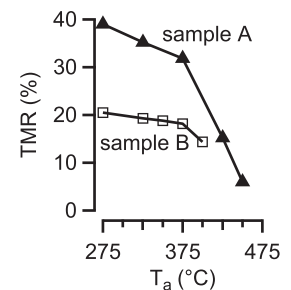

Figure 39: Comparison of the two in-situ annealed Co_2MnSi junctions.

In contrast to the samples discussed above, a clear antiparallel state was present, which allowed a determination of the TMR ratio (Figure 38). The values are shown in Figure 39 as a function of ex

situ annealing temperature. We observed a maximum TMR of 39% for the sample *A* (triangles). Further annealing led to lower TMR ratios and the effect nearly vanished for 450°C annealing. The strong decay of TMR at about 375°C may be attributable to Mn diffusion towards the upper barrier interface.

In comparison, sample *B* showed a reduced TMR value even for the lowest annealing temperature. The initial ratio of about 20% decreased with increasing annealing temperature and the decay at 375°C, which hints to Mn diffusion, could also be found.

lowering the crystallization temperature

Multilayered half junctions were prepared to lower the crystallization temperature of the Co_2MnSi. Here, the lower electrode consisted of Co_2FeAl (5 nm)/Co_2MnSi (5 nm)/Co_2FeAl (5 nm)/Co_2MnSi (5 nm) was capped by a 1.8 nm thick MgO layer. The idea was to induce the crystallization of Co_2MnSi, by combination with the low temperature crystallizing Co_2FeAl.[96] We performed a similar experiment for (011) oriented multilayered Co_2MnSi and Co_2FeSi Heusler compounds.[97]

[96] D. Ebke et al., J Magn Magn Mater **322**, 996 (2010)

[97] D. Ebke et al., Appl Phys Lett **89**, 162506 (2006)

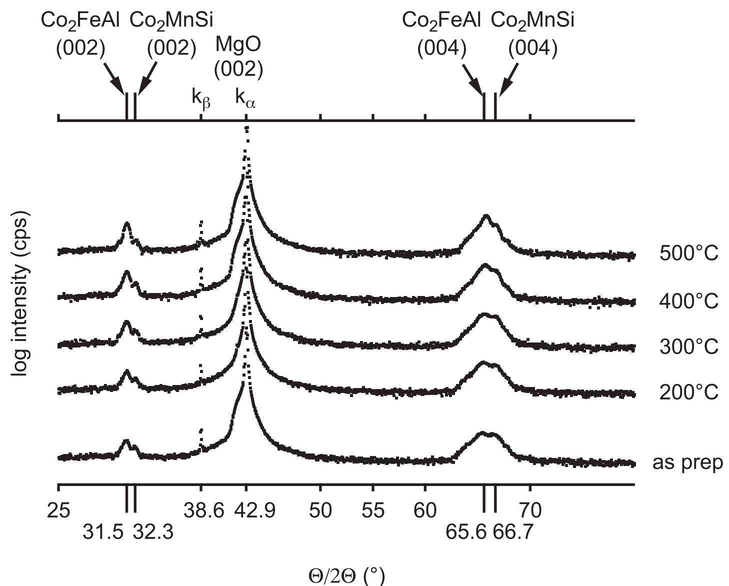

Figure 40: X-ray diffraction pattern of multilayered Co_2FeAl/ Co_2MnSi half junctions at different annealing temperatures.

Figure 40 shows the obtained XRD pattern of the prepared multilayered Heusler half junctions. The baselines of the patterns are shifted with regard to the applied annealing temperatures. A clear double peak structure was present for all temperatures at the Heusler (004) and (002) peak positions, which indicates that

no intermixing of the two compounds took place. The peaks at 31.5 degrees and 65.6 degrees can be attributed to the Co_2FeAl (002) and (004) peak, respectively. These values are actually comparable to the previously discussed values of the single Co_2FeAl thin film. In contrast, the corresponding Co_2MnSi (002) and (004) peaks at 32.3 and 66.7 degrees shifted to larger angles of 2θ. This can be explained by the corresponding lattice constants.

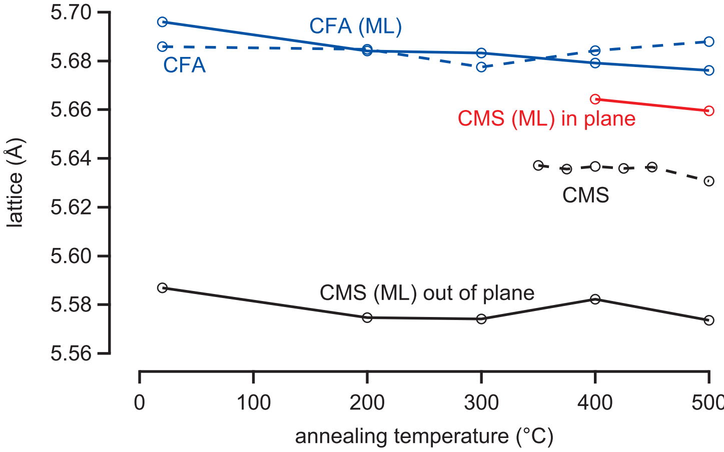

Figure 41: Out of plane lattice constants of the single Co_2FeAl and Co_2MnSi junctions (dashed lines) in comparison with the out of plane lattice of multilayered Co_2FeAl and Co_2MnSi lattice (solid line). The estimated in plane Co_2MnSi lattice of the multilayer is given in red.

Figure 41 shows the averaged lattice constants that were calculated from the (004) and (002) Heusler peaks for different annealing temperatures. As previously discussed, only the out of plane component of the lattice constant is able to be determined by the performed $\theta/2\theta$ scans. As expected from the peak positions, the lattice constants of the single and multilayered Co_2FeAl were almost identical. By contrast, the lattice constant of the multilayered Co_2MnSi was greatly reduced when compared to the out of plane lattice constant of the single Co_2MnSi layer. Assuming a constant lattice volume of $V_{CMS} = a^3_{CMS(SL)}$, ($a_{CMS(SL)}$ is the out of plane component of the single Co_2MnSi layer) the in plane component a_{ip} can be estimated by:

$$a_{ip} = \sqrt{\frac{a^3_{CMS(SL)}}{a_{CMS(ML)}}} \qquad (12)$$

As expected, the in plane lattice constant of Co_2MnSi was close to the Co_2FeAl lattice constant, i.e., the Co_2MnSi lattice was distorted to fit the Co_2FeAl buffer. The effect to the spin polarization was estimated by SPR-KKR DOS calculations, for a cubic and distorted Co_2MnSi lattice and the experimental lattice constants. As

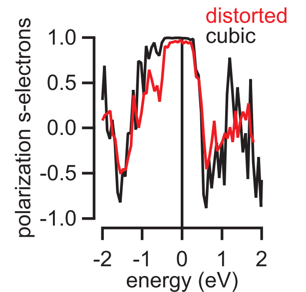

Figure 42: Polarization of s-electrons for a cubic and distorted Co_2MnSi lattice obtained from SPR-KKR calculations.

shown in Figure 42, additional states appear due to the lattice deformation and the spin polarization of the s-electrons is slightly reduced. Nevertheless, a high polarization of about 95% is conserved at the Fermi level and high TMR ratios can be expected.

Figure 43: Room temperature TMR ratios of full MTJs containing Co_2MnSi,Co_2FeAl and Co_2FeSi with the corresponding multilayered Co_2FeAl/ Co_2MnSi and Co_2FeSi/ Co_2MnSi systems as function of ex-situ annealing temperatures. The dashed line represents 1.8nm MgO barrier and the solid 2.1nm, respectively.

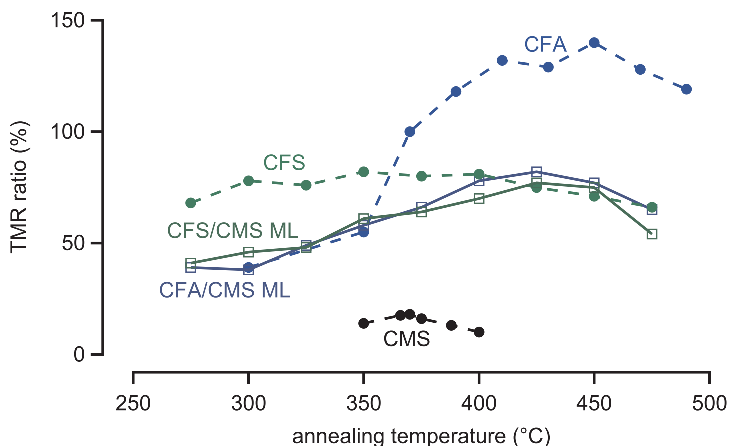

To verify the influence of the lowered Co_2MnSi crystallization temperature, corresponding full tunnel junctions were prepared. In addition, a second, multilayered system containing a Co_2FeSi (5 nm)/Co_2MnSi (5 nm)/Co_2FeSi (5 nm)/Co_2MnSi (5 nm) bottom electrode was prepared for comparison. The resulting TMR ratios are given in Figure 43 in comparison with the single layered junctions of Co_2FeSi, Co_2FeAl and Co_2MnSi. An MgO barrier thickness of 1.8 nm was used in all cases. The TMR of the multilayered junctions was increased with regard to the plain Co_2MnSi layer. For annealing temperatures below 350°C, the ratios were found to be comparable with Co_2FeAl. For temperatures above 400°C, the TMR ratios reached the Co_2FeSi values. A maximum value of about 82% and 77% was achieved at 425°C for the Co_2FeAl and Co_2FeSi based multilayers.

In summary, different approaches were tested to increase the low TMR ratio of the Co_2MnSi junctions. The highest values were reached by reducing the Co_2MnSi crystallization temperature. This was accomplished by Co_2FeAl and Co_2FeSi buffered multilayer junctions. Room temperature TMR ratios of about 80% were reached.

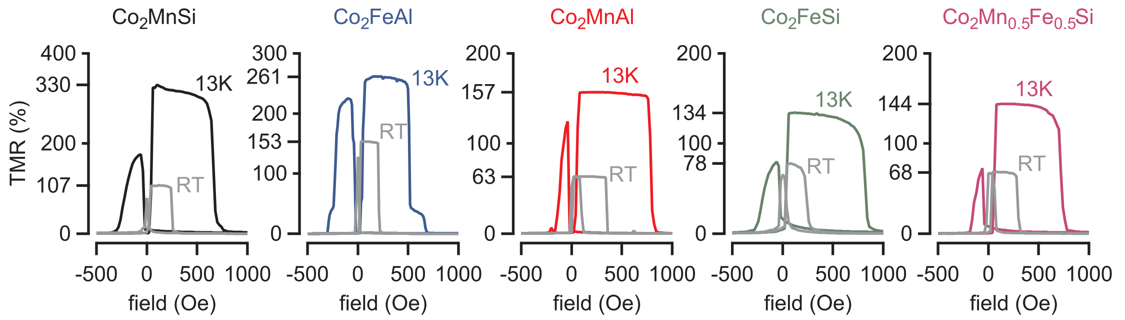

Figure 44: Low temperature (13*K*) and room temperature major loops of the investigated Heusler full junctions.

temperature dependence of the TMR ratio

Giant low temperature TMR ratios of over 750% were reported for MTJs containing a Co_2MnSi Heusler electrode. But the corresponding room temperature values were only about 220%.[98] The proximity of the Fermi level to the conductance or valance band is thought to be responsible for the temperature dependence.[99] But the origin of the temperature dependence is still under discussion. Instead of the plain Co_2MnSi junctions, the multilayered Co_2FeAl/ Co_2MnSi junctions were investigated because of the previously discussed higher TMR values. Instead of subsequently annealing, identical samples were annealed at the optimal temperature and patterned by e-beam lithography. Au contact pads were again deposited. As shown in Figure 33, the highest room temperature TMR ratios of about 150% were found for Co_2FeAl junctions. The same junctions showed about 260% TMR at 13 K. The corresponding major loops can be seen in Figure 44. The pinned upper electrode allows a well defined determination of the TMR ratio for all temperatures. The major loops of the other investigated Heusler full junctions are also given. The highest ratio at 13 K of about 330% can be achieved for Co_2MnSi. This is in contrast to the observed room temperature TMR values but reproduced the reported strong temperature dependence of the TMR ratio for this compound.[100]

[98] S. Tsunegi et al., J. Phys. D: Appl. Phys. (2009)

[99] K. Inomata et al., Phys. Rev. B (2008)

[100] S. Tsunegi et al., Appl Phys Lett **93**, 112506 (2008)

All dependences are given in Figure 45 for the measured TMR ratios (left) and the corresponding normalized TMR (right). We define the ratio of low temperature (13 *K*) to room temperature (RT) TMR value as Γ. The achieved TMR values are also summarized in Table 6.

The temperature dependence of the Fe containing compounds Co_2FeAl and Co_2FeSi ($\Gamma_{CFA} = \Gamma_{CFS} = 1.7$) was as weak as re-

Figure 45: Temperature dependence of TMR ratios for different Heusler compounds (left) and the corresponding normalized TMR ratio (right).

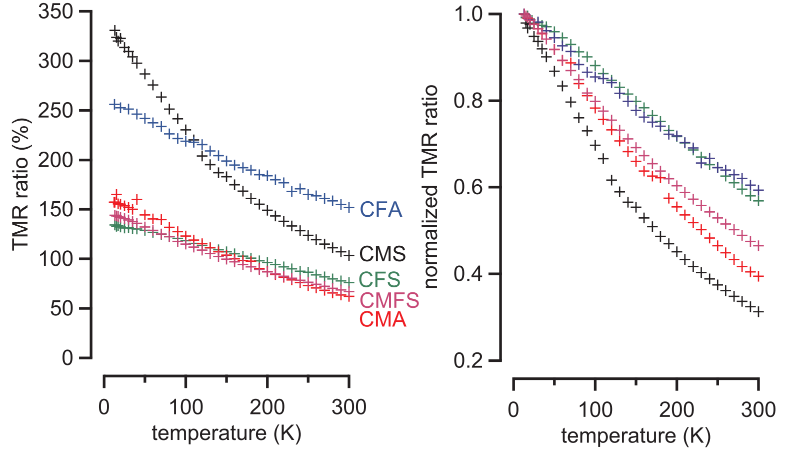

[101] W. Wang et al., Appl Phys Lett **95**, 182502 (2009)

[102] N. Tezuka et al., Appl Phys Lett **94**, 162504 (2009)

ported by Wang ($\Gamma_{CFA} = 2.1$)[101] and Tezuka ($\Gamma_{CFAS} = 2.1$)[102] for $B2$ structured Co_2FeAl and ideal $L2_1$ structured $Co_2FeAl_{0.5}Si_{0.5}$. The reported high room temperature TMR ratios of the latter compound are thought to be caused by a shift of the Fermi level into the middle of the band gap.

Table 6: Summary of found room and low temperature TMR values and the corresponding ratio $\Gamma = TMR(LT)/TMR(RT)$ for the investigated compounds.

compound	TMR (13K)	TMR (RT)	Γ
Co_2FeAl	261%	153%	1.7
Co_2FeSi	134%	78%	1.7
Co_2MnAl	157%	63%	2.5
Co_2MnSi (ML)	330%	107%	3.1
$Co_2Mn_{0.5}Fe_{0.5}Si$	144%	68%	2.1

The achieved temperature dependences of our Mn containing junctions were higher. For Co_2MnAl junctions it was determined to be $\Gamma_{CMA} = 2.5$ and for Co_2MnSi to be $\Gamma_{CMS} = 3.1$. A weak dependence is expected for the quaternary compound $Co_2Mn_{0.5}Fe_{0.5}Si$. The predicted shift of the Fermi level into the middle of the band gap should have led to a lower Γ, as found for Co_2MnSi and Co_2FeSi. Our ratio of $\Gamma_{CMFS} = 2.1$ was obviously lower than Γ_{CMS} but higher than Γ_{CFS}. In contrast to the linear progression of the weakly temperature dependent slopes, a convex TMR(T) curve was present for the stronger dependencies of Co_2MnAl and Co_2MnSi. A similar convex behavior was reported for epitaxial (001) textured Co_2MnSi tunnel junctions in $L2_1$ structure.[103] Here, the reported temperature dependencies were considerably higher. For a sputtered MgO barrier Γ_{sp} it was determined to be 4.1 and for an e-beam evaporated MgO barrier Γ_{eb} it was 3.5.[104] The difference is most likely attributable to barrier (interface) properties. Probably, disorder is less important for the temperature dependence.

[103] S. Tsunegi et al., J. Phys. D: Appl. Phys. (2009)

[104] S. Tsunegi et al., Appl Phys Lett **93**, 112506 (2008)

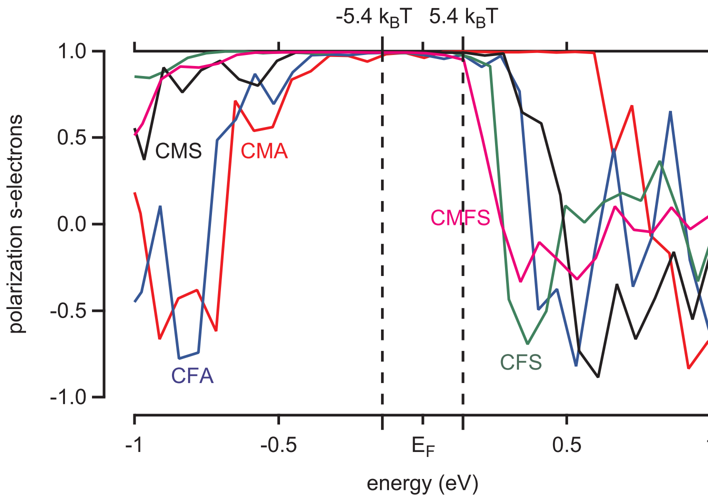

Figure 46: Polarization of s-electrons for ideal $L2_1$ structured Heusler compounds Co_2FeAl, Co_2FeSi, Co_2MnSi and Co_2MnAl. The dashed lines represent the assumed broadening due to thermal smearing.

One can assume that a certain position of the Fermi level can not be the (only) reason for temperature dependence. This can be illustrated by SPR-KKR calculations.[105]

The particular DOS were obtained by assuming $L2_1$ structure and the experimentally determined lattice constants. These DOS are in contrast to the cited theoretical publications,[106] which are based on a lattice constant determined by energy minimization calculations. Figure 46 depicts the spin polarization of s-electrons of the investigated Heusler compounds. These electrons dominate the tunneling process.[107]

The dashed lines at $\pm 140\,\mathrm{meV}$ ($= \pm 5.4\,k_B\mathrm{T}$[108] with regard to the Fermi level) represent the estimated effect of broadening due to thermal smearing. According to this assumption, neither the valence band nor the conductance band is within the range of thermal smearing. The strongest effect would be expected for $Co_2Mn_{0.5}Fe_{0.5}Si$ followed by Co_2FeSi and Co_2FeAl because of the proximity of the Fermi level to the conductance band. But this sequence is in contrast to the dependencies we found in the experiments.

Therefore, it has to be reconsidered if the origin of the reported weak temperature dependence is really related to a shift of the Fermi level into the gap as was previously reported by Tezuka[109] and Balke[110], or if the temperature dependence is more likely generated by the barrier (interface) properties. Very recently Sakuraba[111] reported that the large temperature dependence of $Co_2MnAl_xSi_{1-x}$ junctions is not connected to the position of E_F, but is most likely connected to interface states.

[105] http://olymp.cup.uni-muenchen.de/ak/ebert/SPRKKR/

[106] I. Galanakis, J. Phys.: Condens. Matter **16**, 3089 (2004); S. Picozzi et al., Phys. Rev. B **69**, 1 (2004); and H. C. Kandpal et al., Phys. Rev. B **73**, 1 (2006)

[107] J. Hertz et al., Phys. Rev. B **8**, 3252 (1973)

[108] J. Klein et al., Phys. Rev. B **7**, 2336 (1973)

[109] N. Tezuka et al., Appl Phys Lett **94**, 162504 (2009)

[110] B. Balke et al., Phys. Rev. B **74**, 1 (2006)

[111] Y. Sakuraba et al., Phys. Rev. B **81**, 144422 (2010)

Different effects are reported, which are influencing the bias voltage dependence of magnetic tunnel junctions. On one hand, the insulating barrier can strongly influence the spin polarization of tunneling electrons.[112] On the other hand, impurity-assisted tunneling and spin-flip scattering from defect states will decrease the TMR ratio with increasing bias.[113] Therefore, the bias voltage dependence originates from the superposition of the transport properties in the complex system of electrode / barrier / electrode, and the electrodes belonging DOS. However, the bias voltage dependence for different Heusler junctions also reflects DOS related key features. For example, an achieved kink in the TMR(V) curve of Co_2MnSi at about 300 mV is reported to be a strong change of the effective spin polarization of s-electrons.[114] At even higher bias voltages of more than 1000 mV, the TMR ratio can even be inverted, as reported for AlO_X based (011) textured Co_2MnSi [115] and (001) textured Co_2FeSi [116] junctions. An inverse TMR ratio is not present in (001) textured MgO based Heusler junctions and is assumed to be suppressed in coherent tunneling processes.

[112] J. D. Teresa et al., Phys. Rev. Lett. **82**, 4288 (1999)

[113] A. Bratkovsky, Phys. Rev. B **56**, 2344 (1997)

[114] J. Schmalhorst et al., Phys. Rev. B **75**, 1 (2007)

[115] A. Thomas et al., Appl Phys Lett **89**, 012502 (2006)

[116] F. Keseberg, Master's thesis, Bielefeld University (2007)

However, the bias voltage dependence might help to estimate the position of the Fermi level with regard to the calculated DOS. We used the low temperature bias voltage dependencies to reduce the effect of thermal smearing. These dependencies are compared to the calculated DOS. The dependencies of the (001) textured Heusler junctions are shown in Figure 47. The curves are normalized to the highest TMR values. The electrons are tunneling into the Heusler layer at positive bias voltages and into the Co-Fe counter electrode at negative. Therefore, features in the DOS of unoccupied Heusler s-electron states can be determined at positive voltages. As expected for a coherent tunneling process, a clear positive TMR is present for the measurable range of bias voltage. An asymmetric tunneling characteristic was found due to the various electrodes. The particular bias voltages $V_{\pm 1/2}$, where the TMR ratio dropped to 50% of the TMR ratios found at zero bias, are listed in Table 7.

Table 7: Summary of found bias voltages where the TMR ratios drops to the half of the found value at zero bias. The were achieved at 13K.

	$V_{-1/2}$	$V_{+1/2}$
Co_2FeAl	−151 mV	234 mV
Co_2FeSi	−355 mV	285 mV
Co_2MnAl	−556 mV	> 700 mV
Co_2MnSi (ML)	−44 mV	48 mV
$Co_2Mn_{0.5}Fe_{0.5}Si$	−175 mV	315 mV

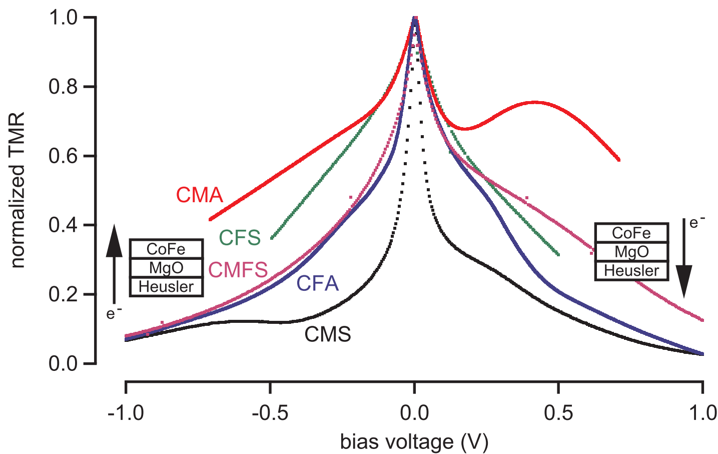

Figure 47: Low temperature (13K) bias voltage dependence of the TMR ratio for different full Heusler junctions. The values are normalized to the achieved maximum TMR value.

Due to the previously discussed low TMR values of the plain Co_2MnSi junctions, the multilayered Co_2FeAl/ Co_2MnSi junctions were investigated instead. Here, the strongest dependence of all compounds was present. The above mentioned kink in the TMR(V) of Co_2MnSi junctions at about +300 mV were also found. In addition, a second shoulder was present for negative bias at about −600 mV. The TMR ratio already dropped to the half for bias voltages of less than 50 mV. A similar strong bias voltage dependence of Co_2MnSi was previously found by Daibou and is reported to be a narrow half-metal gap near the Fermi level.[117]

[117] T. Daibou et al., J Magn Magn Mater **310**, 1926 (2007)

A similar behavior, but with a lowered and less spiky voltage dependence, was found for Co_2FeAl. Two shoulders were present at about +250 mV and −300 mV. We found $V_{-1/2}$ at about −150 mV and $V_{+1/2}$ at about +230 mV. This behavior is in contrast to the reported TMR(V) curve by Wang for similar junctions which indicates a slightly different DOS due to the reported, different film stoichiometry.[118]

[118] W. Wang et al., Appl Phys Lett **95**, 182502 (2009)

The obtained TMR(V) curve of the quaternary Heusler compound $Co_2Mn_{0.5}Fe_{0.5}Si$ is almost coincident to the Co_2FeAl curve for negative bias voltages. The dependence for positive bias voltages was again lowered. A slight shoulder was found at about +500 mV.

By contrast, the TMR(V) of Co_2FeSi showed an almost triangular behavior i.e., the TMR ratio dropped linearly with increasing bias voltages. We found no features in the dependence of the investigated bias range. The junctions were less resistant against higher voltages when compared to all other junctions and actually broke at about ±600 mV. This might indicate a rough barrier

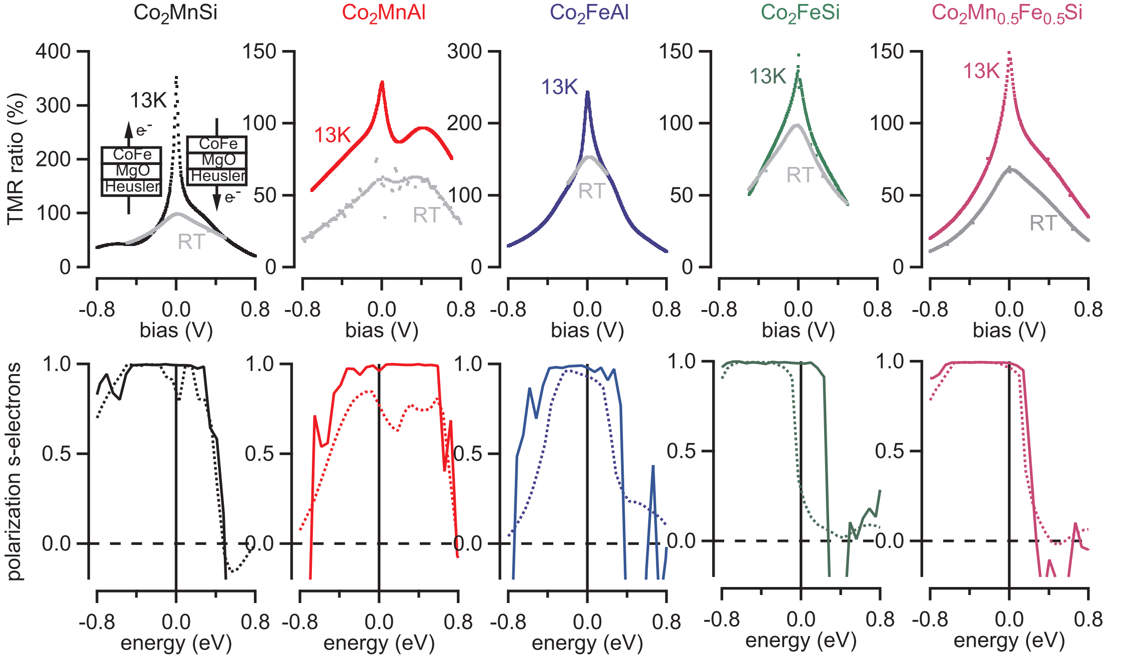

Figure 48: Bias voltage dependence at 13*K* and room temperature, respectively, for different Heusler junctions (top). In comparison, the polarization of the s-electrons that were carried out by DOS calculations for optimal $L2_1$ (solid line) and $B2$ structure (dashed line).

interface or even barrier defects such as pinholes.

The bias voltage dependence of Co_2MnAl was different. The normalized ratios were higher in comparison to all other compounds. $V_{-1/2}$ was reached at about -550 mV and $V_{+1/2}$ could not be reached in the range of $+700$ mV. Furthermore, we found a second maximum at about $+500$ mV. We also verified the values by major loops at higher bias voltages. By contrast, the normalized ratios dropped nearly linearly for negative bias voltages higher than -100 mV.

To illustrate the connection of band structure and voltage dependence, we have depicted the TMR(V) curves at 13 K and room temperature in comparison with the calculated polarization of the s-electrons (Figure 48). The above discussed DOS of the optimum composition X_2YZ in $L2_1$ structure are represented by the solid line. Assuming the experimental film stoichiometries and $B2$ structure, leads to the polarization which is represented by the dashed line. The calculations are based on the previously determined lattice constants.

The spiky bias voltage dependence of the Co_2MnSi junctions at 13 K is not conserved at room temperature, probably due to ther-

mal smearing. As expected from the temperature dependence, considerably lowered TMR ratios were found for low bias voltages. Higher bias resulted in similar values independent of temperature. The observed spiky behavior at $13K$ might be explained by the corresponding DOS calculations and experimental values (lattice, composition). In contrast to a broad gap in the minority band for the optimal $L2_1$ structured compound, the DOS of the $B2$ structured[119] Co_2MnSi show non vanishing states at the Fermi level, represented by a clear dip in the polarization of the s-electrons in Figure 48. An assumed, slightly shifted position of E_F[120] to a half-metallic position might explain the investigated strong bias voltage dependence.

[119] Although we verify $L2_1$ structure in our Co_2MnSi junctions, we have also calculated the DOS for B2, to show the influence of (partly) disorder.

[120] The position of the Fermi level is highly disputed, due to the achieved different positions of E_F for different applied models for calculating the DOS, e.g. SPR-KKR, FLAPW, LDA+U.

The bias voltage dependence of Co_2MnAl is considerably different from the above discussed dependence of Co_2MnSi. The TMR ratio at $13K$ was higher when compared to the obtained values at room temperature, independent of bias voltage. The second maximum, at about $+500\,\text{mV}$, is also conserved at room temperature. The corresponding polarization of s-electrons shows an almost half-metallic behavior for the $L2_1$ structured compound, whereas a considerably lowered polarization of about $P_{B2} = 75\%$ can be found for $B2$ type structure and the experimentally determined film stoichiometry ($Co_2Mn_{0.957}Al_{0.8}$). The presence of the second maximum in the TMR(V) curves can be explained by the high polarization of about 75% of the s-electrons at about 0.5 eV to 0.7 eV which might lead again to a rise of TMR ratio for higher bias voltages. However, the feature can not be explained by the performed calculations of the $L2_1$ structured system.

The voltage dependencies of the Co_2FeAl junctions show very similar behavior for $13K$ and room temperature. The low temperature TMR ratios were increased only in a small range from $-130\,\text{mV}$ to $+130\,\text{mV}$. The present shoulder determined in the TMR(V) curves of the Co_2FeAl junctions can be explained as was explained previously for the Co_2MnSi system. A strong drop of the calculated spin polarization for the disordered $B2$ structured system can be estimated at the same energies.

The almost triangular behavior of the Co_2FeSi TMR(V) curves at $13K$ was also conserved at room temperature. Striking features were not present. In particular, no shoulders could be found, as one would expect from the strong decay of spin polarization at about $+300\,\text{mV}$ of the calculated DOS for ideal $L2_1$ structure. The corresponding polarization of s-electrons and $B2$ structure in X_2YZ composition[121] is considerably different. A reduced gap

[121] The assumption of the experimentally determined film stoichiometry leads to a non convergent solution for the calculated DOS.

width led to a low polarization of about 25% at the Fermi level.

For the quaternary compound $Co_2Mn_{0.5}Fe_{0.5}Si$, the TMR value at $13K$ increased when compared to the room temperature values in the investigated range of bias voltage. We found a shoulder at about $+500$ mV. A strong drop of spin polarization can be found at about these energies for the calculated DOS in $L2_1$ and B2 type structure in X_2YZ stoichiometrie. The differences between these DOS vanished and we found a high spin polarization of s-electrons of about 97%.

In conclusion, we found features in the bias voltage dependence of the Heusler junctions, which can be explained by the calculated spin polarization of s-electrons. For the compounds Co_2FeAl and $Co_2Mn_{0.5}Fe_{0.5}Si$ the features can be explained with the DOS of a $L2_1$ or a B2 structured Heusler. Here, the calculated DOS are only slightly influenced by disorder. This is in contrast to the dependences of Co_2MnSi and Co_2MnAl. The corresponding DOS of the disordered compounds, show a reduced spin polarization at the Fermi level when compared to the DOS of an ideal $L2_1$ structured compound. The observed features in the TMR(V) curves are most likely related to the presence of B2 structure.

spin polarization

The measured TMR value is a superposition of the transport properties in the complex system electrode / barrier / electrode. For an amorphous tunnel barrier like AlO_X, the spin polarization of the involved electrodes can be estimated by the Julliere model.[122] For a crystalline MgO barrier, the tunneling process is coherent. Here, the tunneling current depends on the symmetry of Bloch states in the electrodes and the evanescent states of the tunneling barrier. A different decay length for different symmetries of Bloch states can greatly enhance the resulting TMR ratio.[123] Therefore, the Julliere model can not be applied to a MgO based tunnel junction in order to determine the spin polarization of the containing electrodes.

[122] M. Julliere, Phys. Lett. A **54**, 225 (1975); and J. S. Moodera et al., J Magn Magn Mater **200**, 248 (1999)

[123] W. H. Butler et al., Phys. Rev. B **63**, 1 (2001)

To estimate the Heusler quality in such a system with regard to a high polarization, it is required to directly measure the spin polarization. This is very challenging and two methods will be discussed in the following section. These methods were applied to Co_2FeAl junctions because of the high room temperature TMR ratio which was achieved for this compound.

Spin polarized tunneling into superconductor (SPT): The currents of a spin-transport device were determined by tunneling into a superconductor.[124] We replaced the upper electrode of our stack layout with a thin (4 nm to 7 nm) superconducting layer of Al-Si. The samples were sputtered through shadow masks with cross strip geometry. We carried out the conductance vs. voltage curves with four probe measurements in a ^{3}He cryostat at $0.49K$ and an in plane magnetic field of up to $2.9T$

[124] R. Meservey et al., Phys Rep **238**, 173 (1994)

Due to the Zeeman splitting, an asymmetric tunneling conductance is present and the spin polarization P can be calculated by:

$$P = \frac{(\sigma_4 - \sigma_2) - (\sigma_1 - \sigma_3)}{(\sigma_4 - \sigma_2) + (\sigma_1 - \sigma_3)} \quad (13)$$

Here, the σ_i represent features in the conductance of the normalized dI/dV curve, which is shown in Figure 49 for our Heusler compound Co_2FeAl.

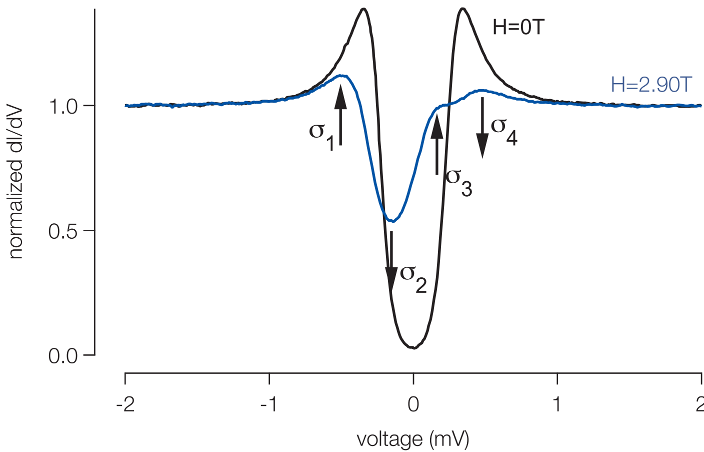

Figure 49: Normalized dI/dV of our Heusler Co_2FeAl with marked conductances σ_i to calculated the polarization. The Figure was taken from our related publication, reported by Schebaum (JAP 107 (2010), 09C717)

For the investigated Co_2FeAl, a spin polarization of $60 \pm 2\%$ can be estimated from this equation. However, the effects of spin-orbit scattering and orbital depairing were neglected. The Maki theory[125] can lead to a more precise value by analyzing the dI/dV curves. From this theory we can conclude a corrected P value of 55%, which is in good agreement to the reported experimental value of $P = 56.2\%$ by Inomata[126] and the theoretical predicted value for $B2$ structured Co_2FeAl of $P = 60.7\%$.[127] More details can be found in our related publication, reported by Schebaum.[128]

[125] P. Fulde et al., Physical Review (1966)

[126] determined by point contact Andreev reflection (PCAR)

[127] K. Inomata et al., Sci. Technol. Adv. Mater. **9**, 014101 (2008)

[128] O. Schebaum et al., Direct measurement of the spin polarization of co2feal in combination with mgo tunnel barriers, 2010

Magnetization dynamics: Recently, Müller[129] established a method to estimate the spin polarization P from a measured demagnetization time τ_M. The calculations are based on a three-temperature model[130] where the electrons, spins and lattice are assumed to different, independent temperatures. The interconnection is given by the particular relaxation rates between spins and electrons, electrons and lattice and lattice and spins. Without going into detail, the demagnetization is measured by a pump probe experiment. In a ferromagnetic material, the laser pulse excitation leads to an increase of the temperature in the electron system and almost instantaneously also leads to an increase of temperature in the spin system. By contrast, the direct channel is blocked in a half-metallic system such as that of Heusler compounds. The energy has to be transferred through lattice excitations which is relatively slow. The spin polarization can then be assumed from the determination of the demagnetization time.

[129] G. M. Mueller et al., Nat Mater **8**, 56 (2009)

[130] E. Beaurepaire et al., Phys. Rev. Lett. (1996)

The experiment was performed by the group of Münzenberg[131] on our previously discussed Heusler half junctions. In this experiment, the spin polarization of Co_2FeAl was estimated to $P_{CFA} = 77 \pm 3\%$[132] which is higher when compared to the values determined for similar junctions above.

[131] University of Göttingen, Germany

[132] A. Mann, Göttingen University, unpublished results

The different obtained spin polarizations from the two experiments for the Heusler compound Co_2FeAl can be explained by the investigated difference of probe depth. In case of the pump probe experiment, the spin polarization of some nm can be assumed.[133] Therefore, the measurements represent more likely the spin polarization of the bulk compound. By contrast, the described method of Meservey and Tedrow evaluates the spin polarized tunneling current. This also includes the barrier properties. In particular, the investigated tunneling electrons originate from the very last layer of the electrode material. Here, the spin polarization might be strongly reduced due to interface defect states, oxides or disorder.

[133] For the used laser wavelength of about 800 nm, a probe depth of about 15 nm is assumed.

off-stoichiometrical composition

The influence of compound stoichiometry has already been discussed above for the half junctions. We prepared corresponding full junctions, containing three different compositions of Co-Fe-Si, to investigate the transport properties.

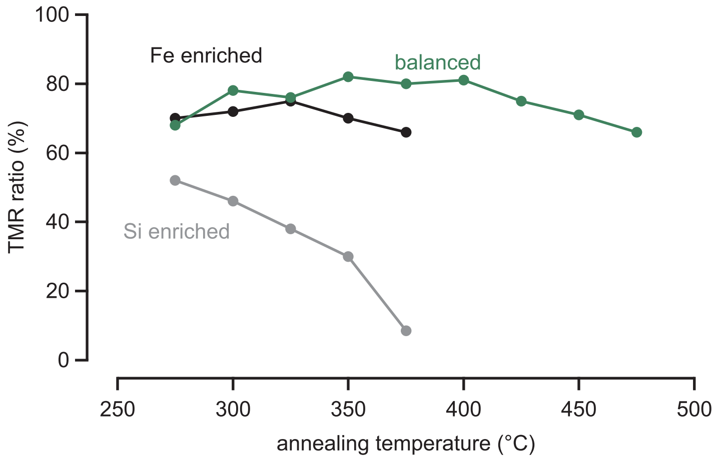

Figure 50: TMR ratio for different annealing temperatures and compositions of Co-Fe-Si.

Figure 50 depicts the achieved room temperature TMR ratios of the off-stoichiometrically Co-Fe-Si tunnel junctions in comparison with the balanced compound for different annealing temperatures. All samples were subsequently vacuum annealed. The MgO barrier thickness was set to 1.8 nm.

The TMR ratios of the Fe enriched Heusler junctions were comparable to the balanced Heusler junctions for low annealing temperatures up to 350°C. Higher annealing temperatures reduced the TMR and the obtained values were considerably lowered in comparison to the balanced Co-Fe-Si. The highest TMR value of about 75% was achieved for 325°C annealing.

By contrast the Si enriched Heusler junction showed a considerably lower TMR ratio, even for the lowest annealing temperature of 275°C.[134] Here, a maximum value of about 50% was achieved. Higher annealing led to a strong decrease. This can be explained by the previously discussed corresponding half junctions, which show a clear crystallographic change within these temperatures. This change might lead to stress at the barrier interface. A decrease of the interfacial magnetic moment was found from XMCD for annealing temperatures above 300°C, which might be attributed to a disordered Heusler compound. Furthermore, low crystallization was found in XRD scans. As discussed for Co_2FeAl, diffusion took place within the grain boundaries. The reduced crystalline growth of the Si enriched Heusler junction might allow diffusion at lower annealing temperatures.

[134] Barrier imperfections can be assumed for low annealing temperatures. Therefore, we set the initial annealing temperature to 275°C.

The same junctions show about 116% (Fe enriched) and 91% (Si enriched) TMR ratio at 13K. The temperature dependence of the obtained TMR values is given in Figure 51 (left) and (right) for

Figure 51: Temperature dependence of TMR ratios for different Co-Fe-Si compositions (left) and the corresponding normalized TMR (right).

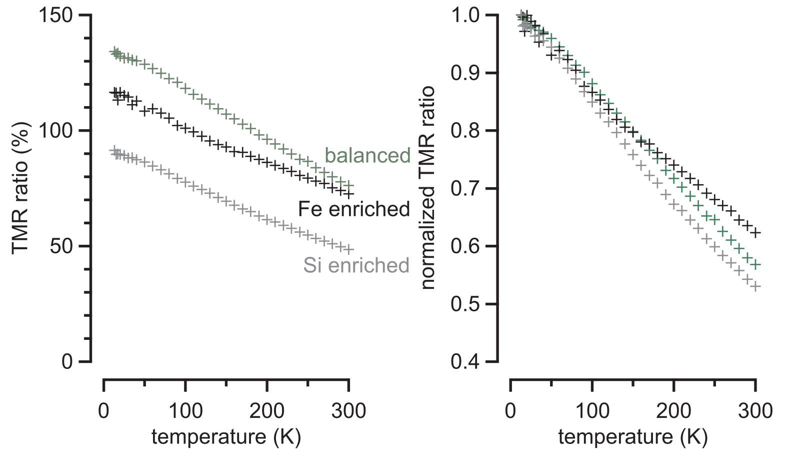

the normalized ratios. In contrast to the above discussed temperature dependences, we found only small deviations for the different Co-Fe-Si compositions. The ratio $\Gamma = TMR(LT)/TMR(RT)$ was slightly weaker for the Fe enriched junctions ($\Gamma_{Fe} = 1.6$) when compared to the balanced ($\Gamma_{CFS} = 1.7$), and slightly stronger for the Si enriched junctions ($\Gamma_{Si} = 1.8$). The achieved values at room temperature and $13K$ are summarized in Table 8.

Table 8: Summary of found room and low temperature TMR values and the corresponding ratio $\Gamma = TMR(LT)/TMR(RT)$ for the investigated Co-Fe-Si compounds.

compound	TMR ($13K$)	TMR (RT)	Γ
balanced	134%	78%	1.7
Fe enriched	116%	74%	1.6
Si enriched	91%	49%	1.8

These results leads again to the assumption that the temperature dependence of TMR ratio is more likely determined by interface properties and not by the reported shift of the Fermi level, which can be precipitated by changing the composition.

In contrast to the previously discussed, considerably different bias voltage dependences for the different Heusler compounds, the found dependencies of the Co-Fe-Si junctions are quite similar. The achieved TMR(V) curves at $13K$ are illustrated in Figure 52. The best agreement can be found for the balanced and the Fe enriched films. In contrast to the more likely triangular slope of the balanced composition, the TMR(V) curves of the Fe enriched junctions show similar features at about -400 mV and $+500$ mV, as previously discussed for the other compounds. The bias voltage dependence of the Si enriched junctions varies only sparsely and is slightly stronger, i.e., the normalized TMR is lower for

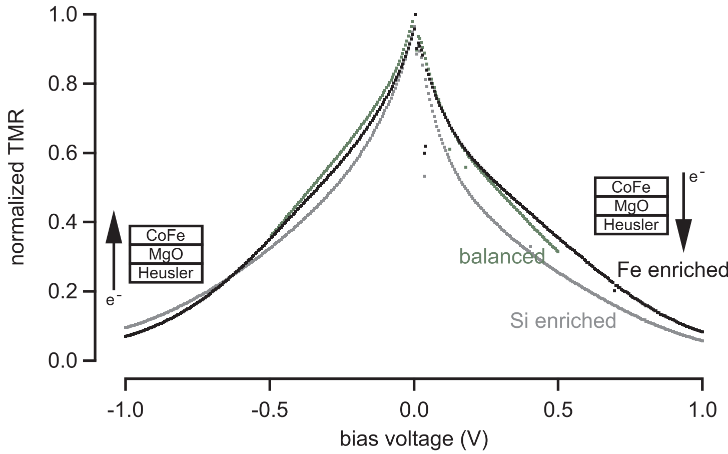

Figure 52: Low temperature bias voltage dependence of different Co-Fe-Si compositions.

the same bias, except for voltages below −600 mV. Remarkably, the off-stoichiometrically compound junctions are more resistant against high voltages than the junctions of the balanced films.

double Heusler junctions

We replaced the Co-Fe counter electrode with a second Heusler electrode to get coherent interfaces and higher TMR ratios. The growth conditions of the second electrode were investigated by XRD, as previously described. The studied layer stacking contains the optimized buffer and Heusler layer that we found before. The investigated layer structure is given in Figure 53. We used Co_2MnSi again as a representative Heusler compound to optimize the second Heusler electrode with regard to crystal growth properties. XRD measurements were performed for samples containing a top Heusler layer thickness of 5 nm, 10 nm, 20 nm and 30 nm. All layers were ex situ subsequently vacuum annealed at 400°C, 450°C and 500°C. To estimate the quality of the Heusler top electrode for different layer thicknesses, the textured fraction was defined as followed:

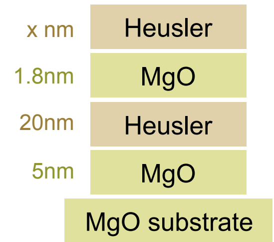

Figure 53: Layer stacking for XRD investigations of the double Heusler junction.

$$\begin{aligned} \textit{textured fraction}_{top} &= \frac{\textit{peak net area}_{top}}{\textit{layer thickness}_{top}} \\ &= \frac{\textit{peak net area}_{total} - \textit{peak net area}_{bottom}}{\textit{layer thickness}_{top}} \end{aligned}$$

We assumed our previously found $\textit{peak net area}_{bottom}$ values. The results are shown in Figure 54 for different annealing temperatures. We found the highest textured fraction for the 5 nm thick top electrode and all investigated temperatures. Thicker layers showed a lowered textured fraction.

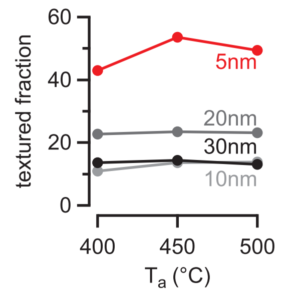

Figure 54: Calculated textured fraction for different Co_2MnSi top electrodes at varying annealing temperatures.

Full magnetic tunnel junctions containing two Heusler compound electrodes were prepared. We used the Heusler compound Co_2FeAl because it resulted in the highest room temperature TMR ratios of our investigated compounds. The layer stacking depicted in Figure 53 was completed with Mn-Ir (10 nm), Ru (40 nm) and Au (20 nm).

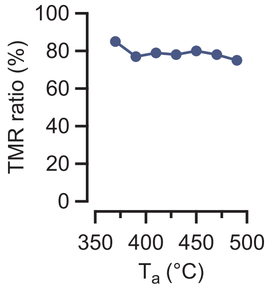

Figure 55: TMR ratio of a subsequently annealed double Heusler junction containing Co_2FeAl electrodes and a 1.8nm thick MgO tunnel barrier.

Figure 55 depicts the obtained TMR ratios for a subsequently annealed junction, containing a 5 nm thick Heusler top electrode. The MgO barrier thickness was set to 1.8 nm and the top electrode was pinned to Mn-Ir. A roughly constant TMR ratio of about 80 % was achieved for the whole investigated range of annealing temperature.

In contrast to the expected improvement of TMR ratio due to the coherent interfaces and the higher spin polarized second electrode, the TMR was reduced to the half when compared to the single Heusler junction. This might be attributed to degraded crystal growth of the top electrode which affects the TMR ratio more strongly for a Heusler compound than for Co-Fe. Furthermore, barrier interface imperfections, due to a different microstructure, are possible. This imperfections would also reduce the TMR ratio, because of eliminated coherent tunneling. This is also reported by Lim for (double) Heusler junctions containing Co_2FeSi electrode(s).[135]

[135] W. C. Lim et al., Ieee T Magn 44, 2595 (2008)

The constant level of TMR ratio is in contrast to the previously found decay at annealing temperatures of about 450°C. Probably, the top Heusler acts as a diffusion barrier for the supposed Mn.

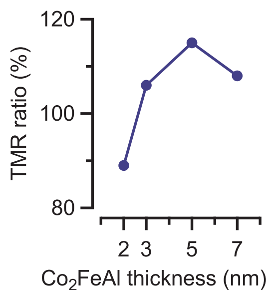

Figure 56: TMR ratio of a Co_2FeAl double Heusler junction with a 2.1 nm thick MgO barrier, annealed for 1h at 410°C.

A gentle variation of the counter electrode thickness in the full junctions also resulted in a maximum TMR ratio for the 5 nm thick second Heusler electrode (Figure 56). This is in good agreement with our XRD investigations. Due to the results found for the single Co_2FeAl electrode, here a MgO barrier thickness of 2.1 nm and an annealing temperature of 410°C was used. The optimized barrier thickness might explain the enhanced TMR ratio when compared to the results above in Figure 55. Nevertheless, the values are below the values of the plain Co_2FeAl junctions with Co-Fe counter electrode.

The above discussed crystal growth properties of the counter electrode influenced the magnetic behavior of the second Heusler layer. The corresponding major loops are plotted in Figure 57. For the 2 nm and 3 nm thick second Heusler layer, a broad switch-

ing is present, which might indicate a certain crystallographic decay and atomic disorder, as previously found for the disordered Co_2MnSi. For layers thicker than 5 nm, the coercive field of the pinned counter electrode was below 80 Oe and a maximum TMR ratio of about 115% was achieved.

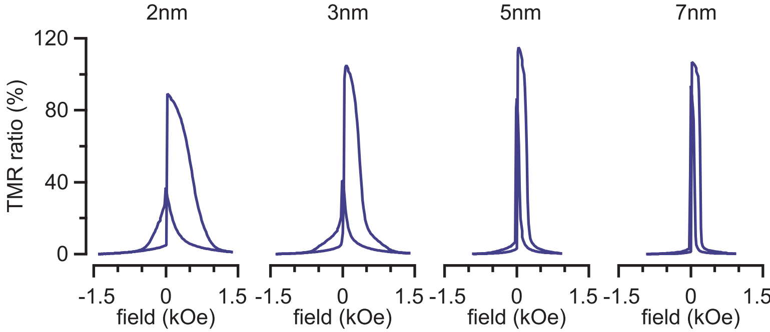

Figure 57: Major loops of double Heusler junctions with varying counter electrode thickness.

In summary the Heusler compounds of the investigated half junctions were integrated into full magnetic tunnel junctions to analyze the transport properties. A maximum room temperature TMR ratio of about 150% (261% at 13K) was achieved for $B2$ structured Co_2FeAl junctions. The obtained area resistances vary from less than $100K\Omega\mu m^2$ for Co_2FeAl to more than $100M\Omega\mu m^2$ for Co_2MnAl. One can conclude that high room temperature TMR values, low area resistances and a low Γ were found for compounds without Mn (Co_2FeAl and Co_2FeSi) and vice versa for compounds containing Mn. In particular, the discussed origin of temperature dependence seemed to be more related to interface properties and not to the reported shift of the Fermi level into a gap of the DOS.

From the different compositions of Co-Fe-Si we found an almost identical Γ, independent of stoichiometry. Furthermore, we can conclude that an excess of Fe is less critical to the transport properties than an excess of Si. As seen before, the excess of Si strongly influences the crystalline growth, as well.

Finally, we have also integrated the promising Heusler compound Co_2FeAl as second electrode into tunnel junctions, in order to generate coherent interfaces and to enhance the TMR ratio. Probably due to a degraded crystal growth on top of the MgO barrier or barrier interface imperfections, a lower TMR ratio is present when compared to a plain Co_2FeAl junction with Co-Fe counter electrode.

Industrial applicability

Within the BMBF[136] project HeuSpin, a collaboration with partners from industry was founded to transfer the knowledge of Heusler preparation. The possible integration of Heusler junctions into relevant applications will be evaluated. This chapter will describe how the limiting conditions can be handled. Preparation techniques and the resulting junction properties of lab and industry samples will also be compared.

[136] Bundesministerium für Bildung und Forschng

seed layer verification

The integration of Heusler compounds to existing systems, e.g., GMR/TMR sensors, is very challenging due to limiting conditions. As previously discussed, the seed layer system of the Heusler is essential for the optimum growth conditions with regard to establish the preferred (001) texture of the compound as well as to induce a high atomic ordering in the crystal structure. For the integration into existing systems fabricated by Siemens AG, one must verify whether the optimized seed layer can be used, as well. The existing sensors were covered with SiN/SiO_2 and polished by chemical mechanical polishing (CMP). Therefore, we used standard SiO_2 wafers to investigate the transport properties of the expected, degraded crystal growth of the Heusler. Co_2FeAl is the preferred compound because of the high room temperature TMR ratios achieved on the MgO substrate.

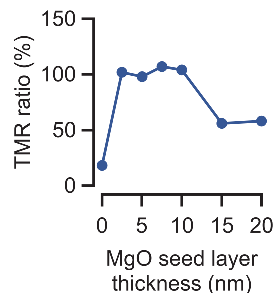

Figure 58: TMR ratio of Co_2FeAl MTJs on SiO substrates with different MgO buffer layer thickness.

Figure 58 depicts the obtained TMR ratios, as a function of MgO buffer layer thickness. All samples were ex-situ vacuum annealed for 1h at 410°C. Clearly visible, is the necessity of a specific MgO buffer. Without an MgO buffer, TMR ratios of about 20% can be reached. In the buffer thickness range of 2.5 nm to 10 nm the achieved ratio is almost on a constant level of about 100%. For a thicker seed layer, the TMR values decreased again to about half. The lowered TMR, when compared to the junc-

tions that were deposited on (001) MgO substrates, is reasonable. The impaired crystal growth of similar junctions has already been discussed previously. For the integration into existing systems an optimum MgO buffer of 5 nm thickness was assumed. The first results of our Heusler layers, deposited on SiO_2 wafers which were further processed at Siemens AG, are very promising. A TMR ratio of about 80% can be achieved for junctions that were moderately annealed at 250°C. Further annealing is planned and higher values are expected.

Frequently, Benzocyclobutene (BCB) based polymers are used in microelectronic processing. The photosensitive BCB is used for wafer level applications, where a protective layer is needed for passivation, or where a thin dielectric layer is required.[137] One limiting condition of this substrate is the restricted annealing temperature that can be applied to the BCB, depending on the cure.[138] The required annealing temperatures for crystallization of the MgO barrier and for inducing the atomic ordering of the Heusler compound would probably melt the BCB.

[137] http://www.dow.com/cyclotene/prod/402440.htm

[138] The full cure time of BCB can take several days depending on thickness and baking temperature.

However, we have prepared full junctions of 5 nm MgO buffered Co_2FeAl to investigate the transport properties. The junctions were annealed for 1h at 360°C. We found a TMR ratio of 58% at room temperature, which is comparable to the achieved values on MgO substrates. Probably, the very smooth surface of the BCB causes the relatively high TMR ratios. Furthermore, subsequent annealing of the junctions is planned.

In summary, high TMR ratios in Co_2FeAl junctions could be achieved even on SiO_2 and BCB substrates, where a degraded crystal growth of the Heusler layer would be expected. The previously found *B*2 ordering at low annealing temperatures on MgO substrates could probably be conserved on other substrates, as well. Due to the easy fabrication of Co_2FeAl onto technologically relevant substrates, it is an interesting material in the class of Heusler compounds.

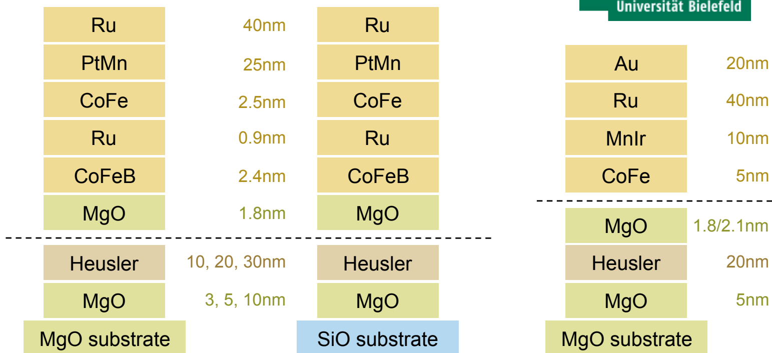

Figure 59: Layer stacking of the Singuls half and full tunnel junctions in comparison with the previously investigated Bielefeld junctions.

properties of industrially prepared Heusler layers

For an optimal comparison of Heusler junctions which were prepared in the lab and under industrial conditions, Co_2FeSi targets from the same supplier[139] were used. Half and full junctions from an identically composed Heusler target were prepared by Singulus NDT GmbH. A lower base pressure as well as a higher film homogeneity can be achieved within the sputtering system which probably leads to an improved crystalline growth of the buffered Heusler thin film and smoother interfaces.

[139] Williams Advanced Materials

The detailed layer structures of the junctions are given in Figure 59. SiO_2 as well as MgO substrates were used. In contrast to our half junctions, the Singulus half junctions ended up with the Heusler layer instead of a MgO capping layer. For the intended investigations by X-ray diffraction, to estimate the quality of crystal growth, this difference can be ignored.

Figure 60 shows an overview of a XRD pattern of the Singulus half junctions of the two different substrates. In the case of the MgO substrate (top), a clear Co_2FeSi (004) and (002) peak was found at 65.9 degrees and 31.5 degrees, respectively. The (002) peak of the single crystalline MgO substrate is located at 42.9 degrees. This is in contrast to the obtained pattern from the SiO_2 based half junctions. Here, no (004) and (002) Co_2FeSi peaks are visible at the expected positions. Instead, a very slight (022) peak can be estimated at 45.1 degrees. The clear (004) and (002) substrate peaks are located at 69.2 degrees and 33 degrees, respectively. A weak (002) peak of the sputtered 5 nm MgO buffer layer can be observed at 42.5 degrees.

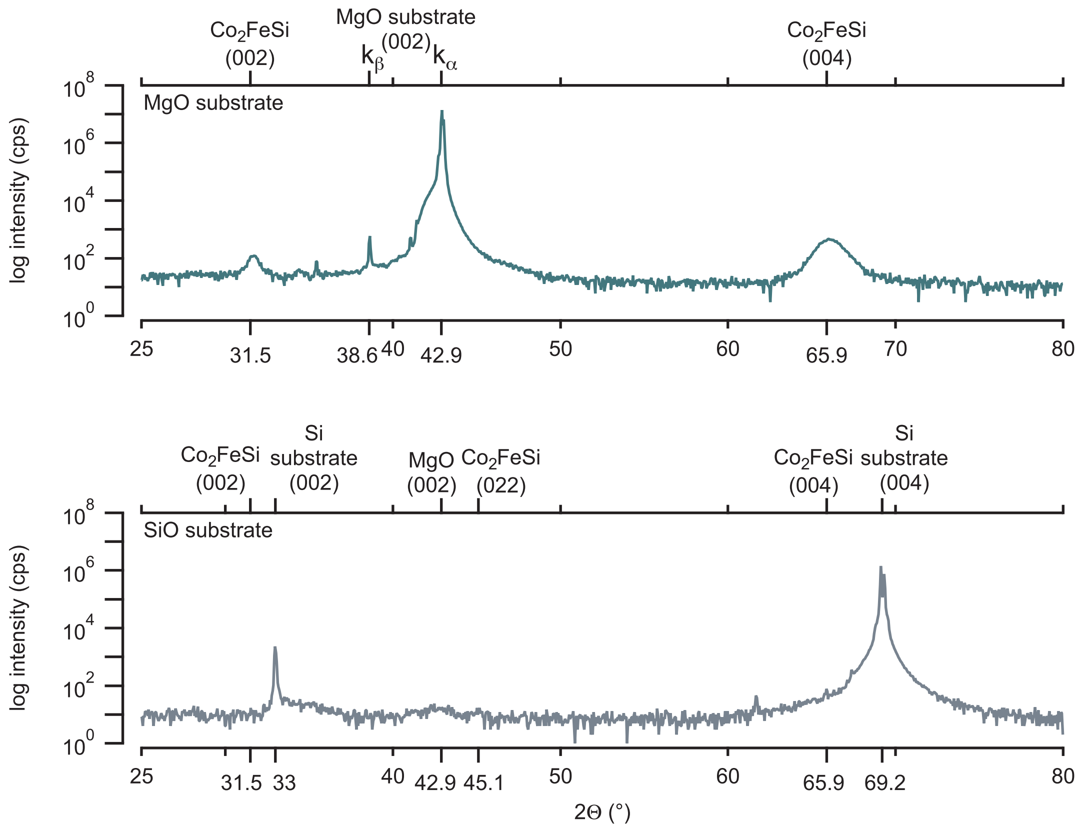

Figure 60: XRD pattern overview of Singulus samples. 20nm Co_2FeSi buffered with 5nm MgO on MgO substrate (top) and SiO substrate (bottom) without annealing process.

The rough XRD overview of the Singulus samples confirms, again, the preferable usage of MgO substrates. Nevertheless, a detailed extract of the (004) Co_2FeSi peaks for all Singulus half junctions is given in Figure 61, to determine the optimal MgO buffer thickness and substrate. Almost no difference in intensity, for 3 nm, 5 nm and 10 nm MgO buffer, was observed for the three investigated different Heusler thicknesses of 10 nm, 20 nm and 30 nm and MgO substrate. The peak intensity increases, as expected, with increasing layer thickness. A small shift in the peak maximum to smaller angles is noticeable with increasing Heusler thickness. This shift is attributed to a change of the lattice constant and will be discussed below.

By contrast no considerable (004) peak of the Co_2FeSi layer is present in all XRD pattern in case of the SiO_2 substrate. As shown in Figure 61 (bottom), only the (004) substrate peak was detected. We found that the MgO substrate is preferable to the industrially prepared Co_2FeSi Heusler thin films, as well. Further investiga-

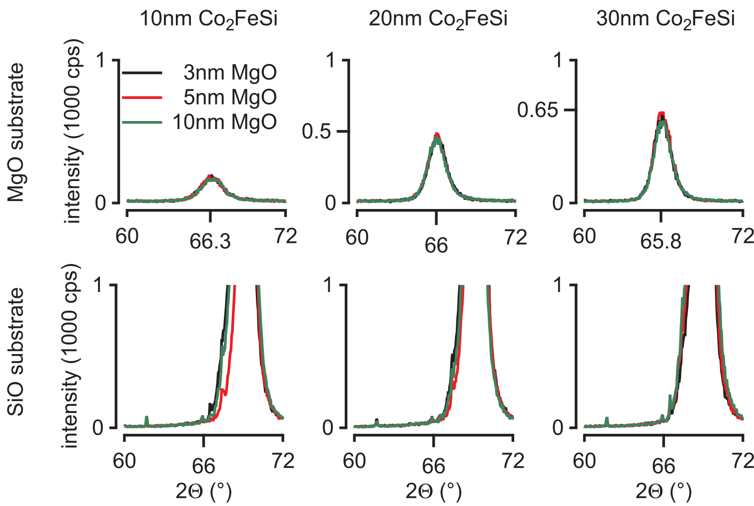

Figure 61: ((004) peak of the MgO buffered 10 nm, 20 nm and 30 nm Co_2FeSi layers, deposited on MgO substrate (top) and SiO_2 substrate (bottom), respectiveley.

tions of the SiO_2 substrate based thin films are rejected in this work.

The investigated (004) peak shift for Co_2FeSi in the case of the MgO substrate (Figure 61 (top)), issues from a change in the lattice parameter. Figure 62 depicts the corresponding lattice, as a function of Co_2FeSi thickness, for different MgO buffer thicknesses. The dashed line represents the bulk value of 5.64 Å.[140] For the 10 nm thick Heusler layer, the lattice constant varies slightly with MgO buffer layer thickness. The lowest value was found for the 10 nm thick buffer; the highest for the 5 nm buffer. For thicker layers of Co_2FeSi, the lattice was unaffected by the buffer thickness and increased with increasing Heusler layer thickness. However, the change of lattice constant was only in the range of hundreds of Å.

[140] S. Wurmehl et al., Phys. Rev. B **72**, 1 (2005)

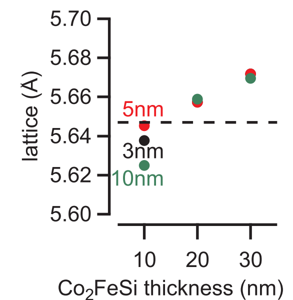

Figure 62: lattice constant of MgO buffered 10nm, 20nm and 30nm Co_2FeSi layers.

To determine the optimum thickness for the Co_2FeSi layer, the textured fraction was calculated from the (004) Heusler peaks. Figure 63 shows that the highest values were reached for the 20 nm thick layer, independent of buffer thickness. These results confirm the previously achieved results from our junctions.

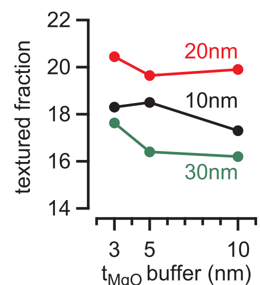

Figure 63: Textured fraction carried out from the (004) Co_2FeSi peak net area of the MgO buffered 10 nm, 20 nm and 30 nm Heusler layers.

To point out the reproducibility of the results, the XRD pattern of our prepared samples (green line) and the prepared samples by Singulus NDT GmbH (red line), are plotted in Figure 64. Both samples contain 20 nm Co_2FeSi on a 5 nm MgO buffer. No annealing process was applied. Both (004) and (002) Heusler peaks

Figure 64: XRD (002) and (004) peaks of Co_2FeSi half junctions. Comparison of Singulus and Bielefeld samples.

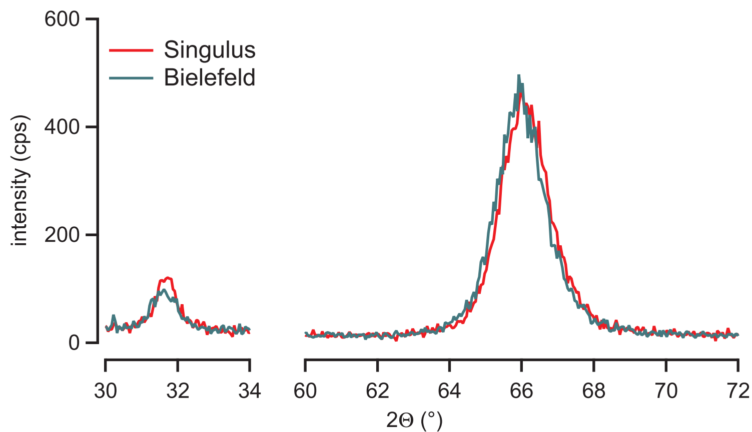

are nearly coextensive. A small deviation in the case of the (004) peak can be estimated which is attributed to a shift in the lattice constant. The (002) peak of the Singulus sample was slightly enhanced, in comparison to our sample. All in all, the differences are negligible and an equal quality of the deposited Co_2FeSi layers can be concluded.

The corresponding lattice constants and the (004) peak net areas of both samples are shown in Figure 65 (top) and (bottom), respectivelys, as a function of annealing temperature. The dashed

Figure 65: Comparison of Singulus and Bielefeld Co_2FeSi half junctions.

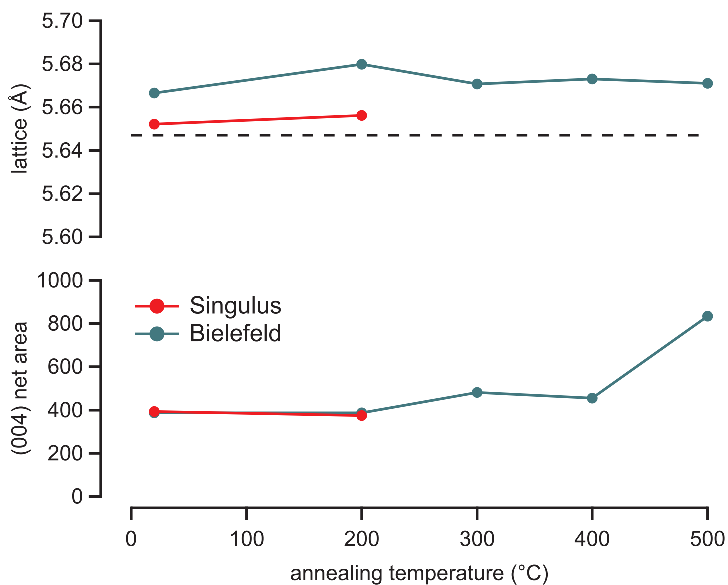

line represents the reported Co_2FeSi bulk lattice.[141] The obtained difference of about 0.02 Å for the compared samples can be ignored. Nevertheless, the lattice of the Singulus samples fits the bulk value even better.

[141] S. Wurmehl et al., Phys. Rev. B **72**, 1 (2005)

The above mentioned good reproducibility can be confirmed by the corresponding net areas that were obtained and are given in the bottom of this Figure. The achieved (004) peak net areas of the as prepared and 200°C annealed Singulus samples, fits the obtained values of the Bielefeld samples perfectly. Further annealing is planed but, due to the good reproducibility, no considerable difference are expected.

A comparable investigation of the bulk magnetic properties, via room temperature AGM measurements, is pending.

The Singulus full junctions were investigated with regard to the transport properties. In contrast to the Bielefeld Heusler full junctions, an artificially pinned Co-Fe-B layer was used as the top counter electrode instead of Co-Fe. The provided samples were capped with a 20 nm Au layer after annealing for better conductance, similar to our previously discussed junctions. The achieved TMR ratios are given in Figure 66, in comparison with our similar Co_2FeSi junctions. For ex situ annealing temperatures of 300°C and 325°C a lower TMR value of about 33% was found although the deposited Heusler thin films show identical properties.

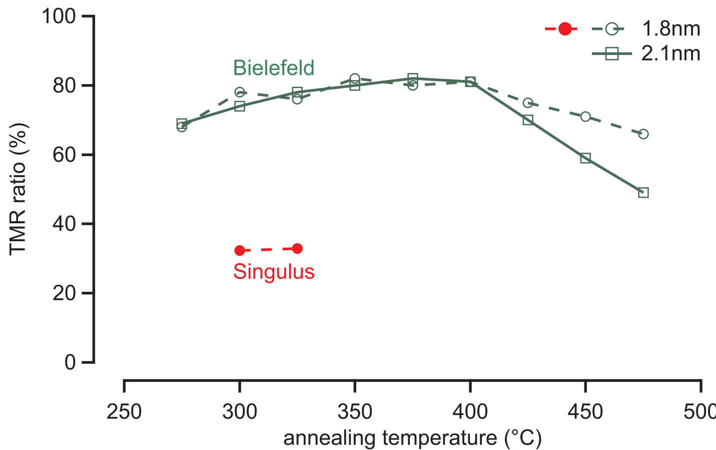

Figure 66: Comparison of achieved TMR ratios from Singulus and Bielefeld Co_2FeSi full junctions.

The reason of the reduced TMR values might be found in the corresponding major loops, which are depicted in Figure 67 for the Singulus sample and in Figure 68 for our sample. Both samples contained a 1.8 nm thick MgO barrier and were subsequently

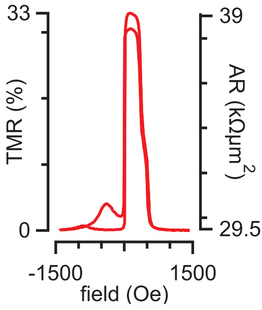

Figure 67: Typical major loop of a Singulus Co_2FeSi junction annealed at 325°C.

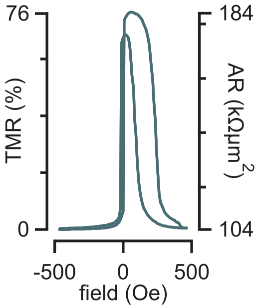

Figure 68: Typical major loop of a Co_2FeSi junction prepared in Bielefeld and annealed at 325°C.

annealed for 1h at 325°C. Apart from the reduced TMR ratio, the area resistance was lowered by a factor of three, compared to similar samples that we have prepared, despite the same barrier thickness. The lower area resistance can probably be explained by a slightly different composition of the MgO barrier, i.e., the Singulus barrier might have a leak of oxygen. On one hand this leak can result in a preferred, low area resistance of the tunnel junctions, but on the other hand might also lead to a lowered TMR ratio, due to barrier imperfections. A similar effect was previously found in common Co-Fe-B/MgO junctions that were prepared by Singulus. The deposition of the MgO layer in a light oxygen atmosphere might improve the barrier quality and enhance the TMR values.

In summary Co_2FeSi Heusler half and full junctions were deposited by Singulus NDT GmbH. The preparation was based on the previously discussed results of our similar junctions. Performed XRD measurements showed almost identical growth properties to the layers we had previously prepared. By contrast, the transport properties showed a considerably lowered TMR ratio, which might be more related to differences in the tunneling barrier than to differences in the Heusler layer properties. Due to the successful integration of the industrially prepared Heusler layer, we can conclude a direct transfer of knowledge from lab to industry.

Conclusions

In summary, we have integrated different Heusler compounds into half and full magnetic tunnel junctions. We have optimized the required seed layer to induce the atomic ordering. The preferred (001) growth direction was achieved. We have found the best results for a 5 nm MgO buffered Heusler layer, deposited on MgO (001) substrates.

We have investigated the crystallographic and magnetic bulk properties of the Heusler thin films as well as the element specific, chemical and magnetic properties at the barrier interface. Except for Co_2MnSi, all investigated compounds were crystalline, even in the as prepared state in $B2$ type structure. A similar behavior was observed for the magnetization. Again, except for Co_2MnSi, all compounds were ferromagnetic even in the as prepared state. Further annealing led to an increase of magnetic moment or magnetization. The highest moment, when compared to the reported bulk values, were achieved for Co_2MnSi and Co_2FeAl. This might be explained by the good agreement of film compositions and of indented X_2YZ Heusler stoichiometry for these compounds. Furthermore, we found that compounds containing Mn usually formed an oxidized barrier interlayer, which we assume to be the origin of the detected lowered TMR ratios, the higher area resistances and the stronger temperature dependence in the tunnel junctions of the Mn containing compounds. By contrast, the Fe containing Heusler junctions show a lower area resistance, which makes them more competitive for industrial applications. The highest room temperature TMR ratios of about 150% were achieved for Co_2FeAl junctions.

From a technological point of view, these TMR values are already sufficient for real applications such as sensors. To realize a Heusler based Application Specific Integrated Circuit (ASIC), we deposited the Co_2FeAl TMR layer stacking onto wafers with existing circuits, provided by PREMA and further processed by

Siemens AG. The preparation of a demonstrator is planed.

Similar full junctions containing the promising Co_2MnSi compound resulted in unexpected low TMR values. This might originate from diffusion prior to crystallization of the compound layer. We investigated different solutions to remedy it (multilayer, in situ annealing, temperature stable counter electrode) and achieved an increase of the TMR ratio to about 110%. Due to the present, strong temperature dependence ($\Gamma = 3.1$) the same junctions showed the highest TMR values at 13K, within the list of compounds that we investigated in this work.

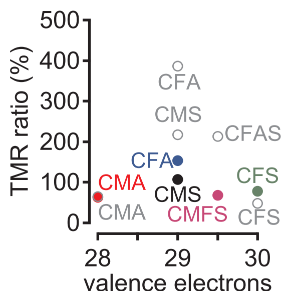

Figure 69: Room temperature TMR values of Heusler junctions with different numbers of valence electrons.

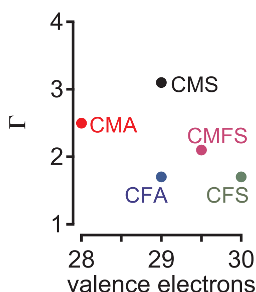

Figure 70: Found ratio $\Gamma = TMR(13k)/TMR(RT)$ as a function of valence electrons.

All room temperature TMR ratios are summarized as a function of valence electrons in Figure 69. The trend of highest TMR ratios for Heusler compounds with 29 valence electrons (Co_2MnSi and Co_2FeAl) can be confirmed by the reported, highest values found in literature (open circles). By contrast, we can not confirm the supposed connection of temperature dependence and position of the Fermi level (or numbers of valence electrons). As depicted in Figure 70, our determined Γ is independent of valence electrons. Here, the origin seems to be more related to barrier interface properties. In particular, the Mn containing compounds show a considerably stronger temperature dependence.

It was shown by Wang that TMR values of over 300% can be realized with the $B2$ structured Heusler composition Co_2FeAl, which was optimized in an attempt to get smooth interfaces.[142] Therefore, the investigation of interface properties is essential to understand the temperature dependence, the influence of roughness and spin polarization for future preparation of highly spin polarized materials. As a first step, we performed tunneling spectroscopy for the Heusler compound Co_2FeAl.[143] Similar measurements are planed for other compounds, as well. The evaluation of these measurements, in addition to the present data, is helpful to understand the interface effects. Furthermore, the investigation of XAS and XMCD will be extended. Ab initio atomistic thermodynamics of the interface in a Co_2MnSi/ MgO system have shown a variant spin magnetic moment of the interfacial atoms for different terminations.[144] Surface sensitive XMCD measurements[145], which were performed by Krumme, on our samples indeed confirmed the predicted interface termination. In 2006, Schattenschneider[146] reported the experimental detection of magnetic circular dichroism in a TEM (named EMCD), which allows a mapping of element specific magnetic moment at the barrier interface on a nanoscale.[147] Initial EMCD measurements of our

[142] W. Wang et al., Appl Phys Lett **95**, 182502 (2009)

[143] D. Ebke et al., Appl Phys Lett **95**, 232510 (2009)

[144] B. Hülsen et al., Phys. Rev. Lett. **103**, 046802 (2009)

[145] The in situ subsequent deposition of a thin Cu capping layer between the measurements improves the interface probing.

[146] P. Schattschneider et al., Nature **441**, 486 (2006)

[147] P. Schattschneider et al., Ultramicroscopy (2009)

Heusler half junctions have already been performed by Ennen and are currently under evaluation.

This work showed that the preparation of highly spin polarized materials is very challenging and the demand of such materials is great. In the future, we can prepare improved junctions. Very recently, a new sputter chamber was put into operation. The available deposition on heated substrates (up to 1000°C) should enhance the crystalline growth. A co-deposition of several materials is also possible. In particular, Heusler layers can be prepared with an adjusted film stoichiometry or dusted interfaces. A crystalline MgO barrier can be formed by common RF sputtering or electron beam evaporation. Furthermore, we have successfully prepared our first Heusler thin films by molecular beam epitaxy (MBE). The adjustable film composition can be realized and a deposition on heated substrates is possible. In particular, the dusting of interfaces might by very interesting for the conservation of a high bulk spin polarization. Recently, Miura showed that the half-metallic tunneling conductance of MgO based Co_2MnSi tunnel junctions can be conserved, with an insertion of a thin Co_2MnAl interlayer at the barrier interface.[148]

[148] Y. Miura et al., Journal of Physics: Conference Series **200**, 052016 (2010)

Even though higher room temperature TMR ratios can nowadays be realized without Heusler compound electrodes, these materials are of great interest for the integration into magnetic tunnel junctions. For example, it was shown by Albon that a wider range for the detection of nano particles can be realized with Heusler based junctions, due to the very small anisotropy of the compounds.[149] Furthermore, this property leads to a less noisy signal, which is essential for the detection of small magnetic fields.

[149] C. Albon, PhD thesis, Bielefeld University (2009)

Additionally, the reported low damping constant of half-metallic Heusler compounds is very interesting with regard to spin current induced switching and the expected low critical current densities within such junctions.

However, the international technology roadmap for semiconductors predicts a further shrinking of the cells in common devices, such as the DRAM (dynamic random access memory) within the next years. A half pitch size, which is half the distance between cells of a memory chip, of 22 nm is supposed for 2011-2012. From a physical point of view, the change to perpendiculary magnetized materials is absolutely essential to realize future magnetic tunnel junctions. This was predicted by Daalderop[150] for multilayers of $(Co)_n/(X = Cu, Ag, Pd)$ and experimentally verified for Co/Pd multilayers by Carcia.[151] The class of Heusler compounds also

[150] G. Daalderop et al., Phys. Rev. B **42**, 7270 (1990)

[151] P. Carcia et al., Appl Phys Lett **47**, 178 (1985)

provides promising materials. Mn_3Ga is predicted to show half-metallicity and perpendicular anisotropy.[152] Furthermore, Mn_3Ga is expected to be a completely compensated-ferrimagnetic, i.e., no magnetic moment is present, which is very attractive for devices based on spin induced magnetization switching. We have already performed initial experiments and the integration into tunnel junctions is planed.

[152] S. Wurmehl et al., Journal of Physics-Condensed Matter **18**, 6171 (2006)

Appendix

data summary

Summary of achieved experimental data of the investigated Heusler compounds. The first table summarizes the results of Co_2FeAl, Co_2FeSi, Co_2MnAl, Co_2MnSi and $Co_2Mn_{0.5}Fe_{0.5}Si$. The results of the half junctions are given in the first part of the table, the results of the full junctions in the second part, respectively.

	Co_2FeAl	Co_2FeSi	Co_2MnAl	Co_2MnSi	$Co_2Mn_{0.5}Fe_{0.5}Si$
# valence electrons	29	30	28	29	29.5
target composition	$Co_2Fe_1Al_1$	$Co_2Fe_1Si_1$	$Co_2Mn_1Al_1$	$Co_2Mn_{1.28}Si_{1.29}$	$Co_2Mn_{0.5}Fe0.5Si_1$
film composition	$Co_2Fe_{0.98}Al_{0.985}$	$Co_2Fe_{0.953}Si_{0.925}$	$Co_2Mn_{0.957}Al_{0.8}$	$Co_2Mn_{0.985}Si_{0.968}$	$Co_2Fe_{0.473}Mn_{0.383}Si_{0.912}$
max. magnetization	1099 kA/m	1090 kA/m	535 kA/m	1039 kA/m	941 kA/m
max. magn. moment	5.45 μ_B	5.36 μ_B	2.70 μ_B	5.02 μ_B	4.62 μ_B
at annealing temp.	500°C	500°C	500°C	400°C	500°C
lattice	5.688 Å	5.671 Å	5.719 Å	5.637 Å	5.667 Å
max. TMR (RT)	153%	78%	63%	107%	68%
max. TMR (13K)	261%	134%	157%	330%	144%
at annealing temp.	410°C	400°C	400°C	425°C	350°C
Γ	1.7	1.7	2.5	3.1	2.1

	Co_2FeSi	Co-Fe-Si (Fe+)	Co-Fe-Si (Si+)
# valence electrons	30		
target composition	$Co_2Fe_1Si_1$	$Co_2Fe_{1.43}Si_{1.22}$	$Co_2Fe_{1.09}Si_{1.37}$
film composition	$Co_2Fe_{0.953}Si_{0.925}$	$Co_2Fe_{1.313}Si_{0.894}$	$Co_2Fe_{1.019}Si_{1.205}$
max. magnetization	1090 kA/m	1310 kA/m	811 kA/m
max. magn. moment	5.36 μ_B	6.42 μ_B	3.47 μ_B
at annealing temp.	500°C	500°C	300°C
lattice	5.671 Å	5.665 Å	5.607 Å
max. TMR (RT)	78%	74%	49%
max. TMR (13K)	134%	116%	91%
at annealing temp.	400°C	325°C	275°C
Γ	1.7	1.6	1.8

XAS and XMCD

The room temperature XAS of the Co-, Mn- and Fe-$L_{3,2}$ edges for the Heusler compounds Co_2FeSi, Co_2MnSi and $Co_2Mn_{0.5}Fe_{0.5}Si$ are illustrated in the following Figures. The spectra of the off-stoichiometrically Co-Fe-Si films are given, too. Prominent XAS features are marked with arrows. The corresponding XMCD of each compound is given in the bottom of the Figures.

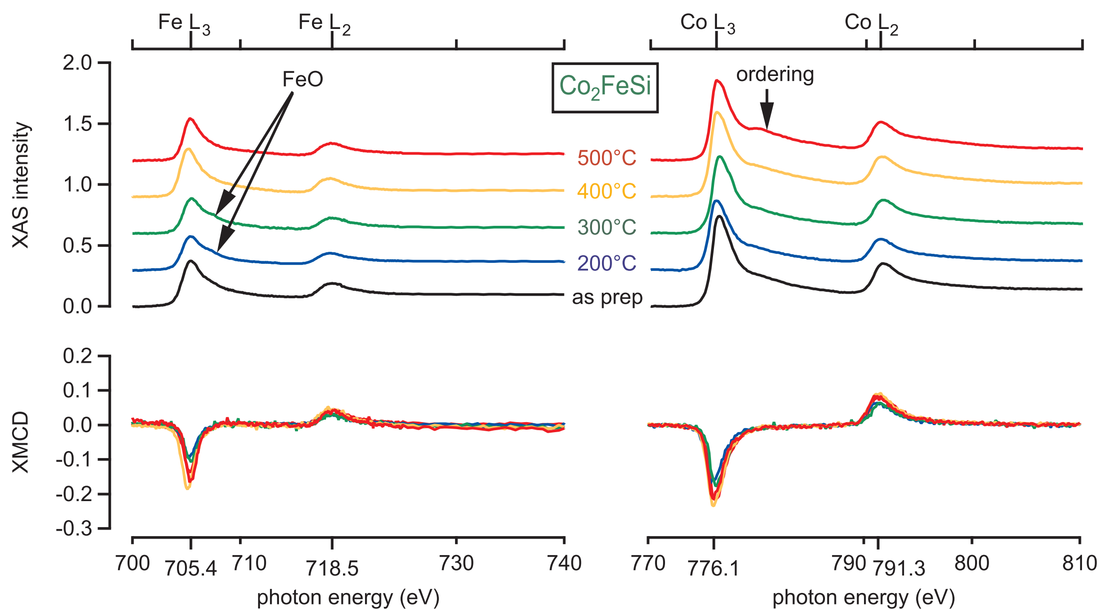

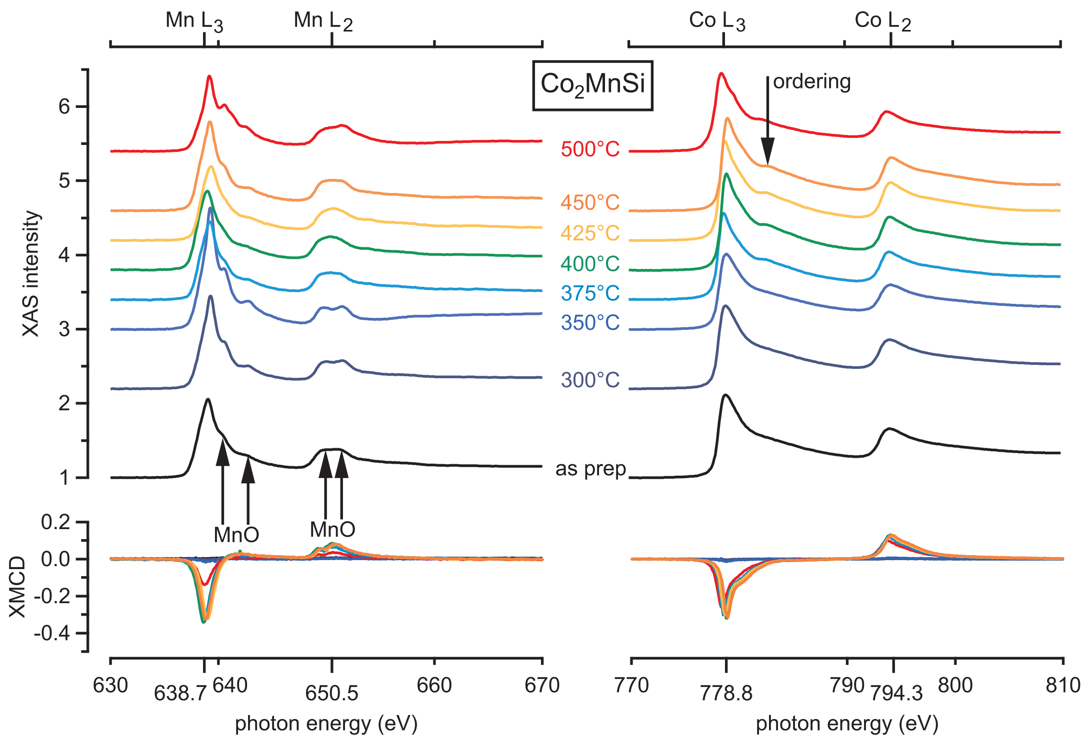

Mn L3
Mn L2
Co L3
Co L2
Co2MnSi
ordering
500°C
450°C
425°C
400°C
375°C
350°C
300°C
as prep
XAS intensity
MnO
MnO
XMCD
photon energy (eV)
photon energy (eV)

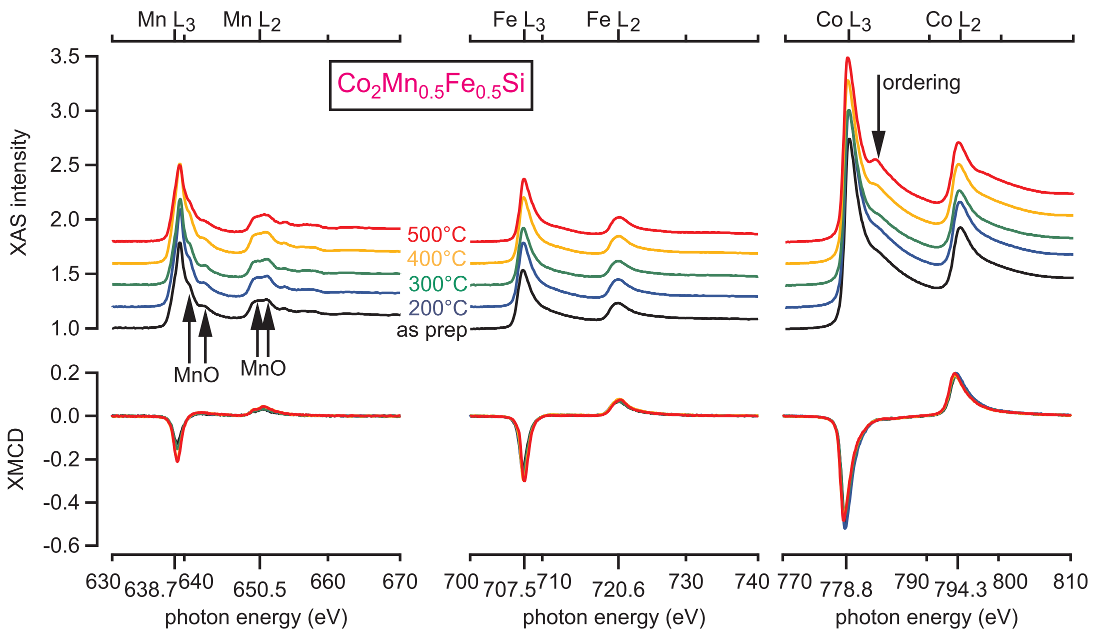

Mn L3
Mn L2
Fe L3
Fe L2
Co L3
Co L2
Co2Mn0.5Fe0.5Si
ordering
500°C
400°C
300°C
200°C
as prep
XAS intensity
MnO
MnO
XMCD
photon energy (eV)
photon energy (eV)
photon energy (eV)

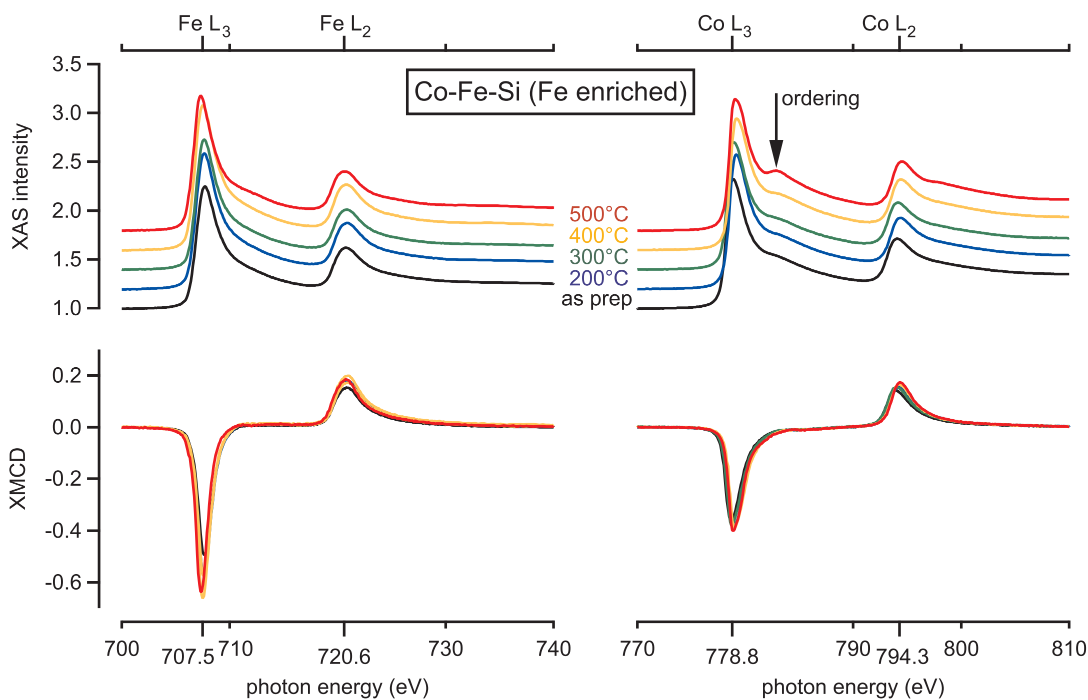
Fe L$_3$
Fe L$_2$
Co L$_3$
Co L$_2$
Co-Fe-Si (Fe enriched)
ordering
XAS intensity
500°C
400°C
300°C
200°C
as prep
XMCD
700
707.5
710
720.6
730
740
770
778.8
790
794.3
800
810
photon energy (eV)
photon energy (eV)

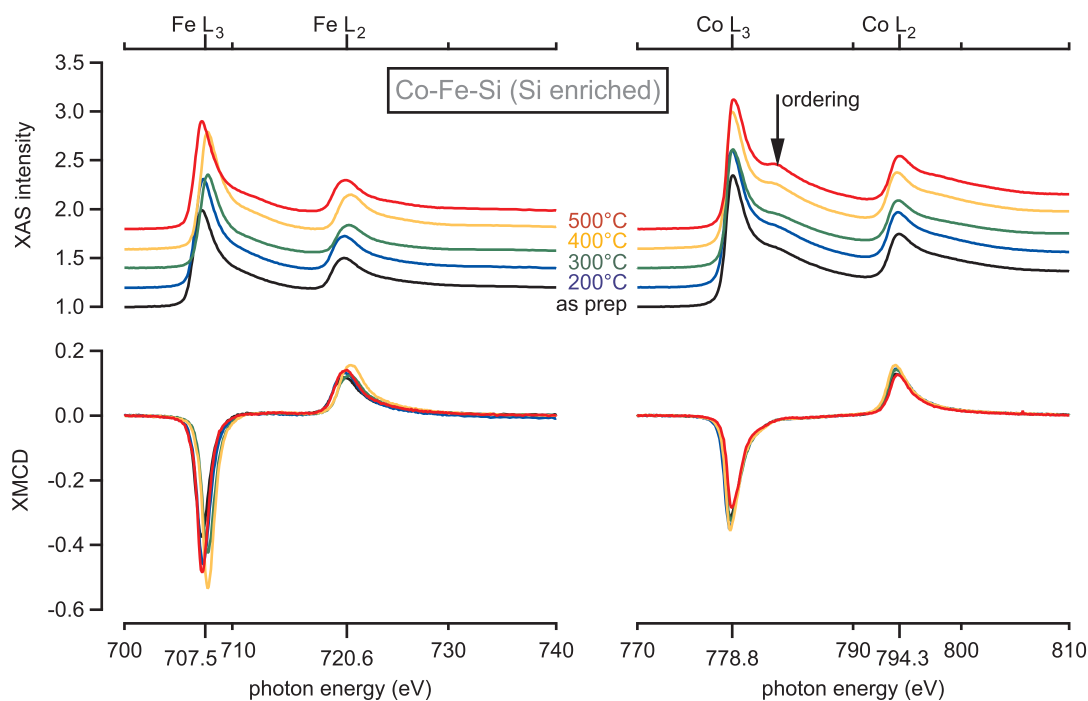
Fe L$_3$
Fe L$_2$
Co L$_3$
Co L$_2$
Co-Fe-Si (Si enriched)
ordering
XAS intensity
500°C
400°C
300°C
200°C
as prep
XMCD
700
707.5
710
720.6
730
740
770
778.8
790
794.3
800
810
photon energy (eV)
photon energy (eV)

Journal of Magnetism and Magnetic Materials 322 (2010) 996–998

Contents lists available at ScienceDirect

Journal of Magnetism and Magnetic Materials

journal homepage: www.elsevier.com/locate/jmmm

Low B2 crystallization temperature and high tunnel magnetoresistance in $Co_2FeAl/MgO/Co-Fe$ magnetic tunnel junctions

D. Ebke *, P. Thomas, O. Schebaum, M. Schäfers, D. Nissen, V. Drewello, A. Hütten, A. Thomas

Thin Films and Physics of Nanostructures, Bielefeld University, Germany

ARTICLE INFO

Article history:
Received 19 November 2009
Available online 11 December 2009

Keywords:
Tunnel magnetoresistance
Heusler
Magnetic thin film

ABSTRACT

We present tunnel magnetoresistance values of up to 147% at room temperature and 273% at 13 K for MgO-based magnetic tunnel junctions with Co_2FeAl and Co–Fe electrodes. The magnetic moment and coercive field were examined as a function of the annealing temperature by alternating gradient magnetometer investigations. This is compared with X-ray diffraction studies of the same samples and all results are contrasted to similar layer stacks based on the Heusler compound Co_2MnSi.

© 2009 Elsevier B.V. All rights reserved.

1. Introduction

To date, four kinds of materials have been theoretically predicted to show half metallic behavior, i.e. they are 100% spin polarized at the Fermi level E_F. These material classes are oxide compounds such as Fe_3O_4 and CrO_2 [1], perovskites (e.g. $LaSrMnO_3$ [2]), zinc-blende-type CrAs [3] and Heusler compounds [4]. In particular, Co-based Heusler compounds are the promising materials for spintronics applications due to the required high Curie temperatures T_C [5]. A Heusler compound is given by the composition X_2YZ in the $L2_1$ structure, where X and Y are transition metal elements and Z is a group III, IV or V element.

In 2004, room temperature tunnel magneto resistance (TMR) ratios of more than 100% were reported for MgO-based magnetic tunnel junctions (MTJs) [6,7]. Recently, Ikeda et al. presented TMR ratios of over 600% at room temperature and over 1100% at low temperatures [8]. High room temperature TMR ratios have also been reported for magnetic tunnel junctions containing $L2_1$- type-structured Heusler compounds as electrodes: 217% for Co_2MnSi [9] and 220% for $Co_2Fe_{0.5}Al_{0.5}Si$ [10]. A maximum TMR ratio of about 50% was found for B2-type-structured Co_2FeAl so far [10,11].

The predicted half-metallicity for Heusler compounds should lead to much higher TMR ratios. Nevertheless, one has to meet two challenges to achieve half-metallicity: $L2_1$ structure of the Heusler electrode(s) and coherent interfaces of the Heusler compound and the MgO tunnel barrier. It was reported by Tezuka et al. that Si is important for a good ordering of the Heusler compound $Co_2FeAl_{0.5}Si_{0.5}$ [18], because Co_2FeSi is easy to fabricate in the $L2_1$ structure, whereas Co_2FeAl has only B2-type structure. Here, we present high room temperature TMR ratios for the Heusler compound Co_2FeAl. Additionally, the low B2 crystallization temperature allows us to propose Co_2FeAl as a buffer layer for other Heusler compounds.

2. Preparation

DC/RF magnetron sputtering was used for the preparation of our magnetic tunnel junctions. All films were deposited at room temperature. A base pressure of 1.0×10^{-7} mbar of the sputtering system can be achieved; the Argon process pressure is about 1.5×10^{-3} mbar. The layers were deposited on an MgO (0 0 1) substrate covered by a 5 nm thick MgO buffer layer to coat surface contaminations. Thereafter, the lower electrode containing of 20 nm Co_2FeAl (or Co_2MnSi) was deposited from a stoichiometric target and followed by the MgO tunnel barrier. The lattice mismatch of about 5% of MgO ($4.21 \times \sqrt{2} = 5.95$Å [12]) and the Co_2FeAl compound (5.69 Å in our case) rotated by 45° allows for a coherent growth of the layer stack. Afterwards, the counter electrode composed of 5 nm of $Co_{70}Fe_{30}$, 10 nm of $Mn_{83}Ir_{17}$, 40 nm of Ru and 20 nm of Au was deposited. This electrode was omitted for the AGM and XRD measurements. The layer stacks were ex situ vacuum annealed at different temperatures to induce crystallization and ordering of the lower layer stack up to the Co–Fe electrode. The samples were cooled in a magnetic field of 0.65 T to set the exchange bias of the pinned electrode and patterned by optical lithography and ion beam etching. All transport characterizations were carried out by conventional two-terminal measurements.

3. Results and discussion

The magnetic major and minor loop of the junction with the highest TMR ratio is shown in Fig. 1. A TMR ratio of about 147% at

* Corresponding author.
E-mail address: debke@physik.uni-bielefeld.de (D. Ebke).
URL: http://www.spinelectronics.de (D. Ebke).

0304-8853/$ - see front matter © 2009 Elsevier B.V. All rights reserved.
doi:10.1016/j.jmmm.2009.12.003

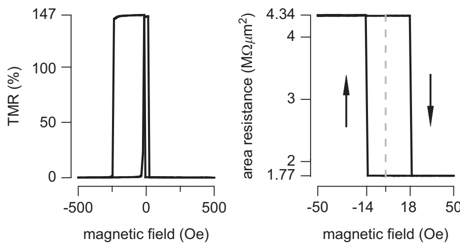

Fig. 1. Magnetic major and minor loops of a Co_2FeAl/MgO(2.1 nm)/Co–Fe/Mn–Ir magnetic tunnel junction annealed at 450 °C and measured at room temperature. The pinned upper electrode allows a well-defined determination of the TMR ratio in Fig. 4.

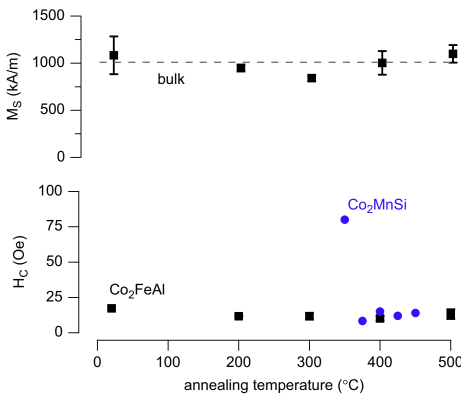

Fig. 2. Room temperature AGM investigations of MgO/Co_2FeAl/MgO layers. Top: magnetization, bottom: coercive field in comparison with Co_2MnSi MOKE investigations. Co_2MnSi is not ferromagnetic for annealing temperatures below 350 °C.

room temperature and more than 270% at 13 K was achieved. This is about 3 times the value previously reported by Inomata/Tezuka et al. for this compound [10,11].

Fig. 2 shows the magnetization for different annealing temperatures of the Co_2FeAl layers investigated by an alternating gradient field magnetometer (AGM) at room temperature. The calculated bulk magnetic moment of $4.99\mu_B$ (1007 kA/m and assuming $L2_1$ structure with a lattice constant of 5.69 Å) represented by the dashed line is reached independently of the annealing temperature. This is in good agreement with the Slater–Pauling behavior and the calculated total moment by Galanakis in 2005 [13].

The coercive field H_c of the soft magnetic Heusler electrode is about 20 Oe for all annealing temperatures in the case of Co_2FeAl. The Co_2MnSi exhibits a change in H_c from 80 to 9 Oe between 350 °C and 375°C, which hints to a structural change between these temperatures.

The high magnetization as well as the low coercive field of the Co_2FeAl suggest that crystallization and/or ordering can already be achieved prior to the annealing of the layer stacks. It is planned to investigate the damping parameters in Heusler compounds by, e.g. ferromagnetic resonance [14] and the specific magnon excitations by inelastic electron tunneling spectroscopy [15].

The structural change is further studied by X-ray diffraction (XRD) in Fig. 3 and again compared with Co_2MnSi. Four peaks are visible in the $\Theta/2\Theta$ scan: The MgO substrate shows the (0 0 2) peak of the Cu–K_α at 42.9° and the parasitic Cu–K_β radiation at 38.6°. The peaks at 31.4° and 65.6° can be attributed to Co_2FeAl (0 0 2) and (0 0 4), respectively. The peaks are already present in the as prepared state. In particular, the absent (0 2 2) at 45.0° and (1 1 1) at 27.1° peaks indicate a good (0 0 1) texture of the Co_2FeAl. A B2 structure, represented by the presents of a (0 0 2) peak, can be found for all annealing temperatures. This is in contrast to the behavior reported by Tezuka et al. [18]. Ordering into the $L2_1$ structure can be excluded from performed pole figure scans and the absence of a (1 1 1) peak. We found a lattice constant of $a = 5.69$ Å that is not influenced by the annealing temperature.

The XRD-scans of the Co_2MnSi compound explain the findings of the AGM investigations. No Heusler peaks are visible below 350 °C. Above 350 °C, the (0 0 1) peaks appear indicating a good texture of the films. Further investigations will show if a MgO/Co_2FeAl buffer layer underneath another Heusler compound allows to induce a low crystallization temperature, for example,

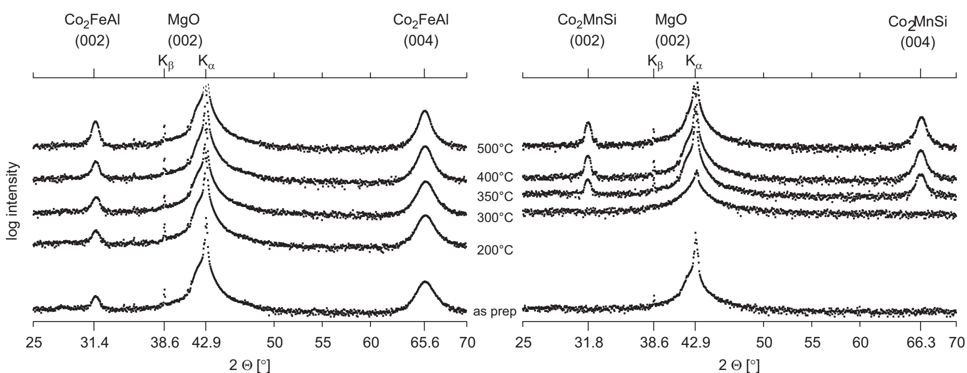

Fig. 3. XRD $\Theta/2\Theta$ scan of MgO/Heusler/MgO deposited on MgO substrates. For comparison, the baseline of the measurements is shifted with regard to the annealing temperature. (left) Co_2FeAl, (right) Co_2MnSi.

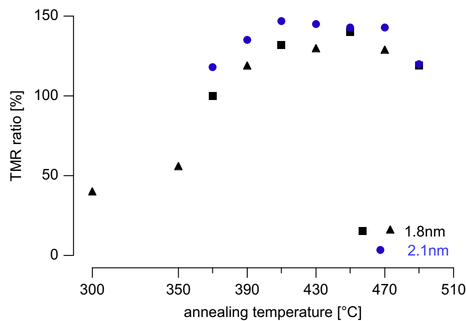

Fig. 4. Room temperature TMR ratios for $Co_2FeAl/MgO/Co{-}Fe$ junctions at different annealing temperatures. The squares and triangles indicate the two different subsequently annealed samples for the 1.8 nm thick MgO barrier.

for Co_2MnSi. This was previously shown for Co_2FeSi/Co_2MnSi multi-layers [16].

The transport properties of magnetic tunnel junctions were measured as a function of the magnetic field for 1.8 and 2.1 nm thick MgO barriers. Except as noted otherwise, all measurements were done at room temperature and the applied bias voltage was 10 mV. Fig. 4 shows increasing TMR ratio with increasing annealing temperature, probably due to an improvement of the crystallinity of the Heusler/tunnel barrier interface. This is commonly found in the conventional Co–Fe–B/MgO/Co–Fe–B MTJs [8].

The junctions show a good annealing temperature stability, the TMR ratio stays roughly constant for temperatures between 410 °C and 470 °C. This is in contrast to other studies, where the Mn diffusion of the Mn–Ir toward the upper barrier interface was thought to be responsible for the decrease of the TMR ratio beyond 400 °C [17]. On the other hand, a similar behavior was reported by Kant et al. and Palusker et al. [19–21].

A maximum TMR ratio of 147% at room temperature can be achieved for junctions with 2.1 nm MgO, which were annealed for 1 h at 450 °C. The same junctions show about 270% TMR at 13 K. The highest room temperature TMR values for Heusler compounds are reported for $Co_2MnSi/MgO/CoFe$ (217% TMR) [9] and $Co_2FeAl_{0.5}Si_{0.5}/MgO/Co_2FeAl_{0.5}Si_{0.5}$ (220% TMR) junctions [10]. In both cases, the high degree of $L2_1$ order rationalizes the high TMR ratios. In addition, the latter paper explains the large TMR values by the shift of the Fermi energy into the middle of the band gap.

In the future, we plan to compare ab initio transport calculations of MgO-based MTJs with Heusler electrodes (cp. Heiliger et al. for Fe/MgO/Fe [22]) to get a more detailed description of those systems. To clarify the detailed structure of the Co_2FeAl electrode, cross-sectional high-resolution transmission electron microscopy (HRTEM) investigations are planed, too [23].

4. Summary

In summary, we investigated the magnetic, structural and transport properties of the Heusler compound Co_2FeAl. We have shown that the full magnetization value of $4.9\mu_B$ and high room temperature TMR ratios of about 150% can be reached. The Co_2FeAl layers show (0 0 1) texture in the B2 structure already in the as prepared state.

The authors gratefully acknowledge the German Bundesministerium für Bildung und Forschung (BMBF) for financial support within the project HeuSpin. We are indebted to C. Heiliger for stimulating discussions.

References

[1] J.M.D. Coey, M. Venkatesan, J. Appl. Phys. 91 (2002) 8345.
[2] W.E. Picket, D.J. Singh, J. Magn. Magn. Mater. 172 (1997) 237.
[3] H. Akinaga, T. Manago, M. Shirai, Jpn. J. Appl. Phys. 39 (2000) L1118.
[4] R.A. de Groot, F.M. Mueller, P.G. van Engen, K.H.J. Buschow, Phys. Rev. Lett. 50 (1983) 2024.
[5] P.J. Webster, J. Phys. Chem. Solids 32 (1971).
[6] S. Yuasa, T. Nagahama, A. Fukushima, Y. Suzuki, K. Ando, Nat. Mater. 3 (2004) 868–871.
[7] S.S.P. Parkin, C. Kaiser, A. Panchula, P.M. Rice, B. Hughes, M. Sament, S.-H. Yang, Nat. Mater. 3 (2004) 862–867.
[8] S. Ikeda, J. Hayakawa, Y. Ashizawa, Y.M. Lee, K. Miura, H. Hasegawa, M. Tsunoda, F. Matsukura, H. Ohno, Appl. Phys. Lett. 93 (2008) 082508.
[9] S. Tsunegi, Y. Sakuraba, M. Oogane, K. Takanashi, Y. Ando, Appl. Phys. Lett. 93 (2008) 112506.
[10] K. Inomata, N. Ikeda, N. Tezuka, R. Goto, S. Sugimoto, M. Wojcik, E. Jedryka, Sci. Technol. Adv. Mater. 9 (2008) 014101.
[11] N. Tezuka, N. Ikeda, A. Miyazaki, S. Sugimoto, M. Kikuchi, K. Inomata, Appl. Phys. Lett. 89 (2006) 112514.
[12] Moscow University Geology Bulletin 47 (1992) 80.
[13] I. Galanakis, Phys. Rev. B 71 (2005) 012413.
[14] K.W. Chou, A. Puzic, H. Stoll, G. Schütz, B. Van Waeyenberge, T. Tyliszczak, K. Rott, G. Reiss, H. Brückl, I. Neudecker, D. Weiss, C.H. Back, J. Appl. Phys. 99 (2006) 08F305.
[15] J. Schmalhorst, S. Kämmerer, G. Reiss, A. Hütten, Appl. Phys. Lett. 86 (2005) 052501.
[16] D. Ebke, J. Schmalhorst, N.-N. Liu, A. Thomas, G. Reiss, A. Hütten, Appl. Phys. Lett. 89 (2006) 162506.
[17] J. Hayakawa, S. Ikeda, Y.M. Lee, F. Matsukura, H. Ohno, Appl. Phys. Lett. 89 (2006) 232510.
[18] N. Tezuka, S. Okamura, A. Miyazaki, M. Kikuchi, K. Inomata, in: 50th Annual Conference on Magnetism and Magnetic Materials, AIP, vol. 99, 2006, p. 08T314.
[19] P.V. Paluskar, C.H. Kant, J.T. Kohlhepp, A.T. Filip, H.J.M. Swagten, B. Koopmans, W.J.M. de Jonge, in: 49th Annual Conference on Magnetism and Magnetic Materials, AIP, vol. 97, 2005, p. 10C925.
[20] C.H. Kant, J.T. Kohlhepp, H.J.M. Swagten, W.J.M. de Jonge, Appl. Phys. Lett. 84 (2004) 1141–1143.
[21] C.H. Kant, J.T. Kohlhepp, P.V. Paluskar, H.J.M. Swagten, W.J.M. de Jonge, J. Magn. Magn. Mater. 286 (2005) 154–157.
[22] C. Heiliger, M. Gradhand, P. Zahn, I. Mertig, Phys. Rev. Lett. 99 (2007) 066804.
[23] H. Sukegawa, W. Wang, R. Shan, T. Nakatani, K. Inomata, K. Ono, Phys. Rev. B 79 (2009) 184418.

APPLIED PHYSICS LETTERS **95**, 232510 (2009)

Tunneling spectroscopy and magnon excitation in $Co_2FeAl/MgO/Co-Fe$ magnetic tunnel junctions

Daniel Ebke, Volker Drewello,[a] Markus Schäfers, Günter Reiss, and Andy Thomas
Thin Films and Physics of Nanostructures, Bielefeld University, 33615 Bielefeld, Germany

(Received 3 November 2009; accepted 16 November 2009; published online 10 December 2009)

Magnetic tunnel junctions with the Heusler compound Co_2FeAl as the soft electrode are prepared. Pinned Co–Fe is used as the hard reference electrode. The junctions show a high tunnel magnetoresistance ratio of 273% at 13 K. The electronic transport characteristics are investigated by tunneling spectroscopy—dI/dV and d^2I/dV^2 are discussed. In the parallel magnetic state the tunneling spectra are asymmetric with respect to the bias voltage, with a pronounced bias-independent region. In the antiparallel state the dependence on bias voltage is much stronger and the curves are symmetric. The findings can be explained with a gap in the minority density of states of Co_2FeAl. © *2009 American Institute of Physics*. [doi:10.1063/1.3272947]

In the recent years spintronic devices have been highly anticipated. It is essential to improve such systems' performance to make them become a commercial reality. In spintronic devices like magnetic sensors, reconfigurable logic, and magnetic random access memory cells[1] it is of crucial interest to increase the tunneling magnetoresistance (TMR) effect of the underlying magnetic tunnel junctions (MTJs). One way to gain this higher effect is by using electrodes with high spinpolarization. Prominent candidates in this category are the Heusler compounds. Recently high TMR ratios were reported with Heusler based MTJs; 217% for Co_2MnSi (Ref. 2) and 220% for $Co_2Fe_{0.5}Al_{0.5}Si$.[3] The high TMR ratios for Heusler based MTJs were explained by the predicted half-metallic behavior of the used Heusler compounds. This explanation was supported by tunneling spectroscopy measurements, which showed a pronounced gap structure.[4–7] The highest reported TMR ratio for Co_2FeAl is 54%[3,9] so far. In this letter we present tunneling spectroscopy measurements (dI/dV and d^2I/dV^2 are discussed) of Co_2FeAl based tunnel junctions with MgO barrier. These junctions show up to 153% and 273% TMR ratio at room and low temperature, respectively.

The MTJs are prepared in a magnetron sputter system with a base pressure of 1×10^{-7} mbar and a Argon working pressure of approximately 1.5×10^{-3} mbar. The layer stack used in this work is MgO (001) substrate/MgO 5/Co_2FeAl (CFA) 20/MgO 2.1/Co–Fe 5/MnIr 10/Ru 40 (all values in nm). The samples are annealed in a vacuum furnace for 60 min at a optimized temperature of 723 K. Details of the preparation and optimization of the samples will be published elsewhere.[8] The samples are patterned by laser lithography and ion beam etching. The resulting patterns are squares of 100 μm^2. These structures are capped with gold contact pads.

The low temperature measurements are done at 13 K in a closed cycle Helium cryostat by a standard two probe technique. The bias voltage is always defined with respect to the upper electrode. Thus, negative bias results in electrons tunneling into the upper electrode. A lock-in technique is used to derive the dI/dV curves which are differentiated numerically to get the inelastic electron tunneling (IET) spectra (d^2I/dV^2). Details of the measurement setup and procedure can be found elsewhere.[10]

Figure 1 shows a major loop of the CFA MTJ at 13 K. The sample exhibits a TMR ratio of 273% with well defined parallel (P) and antiparallel (AP) states. Figure 2(a) shows spectroscopic data obtained in the P state at −500 Oe. The dI/dV data was normalized to $dI/dV(V=0)$ to allow a better comparison. A striking asymmetry in the dI/dV-data is found with respect to the bias polarity. For negative bias the conductance shows a very weak dependence on the bias voltage up to −140 mV. For positive bias up to $V=25$ mV the conductance sharply increases. For $V>25$ mV the slope reduces visibly. At 270 mV the dI/dV-signal has a local maximum, followed by a decrease and a pronounced minimum at 350 mV. These features can more clearly be seen in the IET spectrum. For -140 mV$<V<0$ mV the spectrum shows only small peaks around zero height, while for $0<V<270$ mV the peaks are larger and always positive. The local minimum in the IET spectrum is located at 290 mV with an additional small feature at 350 mV. Figure 2(b) shows the spectroscopic data for the AP state at 250 Oe. The asymmetry is much smaller here. A sharp increase of dI/dV is found for both bias polarities. However, for negative bias a distinct kink is found at −70 mV, whereas for positive bias the transition to the flatter part is much smoother. Again, the IET spectrum can show these features more clearly. For

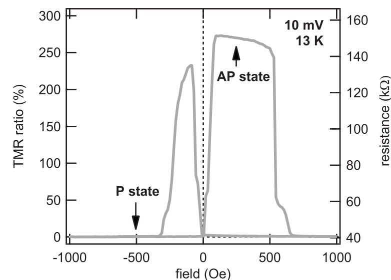

FIG. 1. Major loop of a CFA MTJ. Arrows mark the field and resistance values at which spectroscopy is performed.

[a]Electronic mail: drewello@physik.uni-bielefeld.de.

0003-6951/2009/95(23)/232510/3/$25.00 © 2009 American Institute of Physics

Downloaded 04 Jan 2010 to 129.70.28.22. Redistribution subject to AIP license or copyright; see http://apl.aip.org/apl/copyright.jsp

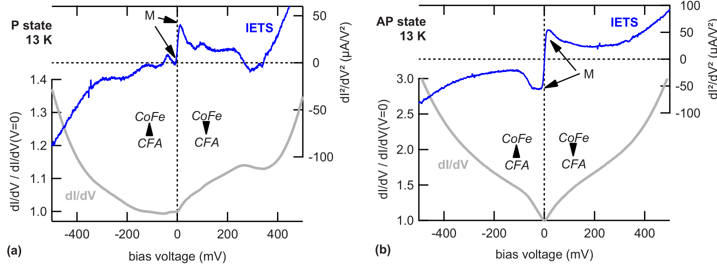

FIG. 2. (Color online) Tunneling and IET spectra of a CFA MTJ in (a) P state and (b) AP state.

-10 mV$<V<0$ mV there is a sharp increase to a broad plateau region up to -50 mV. For $V<-50$ mV the signal rapidly decreases. For positive bias the signal also increases rapidly up to $V=10$ mV. Unlike negative bias there is no plateau and for $V>10$ mV the signal slowly decreases with a small shoulder around 90 mV. For $V<-100$ mV the IETS signal increases monotonically and smoothly. For positive bias $V>200$ mV this is also the case, except for a small feature located at 350 mV as in the P state.

The measurements at small bias in both magnetic states will now be discussed. The flat region for -140 mV$<V<0$ of the dI/dV-curve in the P state can be understood with the assumption that a gap is present in the minority density of states (DOS) of CFA while the majority DOS is not varying much in this region. Majority electrons can tunnel from the CFA into Co–Fe. The constant DOS leads to a constant conductance. Minority electrons are not available to tunnel into Co–Fe. The gap structure ends at approximately -140 mV where dI/dV strongly increases. Here the lower end E_V of the minority gap is reached and electrons can tunnel from the minority "valence band" of CFA in the minority states of Co–Fe. This additional minority tunneling channel increases the conductance for $V<-140$ mV. Similar results have been shown for $Co_2MnSi/Al-O/Co-Fe$,[4,5] for $Co_2Fe_xMn_{1-x}Si/Al-O/Co-Fe$,[6] and for $Co_2FeAl_{0.5}Si_{0.5}/(MgAl_2)-O/Co-Fe$.[7] The immediate rise of dI/dV for $V\geq 0$ can be interpreted as the upper end of the gap just above the Fermi energy E_F. This would mean that the separation of the Fermi energy and the conductance band (in the minority channel) is $E_C\approx 0$.

But there is a different way to look at it. The IET spectrum for the P state [Fig. 2(a)] is not completely flat but shows some features for $V<0$. Especially the first peak (M) is interesting as it shows the excitation of magnons by tunneling electrons with excess energies. Compared to the peak for $V>0$ this peak is very small. In the AP state [Fig. 2(b)] the peaks (M) are of the same size for both bias polarities. Magnon excitation is known to be one of the main reasons for the temperature dependence and low bias behavior of the TMR ratio.[11,12] In Table I an overview of the first-order magnon excitation processes is given. There are four cases regarding to magnetic state and bias voltage polarity. With the assumption of a gap in the CFA minority states none of the processes involving CFA minority electrons are available (marked red/italic). Also, absorption of magnons has a far lower probability at low temperatures than the excitation.

These simple assumptions lead to one case where no magnon excitation is possible: for negative bias voltage in the P state.

Basically, this is what the IET spectra show. The 'forbidden' peak is finite but very small. This can be explained with the assumption of very few minority states in CFA instead of none. Then only very few minority electrons are available to tunnel into the Co–Fe and excite magnons. For positive bias the tunneling essentially is the same as in the case of a distinctive gap. Many minority electrons are available and a tunneling minority electron can excite a magnon, is spin-flip scattered to a majority state of which plenty are available. A small but finite minority DOS could be the result of imperfect ordering. On the other hand, a finite DOS has been predicted below E_F for CFA by some calculations.[13,14] There, most of the residual minority states originate from Fe d-orbitals. As the tunneling electrons are s-like those states are not accessible through the tunneling process. There is also the possibility of interface states that have been predicted[15] and found[16] for other Heusler compounds.

Please note, the presented model gives a reason for the strong increase in conductance, at least for $0<V<25$ mV (in the P state). It can simply be caused by magnons excited only in Co–Fe. Thus, there is no need for a band gap edge near E_F and $E_C\approx 0$ cannot be concluded (nor excluded) in this case.

In Fig. 3 both IET spectra are shown for comparison. The difference for negative bias is obvious, but for positive bias the spectra are comparable. In the AP state the magnon peak is stronger because the magnon excitation only needs majority electrons/states (see Table I). Also the direct tunneling processes are less probable and the relative change

TABLE I. Overview of first order magnon excitation/absorption in the tunneling process. Here, E(e) is an electron in a CFA majority (minority) state, F(f) is an electron in a Co–Fe majority (minority) states and +m(−m) is the emission (absorption) of a magnon. A small DOS or a less probable absorption is marked italic.

	Negative bias	Positive bias
	CFA→Co–Fe	Co–Fe→CFA
P	E→f, *−m*	F→*e*, *−m*
	e→F, +m	f→E, +m
AP	E→F, +m	F→E, +m
	e→f, *−m*	f→*e*, *−m*

Downloaded 04 Jan 2010 to 129.70.28.22. Redistribution subject to AIP license or copyright; see http://apl.aip.org/apl/copyright.jsp

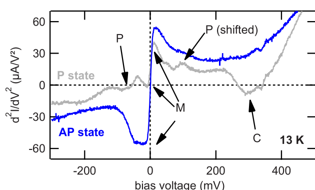

FIG. 3. (Color online) Comparison of IET spectra for both magnetic states.

through magnon excitation is higher. The similarity ends at the large dip at 290 mV in P state. The structure is assumed to be a signature of coherent tunneling in MTJs with MgO barrier.[2,17,18] For negative bias it is not visible, supposedly because of the structure of the minority DOS of CFA.

On a minor note, additional peaks are visible in the IET spectra. They are all much smaller that the magnon peaks around $V=0$. For $V>0$ a shoulder at ≈45 mV and a peak around 100 mV are visible. The shoulder might be related to magnons of higher order. The peak around 100 mV is presumably the peak of barrier phonon excitation, which is typical for tunnel junctions[19] and found at 81 mV[18,20] for Mg–O and 120 mV for Al–O phonons. Here, the position of 100 mV might be related to stress at the CFA/MgO interface or a partial oxidation of the CFA surface (Al–O). This cannot be clarified here. For $V<0$ the IETS signal is much flatter. Additional peaks can only be estimated around −80 to −90 mV. This would fit to the known Mg–O phonon peak position.

In summary, we prepared MTJs with Co_2FeAl bottom electrodes, which show up to 273 and 153% TMR ratio at 13 K and room temperature, respectively. Tunneling spectroscopy measurements showed a large asymmetry of the conductance in the P state, but only small variations in the AP state. These findings can be explained with a gap in the minority DOS of CFA.

We gratefully acknowledge Jan Schmalhorst and Andreas Hütten for helpful discussions and the DFG (Grant No. RE 1052/13-1) and BMBF (Heuspin) for financial support.

[1]G. A. Prinz, Science **282**, 1660 (1998).
[2]S. Tsunegi, Y. Sakuraba, M. Oogane, K. Takanashi, and Y. Ando, Appl. Phys. Lett. **93**, 112506 (2008).
[3]K. Inomata, N. Ikeda, N. Tezuka, R. Goto, S. Sugimoto, M. Wojcik, and E. Jedryka, Sci. Technol. Adv. Mater. **9**, 014101 (2008).
[4]Y. Sakuraba, T. Miyakoshi, M. Oogane, Y. Ando, A. Sakuma, T. Miyazaki, and H. Kubota, Appl. Phys. Lett. **89**, 052508 (2006).
[5]T. Ishikawa, T. Marukame, H. Kijima, K.-I. Matsuda, T. Uemura, M. Arita, and M. Yamamoto, Appl. Phys. Lett. **89**, 192505 (2006).
[6]T. Kubota, S. Tsunegi, M. Oogane, S. Mizukami, T. Miyazaki, H. Naganuma, and Y. Ando, Appl. Phys. Lett. **94**, 122504 (2009).
[7]R. Shan, H. Sukegawa, W. H. Wang, M. Kodzuka, T. Furubayashi, T. Ohkubo, S. Mitani, K. Inomata, and K. Hono, Phys. Rev. Lett. **102**, 246601 (2009).
[8]D. Ebke, P. Thomas, V. Drewello, O. Schebaum, M. Schäfers, D. Nissen, A. Hütten, and A. Thomas (accepted).
[9]N. Tezuka, N. Ikeda, A. Miyazaki, S. Sugimoto, M. Kikuchi, and K. Inomata, Appl. Phys. Lett. **89**, 112514 (2006).
[10]V. Drewello, M. Schäfers, O. Schebaum, A. A. Khan, J. Münchenberger, J. Schmalhorst, G. Reiss, and A. Thomas, Phys. Rev. B **79**, 174417 (2009).
[11]S. Zhang, P. M. Levy, A. C. Marley, and S. S. P. Parkin, Phys. Rev. Lett. **79**, 3744 (1997).
[12]V. Drewello, J. Schmalhorst, A. Thomas, and G. Reiss, Phys. Rev. B **77**, 014440 (2008).
[13]M. Sargolzaei, M. Richter, K. Koepernik, I. Opahle, H. Eschrig, and I. Chaplygin, Phys. Rev. B **74**, 224410 (2006).
[14]K. Özdoğan, B. Aktaş, I. Galanakis, and E. Şaşioğlu, J. Appl. Phys. **101**, 073910 (2007).
[15]Y. Miura, H. Uchida, Y. Oba, K. Abe, and M. Shirai, Phys. Rev. B **78**, 064416 (2008).
[16]T. Ishikawa, N. Itabashi, and T. Taira, K. Matsuda, T. Uemura, and M. Yamamoto, Appl. Phys. Lett. **94**, 092503 (2009).
[17]R. Matsumoto, Y. Hamada, M. Mizuguchi, M. Shiraishi, H. Maehara, K. Tsunekawa, D. D. Djayaprawira, N. Watanabe, Y. Kurosaki, T. Nagahama, A. Fukushima, H. Kubota, S. Yuasa, and Y. Suzuki, Solid State Commun. **136**, 611 (2005).
[18]G.-X. Miao, K. B. Chetry, A. Gupta, W. H. Butler, K. Tsunekawa, D. Djayaprawira, and G. Xiao, J. Appl. Phys. **99**, 08T305 (2006).
[19]E. Wolf, in *Principles of Electron Tunneling Spectroscopy, International Series of Monographs on Physics No. 71*, edited by R. Elliot, J. Krumhansl, W. Marshall, and D. Wilkinson (Oxford University Press, New York, 1989).
[20]J. G. Adler, Solid State Commun. **7**, 1635 (1969).

Downloaded 04 Jan 2010 to 129.70.28.22. Redistribution subject to AIP license or copyright; see http://apl.aip.org/apl/copyright.jsp

X-Ray Absorption and Magnetic Circular Dichroism Studies of Co_2 FeAl in Magnetic Tunnel Junctions

Daniel Ebke[1], Zoë Kugler[1], Patrick Thomas[1], Oliver Schebaum[1], Markus Schäfers[1], Dennis Nissen[1], Jan Schmalhorst[1], Andreas Hütten[1], Elke Arenholz[2], and Andy Thomas[1]

[1]Thin Films and Physics of Nanostructures, Physics Department, Bielefeld University, Bielefeld 33615, Germany
[2]Advanced Light Source, Lawrence Berkeley National Laboratory, Berkeley, CA 94720 USA

The bulk magnetic moment and the element specific magnetic moment of Co_2FeAl thin films were examined as a function of annealing temperature by alternating gradient magnetometer (AGM) and X-ray absorption spectroscopy (XAS)/X-ray magnetic circular dichroism (XMCD), respectively. A high magnetic moment can be achieved for all annealing temperatures and the predicted bulk and interface magnetic moment of about 5 μ_B are reached via heating. We will also present tunnel magnetoresistance (TMR) values of up to 153% at room temperature and 260% at 13 K for MgO based magnetic tunnel junctions (MTJs) with Co_2FeAl and Co-Fe electrodes.

***Index Terms*—Magnetic films, magnetoresistance, thin films, X-ray spectroscopy.**

I. Introduction

SPINTRONIC devices have found a lot of attention in the recent years due to the possible new applications, e.g., a magnetic random access memory (MRAM) [1], [2]. The spin of the electrons is used as an additional degree of freedom. In contrast to common electronic devices. Materials with a high spin polarization are eligible for applications. A half metallic behavior, i.e., they are 100% spin polarized at the Fermi level E_F has been theoretically predicted for some oxide compounds such as Fe_3O_4 and CrO_2 [3], perovskites (e.g., $LaSrMnO_3$ [4]), zinc-blende-type CrAs [5] and Heusler compounds [6]. In particular, Co-based Heusler compounds are promising materials for spintronics applications due to the required high Curie temperatures T_C [7]. A Heusler compound is given by the composition X_2YZ in the $L2_1$ structure, where X and Y are transition metal elements and Z is a group III, IV or V element. The main constituent of many spintronic devices is a magnetic tunnel junction (MTJ) with two ferromagnets separated by a thin insulating tunnel barrier [8]. The resistance of such a device depends on the magnetic orientation of the ferromagnets. Usually, R_{AP} (antiparallel) is higher than R_P (parallel) and a tunnel magnetoresistance (TMR) can be defined as $(R_{AP} - R_P)/R_P$.

Recently, TMR ratios of over 600% at room temperature for a single MgO tunnel barrier [9] and over 1000% for a double MgO barrier were reported [10]. High room temperature TMR ratios have also been reported for magnetic tunnel junctions containing Heusler compounds as electrodes: 217% for Co_2MnSi [11] and very recently 386% for $Co_2FeAl_{0.5}Si_{0.5}$ [12]. Later was grown by using molecular beam epitaxy in place of sputtering deposition. For Co_2FeAl a huge TMR ratio of up to 330% was found very lately, too [13]. The corresponding low temperature TMR ratios are much higher and one challenge is to conserve these values at room temperature, too. This might be realized by shifting the E_F into the middle of the bandgap [12] and is reported to be realized for the compound $Co_2FeAl_{0.5}Si_{0.5}$ which shows a lower temperature dependent TMR ratio compared to Co_2MnSi.

On the other hand, the huge TMR ratio of Co_2FeAl are reported to issue from a extremely flat surface morphology [13].

Here, we present X-ray absorption spectroscopy (XAS) and X-ray magnetic circular dichroism (XMCD) measurements of Co_2FeAl thin films which were performed at beamline 6.3.1 of the Advanced Light Source, Berkeley, USA. The Co- and Fe-$L_{3,2}$ edges were investigated. Surface-sensitive total electron yield TEY was recorded with a grazing angle of incidence of 30° to the sample surface. The XMCD spectra were obtained by applying a magnetic field of max ± 2 T along the x-ray beam direction using elliptically polarized radiation with a polarization of 60%. The XAS intensity and the XMCD effect are defined as $(I_+ + I_-)/2$ and $I_+ - I_-$, respectively. Here, I_+ and I_- name the parallel and antiparallel orientation of photon spin to the magnetic field. Furthermore, full MTJs containing a Co_2 FeAl electrode were prepared. A high room temperature TMR ratio with a similar low temperature dependence as reported for $Co_2FeAl_{0.5}Si_{0.5}$ can be found [12].

II. Preparation of Tunnel Junctions

DC/RF magnetron sputtering was used for the preparation of our magnetic tunnel junctions. All films were deposited at room temperature. A base pressure of 1.0×10^{-7} mbar of the sputtering system can be achieved; the Argon process pressure is about 1.5×10^{-3} mbar. The layers were deposited on a MgO (001) substrate covered by a 5 nm thick MgO buffer layer to coat surface contaminations. Thereafter, the lower electrode of 20 nm Co_2FeAl was deposited and followed by the MgO tunnel barrier. The lattice mismatch of about 5% of MgO ($4.21 \times \sqrt{2} = 5.95$ Å [14]) and the Co_2FeAl compound (5.70 Å in our case) rotated by 45 degrees allows for a coherent growth of the layer stack. Afterwards, the counter electrode composed of 5 nm $Co_{70}Fe_{30}$, 10 nm of $Mn_{83}Ir_{17}$, 40 nm Ru, and 20 nm Au was deposited. This electrode was omitted for the AGM and XMCD measurements. The layer stacks were ex-situ vacuum annealed at different temperatures to induce crystallization and

Manuscript received October 30, 2009; revised December 23, 2009; accepted January 06, 2010. Current version published May 19, 2010. Corresponding author: D. Ebke (e-mail: debke@physik.uni-bielefeld.de).

Color versions of one or more of the figures in this paper are available online at http://ieeexplore.ieee.org.

Digital Object Identifier 10.1109/TMAG.2010.2041049

0018-9464/$26.00 © 2010 IEEE

Authorized licensed use limited to: Universitaet Bielefeld. Downloaded on June 04,2010 at 10:24:58 UTC from IEEE Xplore. Restrictions apply.

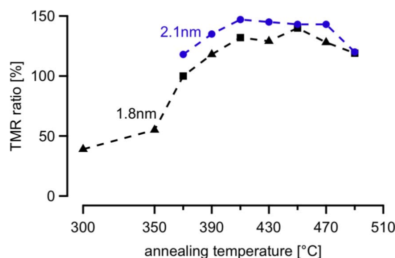

Fig. 1. Room temperature TMR ratios for Co_2FeAl/MgO/Co-Fe junctions at different annealing temperatures. The squares and triangles indicate the two different subsequently annealed samples for the 1.8 nm thick MgO barrier.

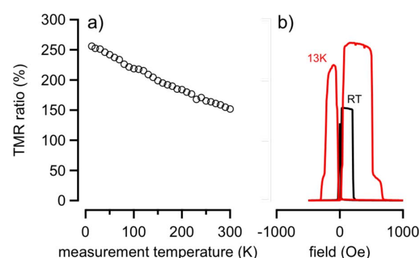

Fig. 2. Temperature dependent TMR ratio for Co_2FeAl/MgO/Co-Fe junctions (a) and the corresponding major loops for RT and 13 K (b).

ordering of the lower layer stack up to the Co-Fe electrode. The samples were cooled in a magnetic field of 0.65 T to set the exchange bias of the pinned electrode and patterned by optical lithography and ion beam etching to form the tunnel junctions. All transport characterizations were carried out by conventional two terminal measurements.

III. Results

The transport properties of the MTJs were measured as a function of an external magnetic field for 1.8 nm and 2.1 nm thick MgO barriers. The measurements were done in a temperature range between 13 K and room temperature. The applied bias voltage was 10 mV.

Fig. 1 depicts an increasing room temperature TMR ratio with increasing annealing temperature. This is also found in conventional Co-Fe-B/MgO/Co-Fe-B MTJs [9] and can probably be attributed to an improvement of the crystallinity of the Heusler/tunnel barrier interface.

Furthermore a good annealing temperature stability can be found for temperatures between 410°C and 470°C. The obtained TMR ratio stays roughly constant in this range. This is in contrast to other studies were the Mn diffusion of the Mn-Ir towards the upper barrier interface was thought to be responsible for the decrease of the TMR ratio beyond 400°C [15]. On the other hand, a similar behavior was reported by Kant *et al.* and Palusker *et al.* [16]–[18].

Fig. 2(a) shows the temperature dependent TMR ratio for a junction with a 2.1 nm thick MgO barrier and annealed for 1 h at 450°C. In contrast to the dependency found for Co_2MnSi [11] junctions ($\Gamma_{\rm CMS} = \rm TMR(LT)/TMR(RT) = 3.5$) it is comparable weak ($\Gamma_{\rm CFA} = 1.7$) as reported for $Co_2FeAl_{0.5}Si_{0.5}$[12] and Co_2FeAl [13] ($\Gamma_{\rm CFAS} = \Gamma_{\rm CFA} = 2.1$). Therefore, it has to be reconsidered if the origin of the reported weak temperature dependence is related to a shift of the Fermi level into the gap [12].

The corresponding major loops for room temperature and 13 K are shown in Fig. 2(b). A TMR ratio of 153% and 260% were achieved, respectively. This is only about half the value reported very recently by Wang *et al.* [13]. The lowered TMR ratio might be attributed to a higher surface roughness, caused by a different seed layer system. Further investigations of the origin are planed.

The element specific magnetic properties of the Co_2FeAl/MgO interface were investigated by surface sensitive X-ray absorption spectroscopy (XAS) and X-ray magnetic circular dichroism (XMCD). Both were measured at room temperature in total electron yield with a sampling depth of about 2 nm [19], [20].

Fig. 3 shows the Fe- and Co-XAS (Fig. 3(a)) and XMCD (Fig. 3(b)) spectra for the as prepared and annealed half junctions. The measured XAS intensity was normalized to the intensity prior the Fe-L_3 and Co-L_3 edge, respectively.

The arrows indicate prominent features in the XAS. In case of Co the shoulder can be attributed to a certain atomic and magnetic order of the Co_2FeAl compound at the barrier interface as previously reported for Co_2MnSi [21]. This feature is already present for the non-annealed sample and is pronounced with increasing annealing temperatures.

By contrast the shoulder in the Fe-XAS of the non-annealed layers is attributed to FeO [22]. The Fe might be oxidized during the sputtering of the MgO barrier. For annealing temperatures higher 200°C no FeO can be found from the XAS. The absent might be explained by the crystallization process of the barrier and the binding of O.

The corresponding Fe- and Co-XMCD in Fig. 3(b) shows an asymmetry for all annealing temperatures, i.e., a magnetic moment can be achieved even for the non-annealed Heusler layer. This is in contrast to the results for Co_2MnSi [21] and emphasizes the low ordering temperature of Co_2FeAl [23].

Fig. 4(a) shows the Fe- and Co-XAS intensity at the L_3 edge (I_{L3}, as defined in Fig. 3(a)) as a function of annealing temperature. Above annealing temperature of 200°C the XAS intensity decreases for Co and Fe, respectively. This might be because of an Al segregation towards the barrier interface to improve the Heusler structure.

The element specific magnetic moment was calculated from the XMCD by applying the sum rules [24]. A number of 3d holes $\rm n_d = 1.93$ for Co and $\rm n_d = 3.29$ for Fe were assumed. This was carried out from SPR-KKR density of band calculation [25]. As shown in Fig. 4(b) the magnetic moment of the Co atoms measure up to the predict value of 1.14 μB for the full

Authorized licensed use limited to: Universitaet Bielefeld. Downloaded on June 04,2010 at 10:24:58 UTC from IEEE Xplore. Restrictions apply.

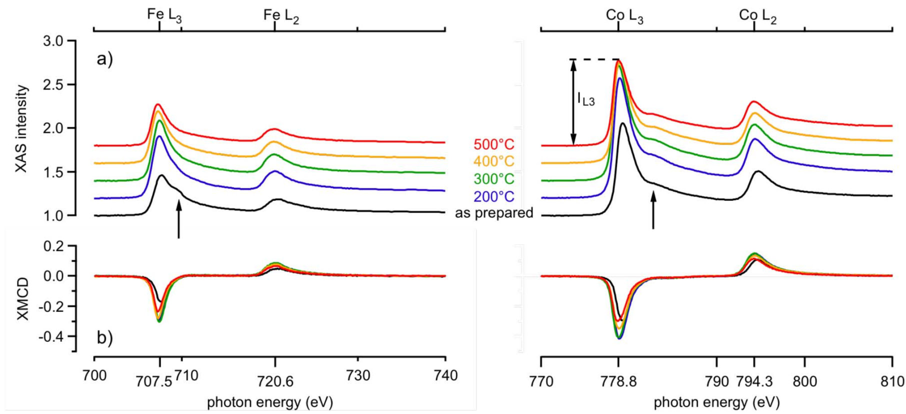

Fig. 3. Room temperature XAS (a) und XMCD (b) spectra at the Fe-$L_{3,2}$ and Co-$L_{3,2}$ edge, respectively for different annealing temperatures. The XAS intensities are normalized to the values prior the L_3 edge. For comparison the baseline of the measurement is shifted in regard to the annealing temperature. The arrows mark prominent XAS features.

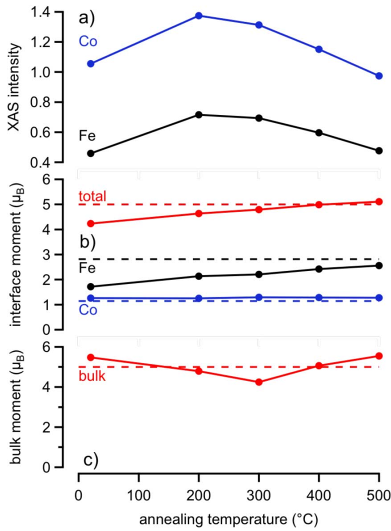

Fig. 4. Room temperature XAS(a), XMCD(b) and AGM (c) investigations of MgO/Co_2FeAl/MgO layers as a function of annealing temperature. (a) XAS intensity at the L3 edge of Co and Fe, respectively. (b) element specific moment (orbital + spin) of the barrier interface and the corresponding total moment $(2 \times m_{Co} + m_{Fe})$. (c) bulk moment of the Co_2FeAl layer.

range of annealing temperature. The reference values are represented by the dashed lines. In contrast the Fe magnetic moment is increased with increasing annealing temperatures and is close to the predicted value of 2.81 μB for the 500°C annealed sample [26]. This might be because of the reduction of FeO. A similar behavior is found for the total moment resulting from $2 \times m_{Co} + m_{Fe}$. The predicted bulk value of 4.99 μB can be reached for annealing temperatures higher 400°C [26].

This is also found for the bulk moment of the Co_2FeAl layers that was investigated by an alternating gradient field magnetometer (AGM) at room temperature. Here, the reported bulk value of 4.99 μB (1007 kA/m and assuming $L2_1$ structure with an experimental lattice constant of 5.69 Å) is reached independently of annealing temperature.

IV. Conclusion

We have investigated the magnetic and electronic transport properties of the Heusler compound Co_2FeAl. A low temperature TMR ratio of up to 260% was achieved. Due to a weak temperature dependence this results in up to 153% at room temperature. The comparatively low values might be attributed to a higher surface roughness of the Heusler layer, due to a different seed layer system that was used in this work.

A high bulk and interface magnetic moment of the Heusler layer are present in the as prepared state. The predicted values for the bulk moment as well as for the element specific interface moment can be reached via annealing.

Acknowledgment

This work was supported by the German Bundesministerium für Bildung und Forschung (BMBF) for within the project HeuSpin. The authors gratefully acknowledge the support of the Advanced Light Source at Berkeley. The Advanced Light Source, Berkeley, CA, is supported by the Director, Office of Science, Office of Basic Energy Sciences, of the U.S. Department of Energy under Contract DE-AC02-05CH11231. The authors thank A. Weddemann for band structure calculations.

Authorized licensed use limited to: Universitaet Bielefeld. Downloaded on June 04,2010 at 10:24:58 UTC from IEEE Xplore. Restrictions apply.

REFERENCES

[1] S. A. Wolf, D. D. Awschalom, R. A. Buhrman, J. M. Daughton, S. von Molnar, M. L. Roukes, A. Y. Chtchelka-Nova, and D. M. Treger, *Science*, vol. 294, no. 5546, pp. 1488–1495, 2001.

[2] G. A. Prinz, *Science*, vol. 282, no. 5394, pp. 1660–1663, 1998.

[3] J. M. D. Coey and M. Venkatesan, *J. Appl. Phys.*, vol. 91, p. 8345, 2002.

[4] W. E. Picket and D. J. Singh, *J. Magn. Magn. Mater.*, vol. 172, p. 237, 1997.

[5] H. Akinaga, T. Manago, and M. Shirai, *Jpn. J. Appl. Phys.*, vol. 39, p. L1118, 2000.

[6] R. A. de Groot, F. M. Mueller, P. G. van Engen, and K. H. J. Buschow, *Phys. Rev. Lett.*, vol. 50, p. 2024, 1983.

[7] P. J. Webster, *J. Phys. Chem. Solids*, vol. 32, 1971.

[8] J. S. Moodera and G. Mathon, *J. Magn. Magn. Mater.*, vol. 200, p. 248, 1999.

[9] S. Ikeda, J. Hayakawa, Y. Ashizawa, Y. M. Lee, K. Miura, H. Hasegawa, M. Tsunoda, F. Matsukura, and H. Ohno, *Appl. Phys. Lett.*, vol. 93, p. 082508, 2008.

[10] L. Jiang, H. Naganuma, M. Oogane, and Y. Ando, *Appl. Phys. Express*, vol. 2, p. 083002, 2009.

[11] S. Tsunegi, Y. Sakuraba, M. Oogane, K. Takanashi, and Y. Ando, *Appl. Phys. Lett.*, vol. 93, p. 112506, 2008.

[12] N. Tezuka, N. Ikeda, F. Mitsuhashi, and S. Sugimoto, *Appl. Phys. Lett.*, vol. 95, p. 162504, 2009.

[13] W. Wang, H. Sukegawa, R. Shan, S. Mitani, and K. Inomata, *Appl. Phys. Lett.*, vol. 95, p. 182502, 2009.

[14] *Moscow University Geology Bulletin*, vol. 47, p. 80, 1992.

[15] J. Hayakawa, S. Ikeda, Y. M. Lee, F. Matsukura, and H. Ohno, *Appl. Phys. Lett.*, vol. 89, p. 232510, 2006.

[16] P. V. Paluskar, C. H. Kant, J. T. Kohlhepp, A. T. Filip, H. J. M. Swagten, B. Koopmans, and W. J. M. de Jonge, in *Proc. 49th Annu. Magn. Magn. Mater. AIP Conf.*, 2005, vol. 97, p. 10C925.

[17] C. H. Kant, J. T. Kohlhepp, H. J. M. Swagten, and W. J. M. de Jonge, *Appl. Phys. Lett.*, vol. 84, pp. 1141–1143, 2004.

[18] C. H. Kant, J. T. Kohlhepp, P. V. Paluskar, H. J. M. Swagten, and W. J. M. de Jonge, *J. Magn. Magn. Mater.*, vol. 286, pp. 154–157, 2005.

[19] R. Nakajima, J. Stöhr, and Y. U. Idzerda, *Phys. Rev. B*, vol. 59, no. 9, p. 6421, 1999.

[20] Y. U. Idzerda, C. T. Chen, H. J. Lin, G. Meigs, G. H. Ho, and C. C. Kao, *Nucl. Instrum. Methods Phys. Res. A*, vol. 347, no. 1–3, pp. 134–141, 1994.

[21] J. Schmalhorst, S. Kämmerer, M. Sacher, G. Reiss, and A. Hütten, *Phys. Rev. B*, vol. 70, no. 2, p. 024426, 2004.

[22] W. Regan, *Phys. Rev. B*, vol. 64, no. 21, p. 214422, 2001.

[23] D. Ebke, P. Thomas, O. Schebaum, M. Schäfers, D. Nissen, A. Hütten, and A. Thomas, *J. Magn. Magn. Mater.* 2009, accepted.

[24] C. T. Chen, Y. U. Idzerda, H.-J. Lin, N. V. Smith, G. Meigs, E. Chaban, G. H. Ho, E. Pellegrin, and F. Sette, *Phys. Rev. Lett.*, vol. 75, no. 1, p. 152, Jul. 1995.

[25] H. Ebert, *Electronic Structure and Physical Properties of Solids*, ser. Lecture Notes in Physics, H. Dreyssè, Ed. Berlin: Springer, 2000, vol. 535, p. 191 [Online]. Available: http://olymp.cup.uni-muenchen.de/ak/ebert/SPRKKR, the Munich SPR-KKR package, Version 3.6

[26] I. Galanakis, *Phys. Rev. B*, vol. 71, no. 1, p. 012413, 2005.

Authorized licensed use limited to: Universitaet Bielefeld. Downloaded on June 04,2010 at 10:24:58 UTC from IEEE Xplore. Restrictions apply.

Direct measurement of the spin polarization of Co_2FeAl in combination with MgO tunnel barriers

Oliver Schebaum,[1,a)] Daniel Ebke,[1] Andrea Niemeyer,[1] Günter Reiss,[1] Jagadeesh S. Moodera,[2] and Andy Thomas[1]
[1]*Thin Films and Physics of Nanostructures, Bielefeld University, 33615 Bielefeld, Germany*
[2]*Francis Bitter Magnet Laboratory, Massachusetts Institute of Technology, Cambridge, Massachusetts 02139, USA*

(Presented 21 January 2010; received 31 October 2009; accepted 3 December 2009; published online 12 May 2010)

It is a truth universally acknowledged that a Heusler compound in possession of a good order must be in want of a high spin polarization. In the present work, we investigated the spin polarization of the Heusler compound Co_2FeAl by spin polarized tunneling through a MgO barrier into a superconducting Al–Si electrode. The measured spin polarization of $P=55\%$ is in good agreement with the previously obtained tunnel magnetoresistance values and compared to the data by other groups. © *2010 American Institute of Physics*. [doi:10.1063/1.3358245]

I. INTRODUCTION

Heusler compounds are of great interest in materials science due to the predicted 100% spin polarization.[1] A large tunnel magnetoresistance (TMR) ratio is a key requirement for applications.[2] Thus, Heusler compounds are promising candidates as ferromagnetic electrodes in future spintronic devices based on magnetic tunnel junctions (MTJs). In the previous years, the room temperature TMR ratio of MTJs with Heusler electrodes could be increased to 220%.[3,4] The commonly used CoFeB/MgO/CoFeB MTJs show a maximum TMR ratio of 600% at room temperature[5] (1000% TMR ratio for double barrier systems[6]). Nevertheless, the enormous TMR ratio expected for very high—or even 100%—spin polarized electrodes has not been observed. The direct measurement of the spin polarization of the tunneling electrons is therefore an important method for further understanding and optimization of ferromagnetic Heusler compounds. While a lot of publications investigated the common ferromagnets[7] only few results for half-metallic ferromagnets[8,9] and very few results for ferromagnet/MgO/superconductor junctions are published.[10,11] In this work, we report about the direct observation of the spin polarization[7,12] of the compound Co_2FeAl by tunneling through MgO barrier into a superconducting counter electrode.

In the previous work, MTJs with a Co_2FeAl electrode and a Co–Fe counter electrode have been investigated by Ebke *et al.*[13] The optimized system MgO(5)/Co_2FeAl(20)/MgO(2.1)/CoFe(5)/MnIr(10) (all numbers in nanometers) system showed good ordering of the Heusler electrode for low annealing temperatures (250 °C) and a TMR ratio of up to 153% at room temperature for annealing temperatures of 450 °C. A TMR major loop of the described MTJ is shown in Fig. 1. The 5 nm thick MgO buffer layer proofed to be necessary to achieve the low ordering temperature of the Co_2FeAl electrode. X-ray diffraction investigations revealed a B2(001) structure of the Heusler films. Due to the high TMR ratio and the low ordering temperature Co_2FeAl is an interesting candidate for the experiments described in this publication.

In the present work, the spin polarization of this electrode was measured by replacing the upper electrode layers by a thin superconducting Al–Si electrode. Yang *et al.*[11] investigated the properties of superconducting Al–Si electrodes when using MgO tunnel barriers and found differences to systems with Al_2O_3 tunnel barriers. In our system, the substrate, the buffer layer and the tunnel barrier consist of MgO. Therefore, we investigated the dependence of the transition temperature on the thickness and the annealing temperature for thin Al–Si layers in proximity with MgO substrate and buffer layer. This way, we determined the optimal Al–Si conditions for the planned measurements of the spin polarization.

II. SAMPLE FABRICATION AND MEASUREMENTS

The samples were prepared using DC- and RF-magnetron sputtering at room temperature in a computer

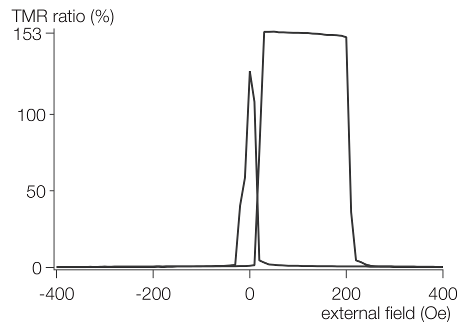

FIG. 1. TMR vs external magnetic field loop for a MgO(5)/Co_2FeAl(20)/MgO(2.1)/CoFe(5)/MnIr(10) MTJ. The sample has been annealed at 450 °C for one hour and successively field cooled.

a)Electronic mail: schebaum@physik.uni-bielefeld.de.

© 2010 American Institute of Physics

Downloaded 14 Jun 2010 to 129.70.28.22. Redistribution subject to AIP license or copyright; see http://jap.aip.org/jap/copyright.jsp

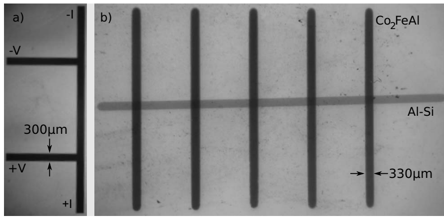

FIG. 2. (a) Layout for the measurement of the transition temperature T_c. A constant current of 1 μA was applied through the leads marked with $\pm I$ and the voltage drop measured between the leads marked $\pm V$. The width of the lines was 300 μm. (b) Cross strip geometry of the conductance vs voltage samples. The long-strip consists of the superconducting Al–Si electrode, the cross-strips are made of Co_2FeAl. Long- and cross-strip are separated by the MgO tunnel barrier.

controlled sputtering system with a base pressure of 1×10^{-7} mbar. The samples were post annealed for one hour at various temperatures in a vacuum furnace with a base pressure of 1×10^{-7} mbar. Optical lithography was used to define the lateral structure of the sample for the measurement of the transition temperature (T_c). The structure is shown in Fig. 2(a). The T_c measurements have been taken in a ^{4}He cryostat by applying a constant current of 1 μA to the outer leads and measuring the voltage drop between the inner leads while reducing the temperature. In contrast, the samples for measuring the spin polarization were directly sputtered *in situ* through shadow masks with the cross-strip geometry shown in Fig. 2(b).

In Fig. 3 (left) T_c is shown for different Al–Si thicknesses and different annealing temperatures, because the transition to the superconducting state is influenced by both the thickness of the superconducting layer and the annealing temperature. T_c is increasing with decreasing thickness and with increasing annealing temperature. For annealing temperatures above 400 °C the normal state resistance of the samples increased dramatically and no transition to the superconducting state could be observed. In Fig. 3 (right) the resistivity at T=4.2 K for the different thicknesses and annealing temperatures is shown. The thinnest layer of 4 nm shows a significantly increased resistivity compared to the 5, 6, and 7 nm thick layers for all annealing temperatures. With regard to this increase an Al–Si thickness of 5 nm was chosen for the conductance versus voltage measurements.

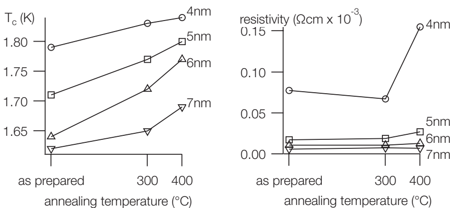

FIG. 3. Left: dependence of T_c on thickness and annealing temperature. Right: resistivity at 4.2 K for different thicknesses in dependence of the annealing temperature.

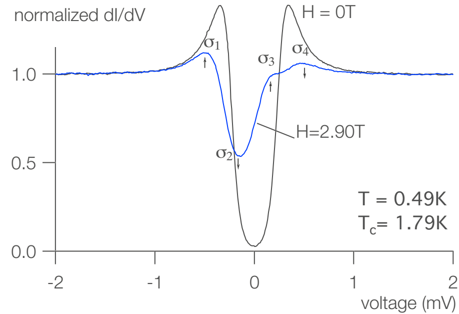

FIG. 4. (Color online) Normalized dI/dV measurements for H=0 T and H=2.90 T. The arrows indicate the contributions of the different spin-up and spin-down electrons. The σ_i are the conductances used to calculate the spin polarization according to Eq. (1).

The conductance versus voltage measurements have been carried out in a ^{3}He cryostat at a temperature of 0.49 K with a magnetic field applied in the plane of the samples to show the superconducting gap. In Fig. 4, the conductance versus voltage measurements for 0 and 2.9 T external in-plane magnetic field is shown. A spin polarization of the tunneling current results in an asymmetry in the conductance curves when a magnetic field is applied due to the Zeeman splitting of the BCS density of states (DOS). The spin polarization P can be calculated using the following equation:[7]

$$P = \frac{(\sigma_4 - \sigma_2) - (\sigma_1 - \sigma_3)}{(\sigma_4 - \sigma_2) + (\sigma_1 - \sigma_3)}. \tag{1}$$

For the Co_2FeAl electrode a value of P=60±2% can be deduced from this equation. Please note that neither spin-orbit scattering nor orbital depairing are accounted in this calculation.

A corrected value can be found by analyzing the dI/dV curves with the Maki theory. Generally, such curves can be modeled by this theory, which includes an orbital depairing parameter ζ and a spin-orbit scattering rate b.[14,15] A phenomenological parameter representing a lifetime broadening in the quasiparticle DOS has to be taken into account to achieve an adequate agreement of the theory and conductance curves.[7,11] In our samples the challenging ratio of the measuring temperature and T_c resulting in broadened BCS peaks complicate the analysis. A comparison between the theoretical curve obtained with the Maki theory and the measured data is given in Fig. 5. We find the best adjustment for a spin polarization P^*=55%, an orbital depairing parameter of ζ=0.04 and an spin-orbit scattering parameter of b=0.12. An additional, magnetic field dependent pair-breaking parameter of p=0.07 was included in the calculation. The corrected value for the spin polarization P^*=55% for the Co_2FeAl electrode is in good agreement with the value P=56.2% given by Inomata *et al.*[4]

In future experiments, we plan to investigate our samples by cross sectional high resolution electron microscopy and to compare *ab initio* transport calculations of Al/

Downloaded 14 Jun 2010 to 129.70.28.22. Redistribution subject to AIP license or copyright; see http://jap.aip.org/jap/copyright.jsp

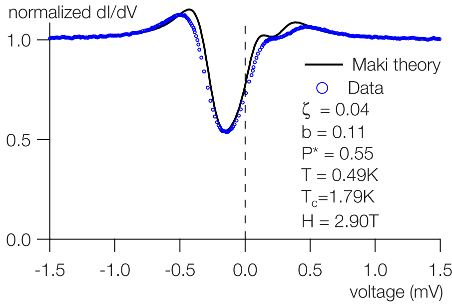

FIG. 5. (Color online) Maki fit vs measured data. The best adjustment of the theory to the data could be found for a spin polarization of $P^* = 55\%$. An orbital depairing parameter of $\zeta = 0.04$ and a spin-orbit scattering parameter of $b = 0.12$ are necessary. An additional pair-breaking parameter of 0.07 was used.

MgO/Heusler structures with the obtained results (cf. Heiliger *et al.*[16]).

III. SUMMARY

In summary, we investigated the spin polarization of the tunneling current from the Heusler compound Co_2FeAl through a MgO tunnel barrier by spin polarized tunneling into superconducting Al–Si electrodes. We found a spin polarization of the tunneling current of 55% which is in good agreement with the TMR ratio and the values found by Inomata *et al.*[4]

ACKNOWLEDGMENTS

The authors would like to thank the Deutsche Forschungsgemeinschaft DFG for financial funding and J. Schmalhorst for inspiring discussions. The work at MIT was supported by NSF Grant No. DMR 0504158 and ONR Grant No. N00014-09-1-0177.

[1] R. A. de Groot, F. Mueller, P. G. van Engen, and K. H. J. Buschow Phys. Rev. Lett. **50**, 2024 (1983).
[2] G. A. Prinz, Science **282**, 1660 (1998).
[3] S. Tsunegi, Y. Sakuraba, and M. Oogane, Appl. Phys. Lett. **93**, 112506 (2008).
[4] K. Inomata, N. Ikeda, N. Tezuka, and R. Goto, Sci. Technol. Adv. Mater. **9**, 014101 (2008).
[5] S. Ikeda, J. Hayakawa, Y. Ashizawa, and Y. Lee, Appl. Phys. Lett. **93**, 082508 (2008).
[6] L. Jiang, H. Naganuma, M. Oogane, and Y. Ando, Appl. Phys. Express **2**, 083002 (2009).
[7] R. Meservey and P. M. Tedrow, Phys. Rep. **238**, 173 (1994).
[8] P. C. Sullivan and J. S. Rogers, Solid State Commun. **45**, 977 (1983).
[9] C. Tanaka, J. Nowak, and J. Moodera, J. Appl. Phys. **86**, 6239 (1999).
[10] S. S. P. Parkin, C. Kaiser, A. Panchula, P. M. Rice, B. Hughes, M. Samant, and S.-H. Yang, Nature Mater. **3**, 862 (2004).
[11] H. Yang, S.-H. Yang, S. S. P. Parkin, T. Leo, and D. J. Smith, Appl. Phys. Lett. **90**, 202502 (2007).
[12] A. Thomas, J. Moodera, and B. Satpati, J. Appl. Phys. **97**, 10C908 (2005).
[13] D. Ebke, P. Thomas, O. Schebaum, M. Schäfers, D. Nissen, V. Drewello, A. Hütten, and A. Thomas, J. Magn. Magn. Mater. **322**, 996 (2010).
[14] P. Fulde and K. Maki, Phys. Rev. **141**, 275 (1966).
[15] D. Worledge and T. Geballe, Phys. Rev. B **62**, 447 (2000).
[16] C. Heiliger, M. Gradhand, P. Zahn, and I. Mertig, Phys. Rev. Lett. **99**, 066804 (2007).

Downloaded 14 Jun 2010 to 129.70.28.22. Redistribution subject to AIP license or copyright; see http://jap.aip.org/jap/copyright.jsp

Danksagung

An dieser Stelle möchte ich allen mein Dank aussprechen, die mich bei der Erstellung dieser Doktorarbeit unterstützt haben.
Mein Dank gilt zunächst meinem Doktorvätern Prof. Dr. Andreas Hütten und PD Dr. Andy Thomas. Vielen Dank für eure Unterstützung!

Bedanken möchte ich mich auch bei Prof. Dr. Günter Reiss, der mir die Gelegenheit gegeben hat in seinem Labor zu Arbeiten, und bei Dr. Jan Schmalhorst, der mit Ideen, konstruktiver Kritik und wissenschaftlichen Diskussionen zu dieser Arbeit beigetragen haben.

Des weiteren möchte ich mich bei allen Teilnehmern der *chinesischen Woche* bedanken: bei Oliver Schebaum für TMR Messungen, bei Markus Schäfers für Lithographie und bonding, bei Patrick Thomas für zahlreiche XRD-Messungen und bei Andy Thomas, der diese sehr erfolgreiche Woche ins Leben gerufen hat. Es hätte noch viele weitere geben sollen!
Oliver Schebaum sei ebenfalls für die hier gezeigten SPT-Messungen gedankt.

Meinem Bürokollegen Volker Drewello danke ich für die durchgeführten LT-Messungen.

Bei Zoë Kugler bedanke ich mich für die gemeinsame Messzeit an der ALS in Berkeley, in der die meisten hier gezeigten XAS und XMCD Spektren entstanden sind. Dr. Jan Schmalhorst und Markus Meinert sei ebenfalls gedankt für die Durchführung von ergänzenden XMCD Messungen.

Dennis Nissen sei gedankt für die ersten Ergebnisse mit Co_2MnAl und der Unterstützung bei TMR-Messungen an Co_2FeAl.
Alexander Weddemann und Alexander Auge möchten ich für die durchgeführten Bandstrukturrechnung danken.

Der guten Seele von D2 Karsten Rott möchte ich meinen

Dank für die Betreuung und Instandhaltung nahezu aller Laboreinrichtungen danken. Auch den namentlich hier nicht aufgeführten Mitgliedern der Arbeitsgruppe von D2 gebührt ein Dankeschön für die angenehme, nahezu familiäre Atmosphäre während und nach der Arbeit.

Bei der (Heusler, Heusler, Heusler-) Arbeitsgruppe von Prof. Dr. Claudia Felser bedanke ich mich für die inspirierende Zusammenarbeit in den letzten Jahren und das bereitgestellte $Co_2Mn_{0.5}Fe_{0.5}Si$ target.

Auch für die Unterstützung der Advanced Light Source in Berkeley zur Durchführung der hier gezeigten XAS und XMCD Messungen an den beamlines 6.3.1 und 4.0.2 sei gedankt. Insbesondere gilt ein großer Dank Elke Arenholz, die uns stets umsorgend betreut hat und die durch die außergewöhnlich gut gewarteten Messaufbauten immer für erfolgreiche Strahlzeiten gesorgt hat. Die Advanced Light Source, Berkeley, USA, wird gefördert von dem Office of Science, Office of Basic Energy Sciences, of the U.S. Department of Energy unter der Vertragsnummer: DE-AC02-05CH11231.

Vielen Dank auch dem Bundesministerium für Bildung und Forschung (BmBF) für die finanzielle Unterstützung im Rahmen des Projekts *HeuSpin*. Hier sei den Kollegen Jürgen Langer und Berthold Ocker von der Singulus NDT GmbH, sowie Manfred Rührig von der Siemens AG, für die gute Zusammenarbeit und die Bereitstellung der Proben gedankt.

Abschließend möchten ich mich bei meiner Frau Wiebke und meinem Sohn Johann für die liebevolle Unterstützung und ihr Verständnis in den letzen Jahren bedanken.